Changes in ocean circulation and carbonate chemistry in the Australian sector of the Southern Ocean during the last 500,000 years

Dissertation

zur Erlangung des Doktorgrades

der Mathematisch-Naturwissenschaftlichen Fakultät

der Christian-Albrechts-Universität

zu Kiel

vorgelegt von

Arne Sturm

Kiel 2003

Referent:	Professor Dr. J. Thiede
Korreferent:	Professor Dr. W.-C. Dullo
Tag der mündlichen Prüfung:	09. Februar 2004
Zum Druck genehmigt:	

Der Dekan

DANKSAGUNG

Bei Herrn Prof. Dr. J. Thiede möchte ich mich für die Vergabe und Betreuung der vorliegenden Dissertation bedanken. Prof. Dr. W.-C. Dullo und Prof. Dr. W. Kuhnt danke ich für die freundliche Übernahme der Zweitgutachten.

Besonders herzlich bedanke ich mich bei Herrn Dr. Ralf Tiedemann für die niemals nachlassende Unterstützung und Betreuung, sowie unsere langjährige Freundschaft.

Für viele fruchtbare Diskussionen und gute Zusammenarbeit danke ich den Kollegen der Abteilung Paläo-Ozeanologie des GEOMAR, besonders Dr. D. Nürnberg sowie J. Schönfeld, die immer mit Rat und Tat zur Seite standen. Ein herzlicher Dank gilt allen Kollegen des TASQWA Projektes, inbesondere Dr. S. Nees, Dr. J. Reijmer, Dr. A. Müller, Dr. S. Roth, Dr. A. Rüggeberg, O. Runze und S. Überall. Für Unterstützung bei labortechnischen Problemen bedanke ich mich recht herzlich bei den Technikern des GEOMAR Dirk Reese, Bastian Fessler, Jutta Pagel, Silvia Koch und Bettina Dohmeyer. Für tatkräftige Unterstützung bei den Laborarbeiten danke ich insbesondere Janne Repschläger, Agnes Heinemann und Henrike Höppner. Für aufmerksames Korrekturlesen der Arbeit sei Carolyn Wegner, Ortrud Runze und Anja Wolf gedankt.

Ein liebes Dankeschön gilt der Doktoranden-Gruppe um Anja Wolf, Carolyn Wegner, Natasja Brughmans, Silke Steph, Lester Lembke und André Kaiser für Diskussionen und Gespräche aller Art, ob im wissenschaftlichen oder privaten Bereich. In diesem Sinne möchte ich mich auch bei Dr. Sven-Oliver Franz und Dr. Shungo Kawagata bedanken.

Ein besonderes Dankeschön gilt Herrn Dr. P. De Deckker für den unkomplizierten und regen Austausch von Proben und Daten und die hilfreichen Gespräche, sowie die familiäre Unterbringung während meines Aufenthaltes in Canberra, Australien.

Finanziell unterstützt wurde diese Arbeit vom Bundesministerium für Bildung und Forschung (Projekt TASQWA) und von der Deutschen Forschungsgemeinschaft (Projekt Ti 240/10-1).

Für die liebevolle Unterstützung meiner Familie kann ich mich gar nicht oft genug bedanken. Allen Freunden einen lieben Dank für die steten Aufmunterungen.

ABSTRACT

Fifteen Pleistocene sediment records from 585 to 4,068 m water depth were studied on a bathymetric transect in the Australian sector of the Southern Ocean between 42° to 56°S and 114° to 170°E. Stable oxygen and carbon isotope records and carbonate dissolution proxy records were used to reconstruct glacial/interglacial changes in ocean circulation, deep-water ventilation and carbonate chemistry for the last 500 kyr.

Carbonate preservation records indicated a longitudinal gradient in Southern Ocean deep-water alkalinity at 110°E that persisted through glacial/interglacial stages. The "Atlantic-type" carbonate preservation pattern was previously considered to have prevailed in the entire Southern Ocean with enhanced carbonate preservation during interglacials and increased carbonate dissolution during glacials. New data from the present study reveal, however, that the reversed "Pacific-type" pattern of glacial/interglacial carbonate preservation expanded from the Pacific into the Australian sector of the Southern Ocean up to 110°E. This result implies that deep-waters in the Australian sector flow westwards against the predominant eastward drift in the Southern Ocean. In general, the lysocline depth fluctuated between ≥4,100 m (glacial) and ≤3,200 m (interglacial) in the Australian sector of the Southern Ocean during the last 500 kyr.

Epibenthic stable carbon isotope records depicted a detailed variability of Pleistocene deep-water circulation and ventilation with new implications for glacial deep-water circulation. The major problem in understanding the glacial deep-water circulation and isotope signatures below 2,500 m derives from the extremely low $\delta^{13}C$ values in the Atlantic-Indian sector of the Southern Ocean. They contrast relatively high $\delta^{13}C$ values in the central Pacific. This difference raises the question whether the nutrient-enriched and poorly ventilated glacial Southern Ocean could be a source of the nutrient-depleted and well-ventilated Pacific deep-waters. The glacial $\delta^{13}C$ signatures of deep-waters in the Australian sector present a mixture of both endmembers and thus link the isotope signatures of both regions. This suggests a westward deep-water flow to the south of Australia, which is consistent with the "Pacific-type" pattern of carbonate preservation in this area. These findings and the even better ventilated water masses towards the east (Chatham Rise) suggest the SW Pacific, in particular the Ross Sea, as a source region for nutrient-depleted Glacial Antarctic Bottom Water. This water mass ventilated both, the Australian sector of the Southern Ocean and the deep Pacific. Modified, well-ventilated Glacial Upper North Atlantic Deep Water may have contributed to the bottom water formation. In contrast, Glacial Antarctic Bottom Water formed in the Atlantic sector (Weddell Sea) possibly suffered from both, increased contribution of older Pacific deep-water masses via the Drake Passage, and a persistent sea-ice coverage that reduced air-sea gas exchange and thus contributed as well to the extremely low $\delta^{13}C$ values.

The comparison of carbonate dissolution and $\delta^{13}C$ initially suggested increased carbonate preservation during glacials when deep-water ventilation was reduced. Considering the intermediate- to deep-water gradient in $\delta^{13}C$ and eliminating the regional glacial/interglacial background, carbonate dissolution proxies and the net depth-related change in $\delta^{13}C$ imply, however, that increased carbonate preservation was associated with a relative increase in deep-water ventilation.

Planktonic oxygen isotope data suggested a glacial/interglacial latitudinal variability of the Subtropical Front to the south of Tasmania on the order of 2° in latitude with a northward, glacial position between 44.2° to 46.5°S. Comparisons of $\delta^{18}O$ records from shallow- and deep-dwelling planktonic foraminifers suggested a long-term change in salinity at a water depth of >250 m. Intermediate-water salinities were apparently lower between 420 to 170 ka than during the last 170 kyr. This shift was most likely associated with a long-term southward displacement of surface water frontal systems. Another prominent feature in upper-ocean water mass signatures are extreme $\delta^{13}C$ minima occurring at glacial terminations. Such minima in planktonic $\delta^{13}C$ are already known from other areas of the Southern Ocean and even from the upwelling regions of the tropical Pacific. Recent studies thus assume that Antarctic Intermediate Water acted as a conduit for transferring $\delta^{13}C$ variability to low latitudes. An epibenthic $\delta^{13}C$ record from the Campbell Plateau at 600 m water depth displayed these minima too during Termination II. This would corroborate the proposed link between high- and low-latitude surface waters via Antarctic Intermediate Water.

TABLE OF CONTENTS

ABBREVIATIONS

Oceanographic fronts, zones and surface currents

STF	Subtropical Front
SAF	Subantarctic Front
APF	Antarctic Polarfront
AD	Antarctic Divergence
SAZ	Subantarctic Zone
PFZ	Polarfront Zone
AAZ	Antarctic Zone
SAC	South Australian Current
ACC	Antarctic Circumpolar Current

Water masses

STSW	Subtropical Surface Water
SASW	Subantarctic Surface Water
AASW	Antarctic Surface Water
SAMW	Subantarctic Mode Water
AAIW	Antarctic Intermediate Water
CPDW	Circumpolar Deep Water
UCPDW	Upper Circumpolar Deep Water
LCPDW	Lower Circumpolar Deep Water
NADW	North Atlantic Deep Water
GNADW	Glacial North Atlantic Deep Water
PCW	Pacific Central Water
AABW	Antarctic Bottom Water

CHAPTER 1

INTRODUCTION

From a paleoceanographic point of view, the non-Atlantic sector of the Southern Ocean has been poorly studied during the past and there are still large gaps in our knowledge on paleoceanographic changes in this area, although it is a key area for the water mass exchange between ocean basins. Its interaction with water masses from the Atlantic, Pacific and Indian oceans is an important element of the global thermohaline circulation, because it influences the salt, heat and nutrient balances of the world ocean and may trigger climate feedback associated with heat transport and the carbon cycle. Variations in the nutrient budget of the Southern Ocean are important to carbon cycling due to their direct effect on atmospheric CO_2, and also because world's intermediate- and deep-waters are ventilated to large parts in the Southern Ocean. This study investigates changes in circulation and chemistry in the Australian sector of the Southern Ocean (Fig. 1-1) for the time interval of the last 500,000 years. It is the most extensive study in this area with regard to Pleistocene reconstructions on oceanography and provided the opportunity of new insights into regional elements of the climate system. The results presented here are based on 15 sediment records forming a deep-water transect from 585–4,070 m water depth and covering an area between 40°–56°S and 120°–170°E. The interpretations are mainly based on the following proxy data:

- Oxygen and carbon isotope data from epifaunal benthic foraminifers to develop an oxygen isotope stratigraphy, and to reconstruct changes and deep- and intermediate-water ventilation and circulation ($\delta^{13}C$) that are critical for the exchange of nutrients between oceans (influencing the productivity in the Southern Ocean),
- Oxygen and carbon isotope data from planktonic foraminifers to monitor changes in near-surface water $\delta^{18}O$ and $\delta^{13}C$ signatures, to assess fluctuations in temperature/salinity ($\delta^{18}O$) and nutrients ($\delta^{13}C$) and to reconstruct climate related changes in subantarctic surface circulation and its effect on intermediate-water formation,
- Carbonate and sand fraction content, and planktonic foraminiferal fragmentation to assess variations in carbonate preservation and lysocline depth that result from changes in deep-water alkalinity and that are associated with atmospheric CO_2-concentrations.

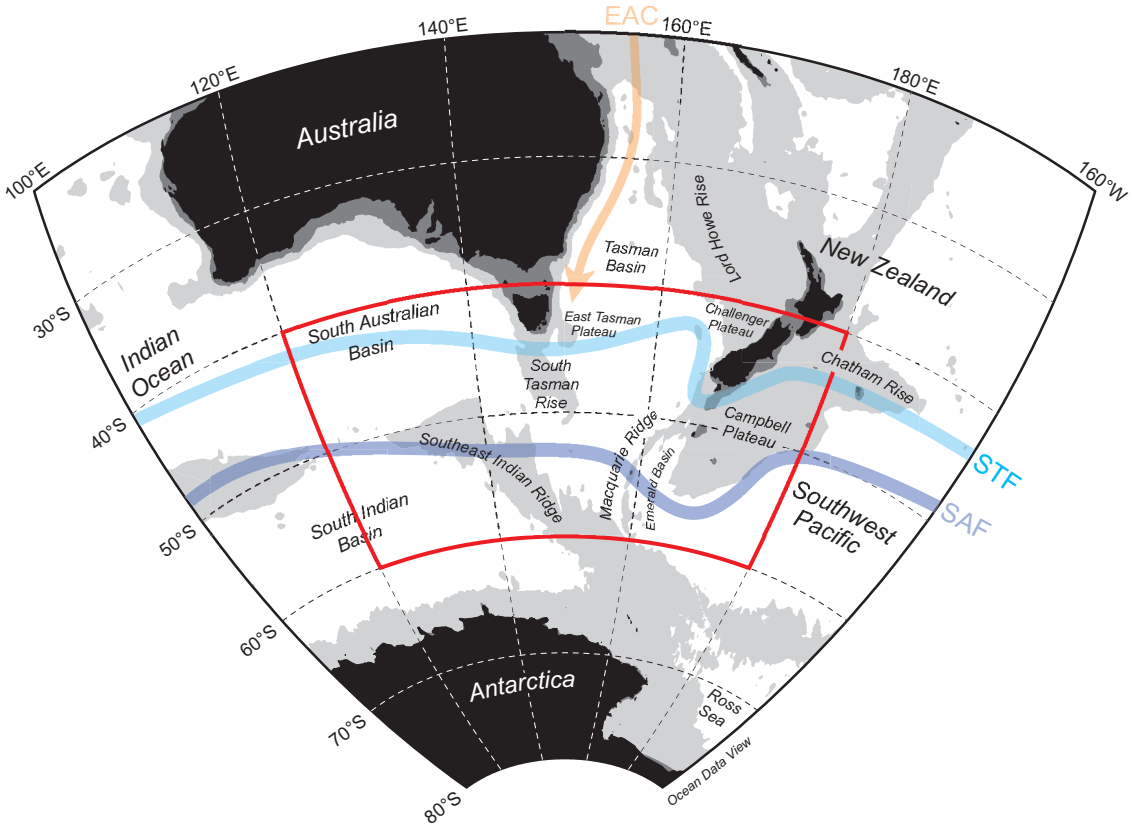

Figure 1-1. Major bathymetric features, oceanographic fronts and currents of the Australian sector of the Southern Ocean. Grey shaded areas indicate water depth above 3,500 m. The red frame marks the research area between 120°–180°W and 40°–60°S (STF = Subtropical Front, SAF = Subantarctic Front, EAC = East Australian Current). A more detailed bathymetry of the research area is given in Figure 1-6.

The time resolution (sampling interval) of these records varies from higher than 1,000 years to about 3,000 years and allows detailed comparisons with high-resolution records from the Atlantic and Pacific and to prove several hypotheses on the Southern Ocean's role in the climate system (see below). This study was initiated during the TASQWA-project („Quaternary variability of water masses in the southern Tasman Sea and the Southern Ocean (SW Pacific sector)", funded by the BMBF) and finished within the DFG-project „Paleoceanographic changes in the Australian sector of the Southern Ocean during the last 500,000 years".

1.1 MAJOR OBJECTIVES AND QUESTIONS

The goals of this study are to test hypotheses on global ocean circulation and climate change by (1) reconstructing Pleistocene variations in Antarctic Intermediate Water formation that is related to variations in subantarctic surface water mass properties and circulation and (2) monitoring changes in deep-water ventilation and carbonate chemistry that are indicative of changes in deep-water alkalinity and its potential for influencing atmospheric CO_2-concentrations. The following paragraphs highlight hypotheses and questions that are relevant to the results and interpretations of this study:

Hypotheses for atmospheric and upper ocean dynamics during glacials and problems:

Glacial to interglacial variations in sea-ice cover, biological nutrient utilization and exposure rates of deep-water in the Southern Ocean have been considered in numerical models to play a key role in explaining the glacial reduction in atmospheric CO_2-concentrations (Sarmiento & Toggweiler, 1984; Michel *et al*., 1995; Francois *et al*., 1997; Toggweiler, 1999; Stephens & Keeling, 2000; Watson *et al*., 2000; Gildor & Tziperman, 2001; Gildor *et al*., 2002). On one hand, such changes modulate the preformed nutrient concentration and ventilation of newly formed subsurface waters (Subantarctic Mode Water, Antarctic Intermediate Water, Antarctic Bottom Water). On the other hand, variations in the strength and northward expansions of the southern hemisphere's westerly winds as well as associated northwards shifts of the Antarctic Polar Front (sea-ice extent) and the Subtropical Front are thought to exert a strong control on the northward export of these water masses which, to large parts, ventilate the global ocean. Conventional models that invoke glacial increases in high-latitude nutrient utilization, however, face a number of apparent disagreements with paleoceanographic proxy data (Sigman & Boyle, 2000), in particular with the Cd/Ca and $\delta^{13}C$. The glacial decrease in Southern Ocean upper surface $\delta^{13}C$ of ~0.7 ‰ as derived from planktonic foraminifers (Charles & Fairbanks, 1990) contrasts with enhanced utilization of nutrients. Variations in Cd/Ca ratios of planktonic foraminifers consistently suggest a glacial nutrient increase of ~0.6 µmol/kg PO_4 in the Antarctic Ocean (Elderfield & Rickaby, 2000), which is as well in conflict with hypotheses of an enhanced nutrient utilization. Moreover, models invoking a glacial increase in the high-latitude biological pump associated with a strong feedback on alkalinity predict a large increase in the depth of the lysocline, which is not observed. A way out of this dilemma seems to be provided by numerical models by combining both, the influence of Antarctic sea-ice on changes in surface water dynamics (Stephens & Keeling, 2000) and/or a decrease in high-latitude vertical mixing (Toggweiler, 1999). Stephens & Keeling (2000) suggest that low glacial atmospheric CO_2-levels might result from reduced deep-water ventilation associated with either year-round Antarctic sea-ice coverage, or wintertime coverage combined with ice-induced stratification during summer. Toggweiler (1999) presented a model that reduced the deep-water ventilation by decreasing the vertical exchange between deep and Antarctic surface waters. Both models are generally consistent with paleoceanographic data (Cd/Ca and $\delta^{13}C$). More recently, Gildor & Tziperman (2001) presented a new mechanism to explain changes in vertical mixing and sea-ice cover changes. The cooling of North Atlantic Deep Water due to northern hemisphere glaciation is transported southward by thermohaline circulation and cools the deep-water upwelled in the Southern Ocean, which, in turn, affects the Southern Ocean stratification and reduces the rate of vertical mixing of the surface-water with the deep-water and increases sea-ice cover.

Other models propose that the glacial sea-ice cover and its thermodynamic effect on $\delta^{13}C$ was only partly responsible of the low $\delta^{13}C$ values (e.g. Broecker & Maier-Reimer, 1992; Charles *et al.*, 1993), but might be explained by a different ocean circulation (Michel *et al.*, 1995). Michel *et al.* (1995) proposed that a deeper enhanced flux of Antarctic Mode Water north of the Subantarctic Front flowed towards the equator and refilled the Atlantic, Indian and Pacific basins. As a consequence, the Southern Ocean was then partially isolated and mostly self-ventilated reducing $\delta^{13}C$ of circumpolar waters to the lowest values in the glacial ocean (Fig. 1-2). Today, the Australian – New Zealand sector is one of the largest regions of mode water formation and the sediment records of this study will be used to verify this hypothesis.

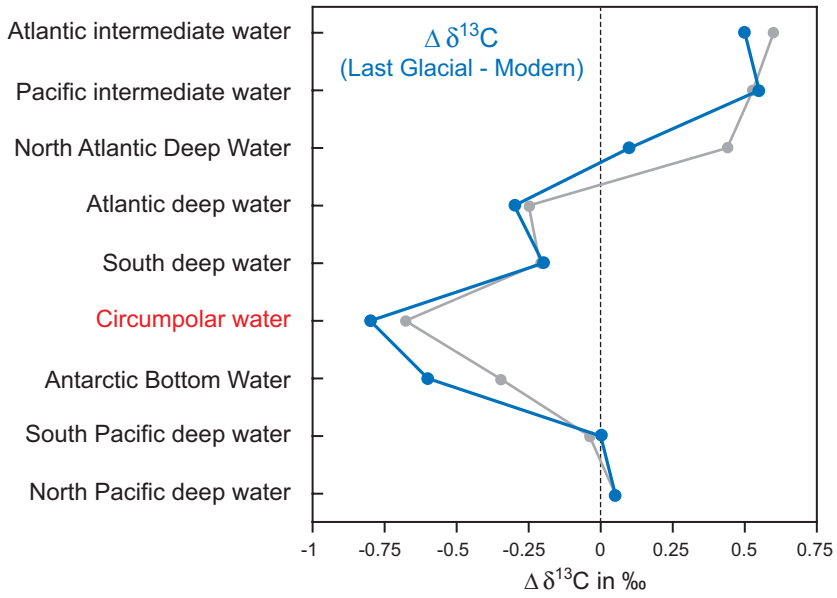

Figure 1-2. Glacial-interglacial differences in $\delta^{13}C$ of epifaunal benthic foraminifers (blue) from different oceanic regions and water masses in comparison to calculated values (grey) derived from a circulation model that simulates an enhanced deep-water production of „Subantarctic Mode Water" during the last glacial (Michel *et al.*, 1995). The glacial values have been corrected for by 0.4 ‰ according to a global decrease in $\delta^{13}C$ (Curry *et al.*, 1988). The circumpolar water masses exhibit the strongest decrease in $\delta^{13}C$ with the most negative values.

Hypotheses for the atmospheric and oceanic frontal system during the Pleistocene:

Paleoceanographic reconstructions based on the distribution of faunal assemblages (radiolarians, foraminifers and diatoms) indicate northward shifts of the frontal system during glacial times on the order of 2–6° within the Atlantic and Indian sector of the Southern Ocean (Howard & Prell, 1992; Brathauer & Abelmann, 1999; Crosta *et al.*, 1998). In the Australian – New Zealand sector, however, northward shifts of the frontal system are restricted by bottom topography of the South Tasman Rise and the Campbell Plateau (Moore *et al.*, 1999), and are also affected by the southward-directed East Australian Current (Fig. 1-1), which today transfers warm and saline subtropical surface water into the Southern Ocean. Therefore, the

frontal system in the study area is assumed to be compressed during glacial periods with stronger sea-surface temperature gradients, because the glacial Subtropical Front was locked to a position south off Tasmania (Armand, 1997). Pleistocene records of ice rafted debris from the Southern Ocean are sparse and limited to the Atlantic sector but indicate that debris-laden icebergs reached as far north as 41°S during the last glacial (Kanfoush *et al*., 2000). Diatom-based paleo-reconstructions of maximum sea-ice extent during the last glacial maximum (Crosta *et al*., 1998) indicate that the ice-edge was displaced northwards by ~5–8° during glacial winters in comparison to its modern position at ~55°S. Similar studies of Armand (1998) suggest a northward expansion of the glacial ice-edge from ~63°S (today) to ~54°S south of Tasmania.

The glacial expansion of Antarctic sea-ice coverage during winter time combined with ice-induced stratification during the summer are considered in general circulation models to play an important role in explaining the lowered atmospheric CO_2-concentrations by limiting the outgassing of CO_2 from the Southern Ocean (Stephens & Keeling, 2000; Sigman & Boyle, 2000). In addition, these models imply also an important feedback on deep- and subsurface-water ventilation, as increased sea-ice cover would lower the Antarctic surface $\delta^{13}C$ values by reducing the air-sea gas exchange.

Questions on Southern Ocean deep-water dynamics during the Pleistocene:

Which role plays the Southern Ocean in actively modulating the thermohaline circulation? Variations in freshwater flux between both hemispheres have long been suggested as a pacemaker of the oceanic thermohaline circulation that may operate with transitions, at least between three settings (Fig. 1-3): a modern, a glacial and the Heinrich mode (Broecker, 1991, 1997; Sarnthein *et al*., 1994; Stocker, 1998; Alley & Clark, 1999; Manabe & Stouffer, 1999). The modern mode is dominated by formation of North Atlantic Deep Water that fills the Atlantic basin up to a depth of ~4,200 m. The glacial mode is characterized by reduced North Atlantic Deep Water formation only up to a depth of <2,500 m and Antarctic-derived waters beneath. The glacial mode, however, is disturbed by the Heinrich mode that operates on millennial timescales. This mode is characterized by ice-rafting and associated meltwater events in the North Atlantic region that further reduces the formation of North Atlantic Deep Water, allowing Antarctic deep-water masses to expand to water depths near 1,000 m in the Atlantic. These glacial variations in the strength of the Atlantic thermohaline circulation often resulted in a temporally offset pattern of polar warming and cooling between both hemispheres (northern hemisphere cooling and southern hemisphere warming relates to reduced Atlantic overturning). This asynchrony of temperature changes between both hemispheres has been observed in sediment and ice-core records (Charles *et al*., 1996; Blunier *et al*., 1998; Kanfoush *et al*., 2000; Blunier & Brook, 2001) and is known as the “bipolar seesaw” (Stocker, 1998).

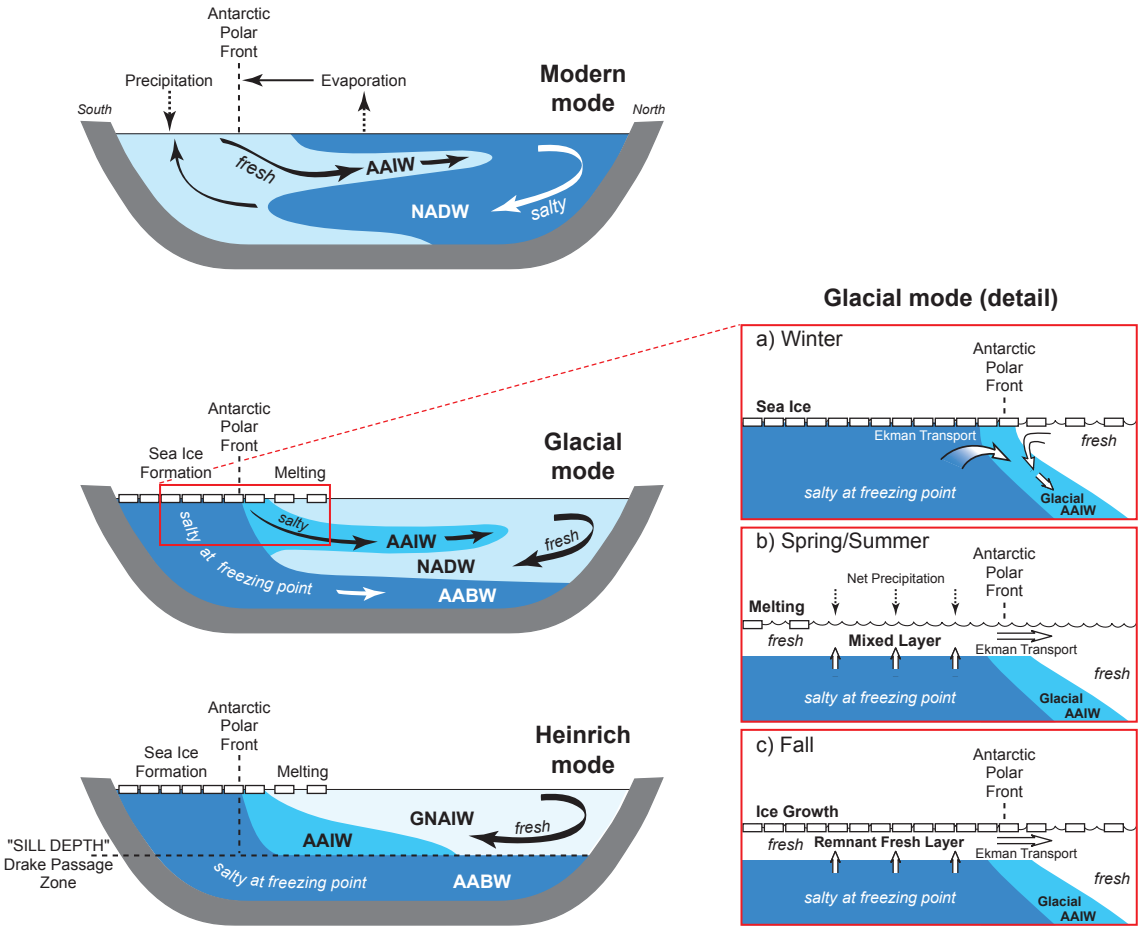

Figure 1-3. Sketch of three states (modern, glacial and Heinrich mode) of oceanic thermohaline circulation with focus on the Southern Ocean (modified after Keeling & Stephens, 2001).

Growing evidence from general circulation models (Toggweiler & Samuels, 1993; Toggweiler, 1999; Keeling & Stephens, 2001; Seidov *et al*., 2001; Brix & Gerdes, 2003) and paleoceanographic data (Vidal *et al*., 1999; Adkins *et al*. 2002; Boyle, 2002) suggest that the Southern Ocean plays a more active role in modulating oceanic changes in the thermohaline circulation rather than just responding to changes in the North Atlantic. Results from general circulation models (Toggweiler & Samuels, 1993; Brix & Gerdes, 2003) propose that the strength of the inflow and outflow through the South Atlantic is determined more by the strength of the wind-field over the Southern Ocean than by the production of North Atlantic Deep Water. Changes in the freshwater input to the Southern Ocean due to the melting of sea-ice and ice sheets on Antarctica may also actively change the Atlantic thermohaline circulation as hypothesized by Seidov *et al*. (2001). In general, meltwater events in one hemisphere may lead to a strengthening of the thermohaline conveyor driven by the source of the opposite hemisphere.

In terms of the freshwater balance of the Southern Ocean, recent results from Adkins *et al.* (2002) propose that the most saline deep-waters were formed in the Southern Ocean during the last glacial maximum with Antarctic Bottom Water to be ~1 PSU higher than North Atlantic Deep Water. If so, the source for saline deep-waters switched during the past 20,000 years from Antarctica to the North Atlantic. In addition, deep-water temperature reconstructions from benthic oxygen isotopes suggest that the Southern Ocean provided the coldest deep-waters, close to the freezing point, during the last glacial (Duplessy *et al.*, 2002). Both, a salinity increase and temperature decrease in glacial Antarctic Bottom Water in combination with enhanced wind stress over the Southern Ocean and sea-ice formation, should have strengthened the role of the Southern Ocean in actively modulating the variability of the glacial thermohaline circulation.

Is there an evidence for a glacial vertical redistribution of nutrients and carbon in the Southern Ocean as predicted by circulation models?

Recently, studies of Ninnemann & Charles (2002) and Hodell *et al.* (2003) in the South Atlantic sector of the Southern Ocean showed that the carbon isotopic signal of mid-depth waters evolved differently from deep-waters during the Pleistocene. Reconstructions of intermediate-to-deep $\delta^{13}C$ gradients revealed a sharp chemocline between 2,100 and 2,700 m dividing well-ventilated water above ~2,500 m from poorly ventilated water below (Fig. 1-4) during most glacial stages of the last 1.1 myr.

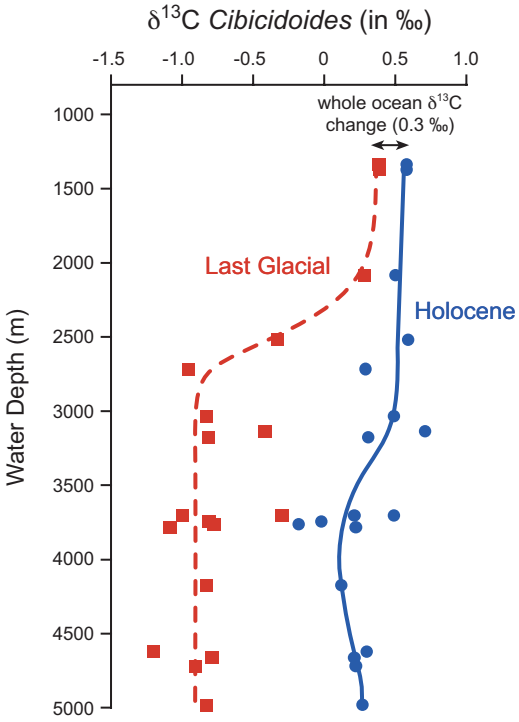

Figure 1-4. Reconstruction of vertical $\delta^{13}C$ gradients in the South Atlantic for the Holocene (blue) and last glacial maximum (red) indicates a chemocline between 2,100 and 2,700 m water depth for the glacial Southern Ocean (Hodell *et al.*, 2003). This chemical difference defines well-ventilated water above ~2,500 m and poorly ventilated water below.

This vertical distribution is in contrast to the Holocene when both deep- and intermediate-waters were generally better ventilated, because North Atlantic Deep Water extended far into the South Atlantic, altering the physical and chemical properties of Circumpolar Deep Water especially above 3,000 m water depth (Charles & Fairbanks, 1990). Similar studies in the Indian and Pacific oceans also reported sharp $\delta^{13}C$ gradients at ~2,000 m water depth during glacial periods (Mix *et al*., 1991; Herguera *et al*., 1992; McCorkle *et al*., 1998; Matsumoto *et al*., 2002). The indications of such a chemical boundary between mid-depth- and deep-waters in the glacial Southern Ocean are supported by models that ascribe reduced glacial atmospheric CO_2-concentrations to the vertical fractionation concept (e.g. Boyle, 1988; Toggweiler, 1999; Gildor & Tziperman, 2001), where a boundary separates low CO_2 intermediate-water from CO_2-rich deep-water. Sediment records of this study will provide details on intermediate- to deep-water gradients in the more eastern part of the Southern Ocean (Australian – New Zealand sector).

What is the role of mid-depth Pacific outflow to the Southern Ocean and the export of Southern Ocean water masses into the Pacific?

Today, the net northward export of water masses from the Southern Ocean is balanced by the deep return flow from the North Atlantic, because modern conditions favor the formation of dense North Atlantic Deep Water. However, during glacial times when North Atlantic Deep Water formation was reduced the Pacific may have become important in balancing the mid-depth return flow. If so, a return flow from the North Pacific containing the largest nutrient pool, would influence the deep-water ventilation and the nutrient budget in the Southern Ocean. This would also change the relationship between dissolved nitrate, phosphate, and silica and would also change the character of upper-ocean productivity in the Southern Ocean. Evidence for glacial changes in Pacific deep- to intermediate-water circulation is provided by benthic $\delta^{13}C$ records from the eastern equatorial Pacific and the North Pacific. In the eastern equatorial Pacific, Mix *et al*. (1991) examined the $\delta^{13}C$ gradient between Pacific deep- and intermediate-water (3,200 m and 1,370 m). They noted that the gradients between these two records might reflect either an enhanced glacial source of high-$\delta^{13}C$ intermediate water in the North Pacific or the Southern Ocean. Today, the surface-water in the North Pacific is too fresh for intermediate-water formation. During the last glacial, however, Keigwin (1998) suggests the Sea of Ochotsk as a potential source for North Pacific Intermediate Water formation that ventilates the North Pacific to a water depth of ~2,000 m. Using benthic $\delta^{13}C$ records from the deep Southern Ocean, the deep equatorial and North Pacific, Zahn *et al*. (1991) suggested that the equatorial deep water at ~3,100 m water depth was better ventilated than that of the Southern Ocean (3,250 m) and the deep North Pacific (>3,500 m). Hence, the Pacific may have been important in balancing the exchange within the Southern Ocean.

Questions about changes in carbonate chemistry during the Pleistocene:

Which carbonate preservation pattern dominates the Australian sector of the Southern Ocean?

Pleistocene variations in carbonate preservation are marked by a contrasting pattern between Atlantic and Pacific. Enhanced North Atlantic Deep Water formation during interglacial times amplified the chemical inter-basin fractionation between Atlantic and Pacific. This is reflected in an increase in Atlantic carbonate preservation and a decrease in Pacific carbonate preservation, which is related to a deepening of the Atlantic and a shoaling of the Pacific lysocline. During times of diminished North Atlantic Deep Water formation this pattern is reversed. The Australian sector of the Southern Ocean is the interface between Pacific and Atlantic deep-water exchange. Today, the influence of nutrient depleted North Atlantic Deep Water can be traced by phosphate concentrations from the South Atlantic to the Indian sector of the Southern Ocean (Fig. 1-5). Thus, any change in the strength of North Atlantic Deep Water production, possibly associated with variations in the return flow of nutrient-enriched and more carbonate-aggressive deep-water masses from the Pacific and Indian Ocean, should leave an imprint on the carbonate preservation and the lysocline depth in the studied area. So far, global reconstructions about changes in carbonate preservation (Catubig *et al.*, 1998) are limited because of small data coverage in the Australian and South Pacific sectors of the Southern Ocean.

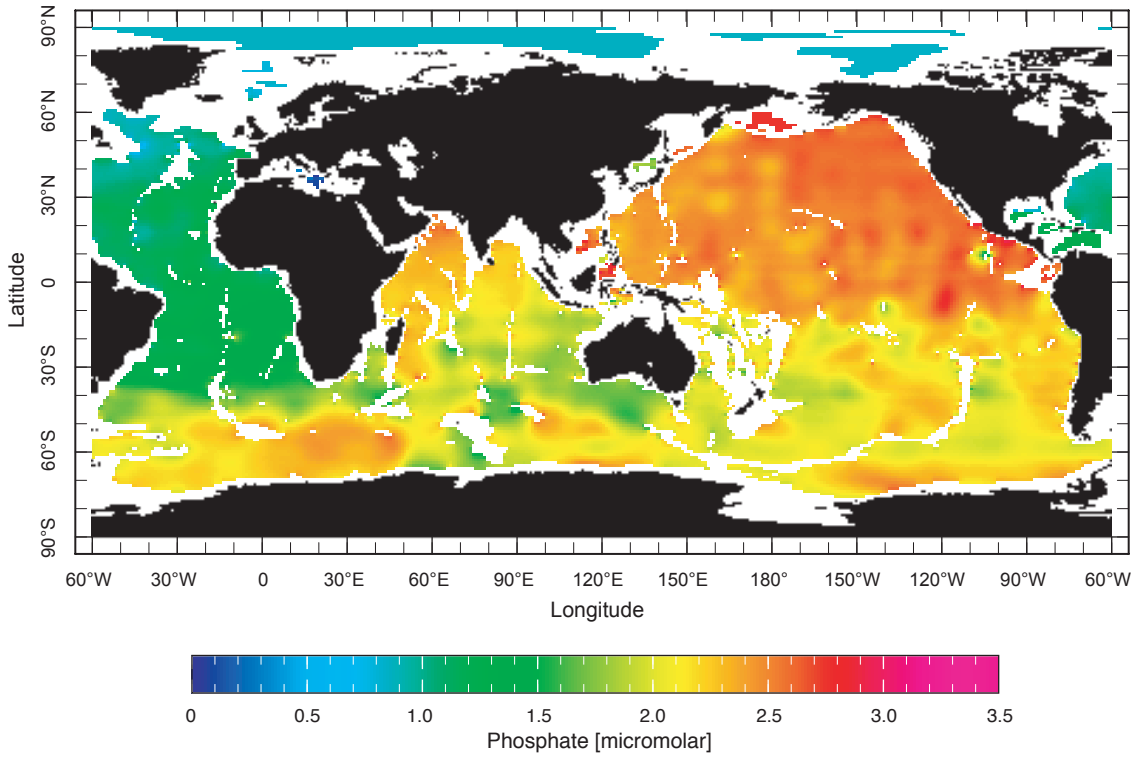

Figure 1-5. Distribution of phosphate concentration at 3,000 m water depth, data are from LEVITUS World Ocean Atlas 1994 (Conkright *et al.*, 1994; illustrated with http://iridl.ldeo.columbia.edu/).

The global distribution of Atlantic-type and Pacific-type patterns in carbonate preservation as well as their differences on glacial to interglacial scales defines the relative changes of the ocean-average lysocline depth. This depth plays an important role in assessing glacial-interglacial changes in deep-ocean alkalinity that drives changes in atmospheric CO_2-concentrations (Sigman & Boyle, 2000). Most models invoking alkalinity changes to explain the glacial reduction in atmospheric CO_2-concentrations predict considerable deepening of the ocean-average lysocline depth (Boyle, 1988; Opdyke & Walker, 1992; Archer & Maier-Reimer, 1994). This means that the Pacific-type pattern of enhanced carbonate preservation should have dominated the glacial ocean. Considerable doubt arises from the findings of Catubig *et al.* (1998) that suggest no significant change in the burial rate of $CaCO_3$ in the deep sea between the Holocene and the last glacial maximum.

1.2 RESEARCH AREA AND SAMPLES

Bathymetry

The Australian sector of the Southern Ocean between 120°E and 180°E is a unique area for paleoceanographic studies because it comprises a complex system of submarine plateaus and ridges (Fig. 1-1 & 1-6), which rise well above the adjacent abyssal plains and which under favorable conditions are protected against deep-water erosion as well as carbonate dissolution.

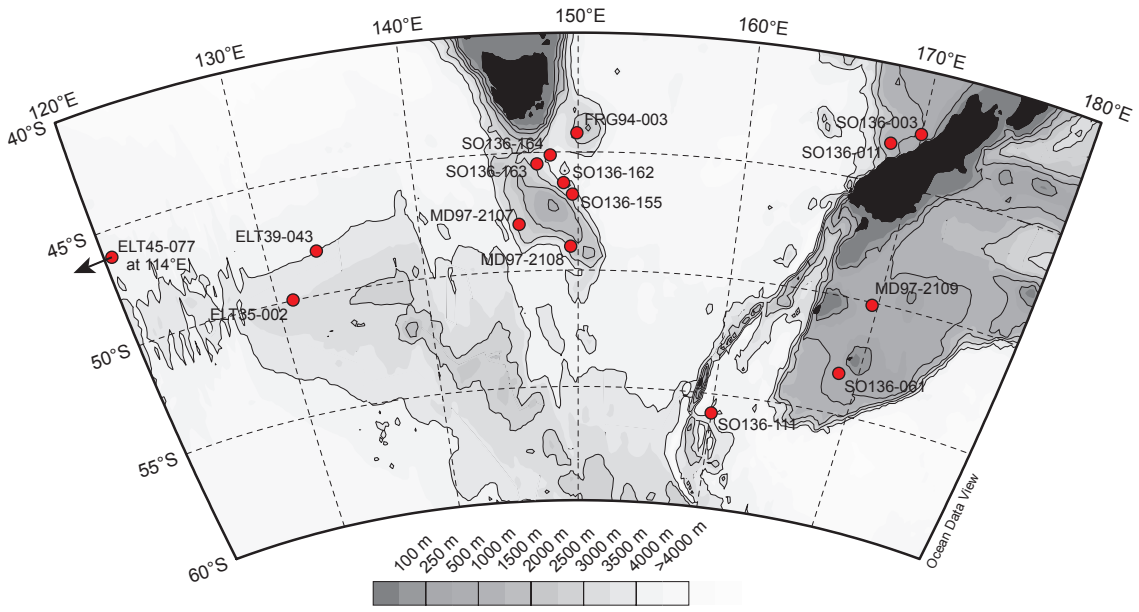

Figure 1-6. Bathymetry of the study area and locations of investigated sediment cores.

The major bathymetric feature in the eastern part of the study area is the Southeast Indian Ridge with zonal orientation at ~50°S that separates the South Australian Basin to the north from the South Indian Basin, elevating to a depth of ~2,000 m below sea level. South of Tasmania at ~145°E, the South Indian Ridge turns abruptly toward the southeast until it emerges with the Macquarie Ridge and the Antarctic continental rise at approximately 160°E. The central part of the study area is dominated by the north-northwest-trending South Tasman Rise, which rises to <1,000 mbsl and is separated from Tasmania by a northwest-trending, ~3,000-m-deep saddle at ~45°S. The abyssal South Tasman Basin east of Tasmania with a maximum depth of ~5,500 mbsl is bounded in the west by the South Challenger Plateau. Southeast of New Zealand, the Emerald Basin is located between the Macquarie Ridge and the Southern Campbell Plateau, which rises to <500 mbsl. An important feature in the study area is the southern position of Tasmania and especially New Zealand with the associated plateaus. The South Tasman Rise, the Macquarie Ridge and the Campbell Plateau form shallower topographical barriers, which represent physical constrictions of the circum-Antarctic circulation. The modern hydrography will be described in Chapter 2.

Sample material

To achieve the objectives of this study, 15 sediment cores were investigated (Table 1-1, Fig. 1-6). Since this study was initiated within the TASQWA-project, the main part of the investigated sediment records were sampled during the TASQWA-cruise (SO136) with the German Research Vessel (RV) *Sonne* in October–November 1998 (Thiede *et al*., 1999). To complement the study in the New Zealand sector and on the South Tasman Rise, three cores from the IMAGES III *Iphis* cruise (MD97) in May 1997 (Nees, 1997) were chosen. RV *Franklin* retrieved the gravity core FR94-003 on East Tasman Plateau in 1994, which extends the latitudinal deep-water transect from the South Tasman Rise farther north. To the east of the South Tasman Rise, three piston cores on the northern edge of the Southeast Indian Ridge at ~114°E and ~132°E, taken by USNS *Eltanin* (Frakes, 1973), were studied. Combined, the selected sediment records form two latitudinal deep-water transects between ~2,100 m and ~4,200 m water depth at ~132°E and ~147°E, located in subantarctic to subtropical waters. The two transects are supplemented by one deep-water core from the Emerald Basin and intermediate-water cores (585–1,560 m) at the Campbell and Challenger Plateau.

Table 1-1. Core locations according to major bathymetric features and core details.

Core	Latitude	Longitude	Water depth (m)	Core recovery (m)
Challenger Plateau				
SO136-003	42°17.74'S	169°52.66'E	958	7.63
SO136-011	43°26.40'S	167°51.04'E	1556	8.77
Campbell Plateau				
SO136-061	53°20.00'S	169°14.69'E	602	2.25
MD97-2109	50°38.00'S	169°23.00'E	585	2.97
Emerald Basin				
SO136-111	56°40.86'S	160°14.49'E	3912	8.61
South Tasman Rise				
SO136-155	47°00.09'S	149°31.30'E	3208	7.56
SO136-162	46°33.20'S	149°05.01'E	3682	8.80
SO136-163	45°56.88'S	147°30.85'E	3236	8.38
SO136-164	45°18.55'S	147°55.24'E	4068	9.78
MD97-2107	47°43.00'S	145°48.00'E	2950	4.15
MD97-2108	48°30.00'S	149°31.30'E	2155	9.11
East Tasman Plateau				
FRG94-003	44°15.00'S	149°59.00'E	2667	4.50
South Australian Basin				
ELT35-002	49°59.20'S	131°36.30'E	3365	5.83
ELT39-043	47°26.30'S	133°00.60'E	3945	4.56
ELT45-077	46°26.90'S	114°20.90'E	3890	3.82

CHAPTER 2

THE SOUTHERN OCEAN – MODERN OCEANOGRAPHIC SETTING

The Southern Ocean stretches from the coast of Antarctica (~70°S) to the Subtropical Front (~40°S). This region represents the most important connection between the three major ocean basins (Fig. 2-1) and thus plays an essential role in thermohaline circulation and global redistribution of heat, nutrients and other properties. In addition, water masses formed in the Southern Ocean ventilate the intermediate and abyssal depths of much of the world ocean. The following chapter describes the modern oceanographic setting of the study area according to the definitions of Gordon & Molinelli (1986) and Rintoul & Bullister (1999). The interpretations of Rintoul & Bullister (1999) are mainly based on results of the repeat section SR3 of the World Ocean Circulation Experiment (WOCE). In general, water masses are conveniently defined by their particular relation between temperature and salinity, and other properties (e.g. dissolved oxygen, silica, phosphate), and transitions observed between such bodies refer to transitional waters that are caused by mixing. Figures 2-2 and 2-3 illustrate vertical signatures of water masses and positions of oceanic fronts on meridional transects from Australia to Antarctica (along 135°E and 157°E, respectively). A summary of the characteristics of the water masses described below is given in Table 2-1.

2.1 THE ANTARCTIC CIRCUMPOLAR CURRENT

The most prominent feature in the Southern Ocean is the deep-reaching Antarctic Circumpolar Current system that is driven by strong, prevailing westerly winds. Today, the Antarctic Circumpolar Current is the current system with the largest water mass transport of ~140 Sv (1 Sverdrup = 10^6 m^3 sec^{-1}) (Rintoul, 2000; Siedler *et al.*, 2001). Thereby, it assimilates and mixes both well-ventilated deep-water masses from the Atlantic and recirculated, older and less oxygenated deep-water masses from the Indian and Pacific oceans. These water masses form the Circumpolar Deep Water. On the other hand, surface-water cooling and the convection process lead to formation of new water masses, which then spread northward such as Antarctic Bottom Water, Antarctic Intermediate Water and Subantarctic Mode Water. At the surface the continuous eastward flow of the Antarctic Circumpolar Current constraints the horizontal

distribution of water mass properties to be relatively uniform in the zonal direction while varying meridional.

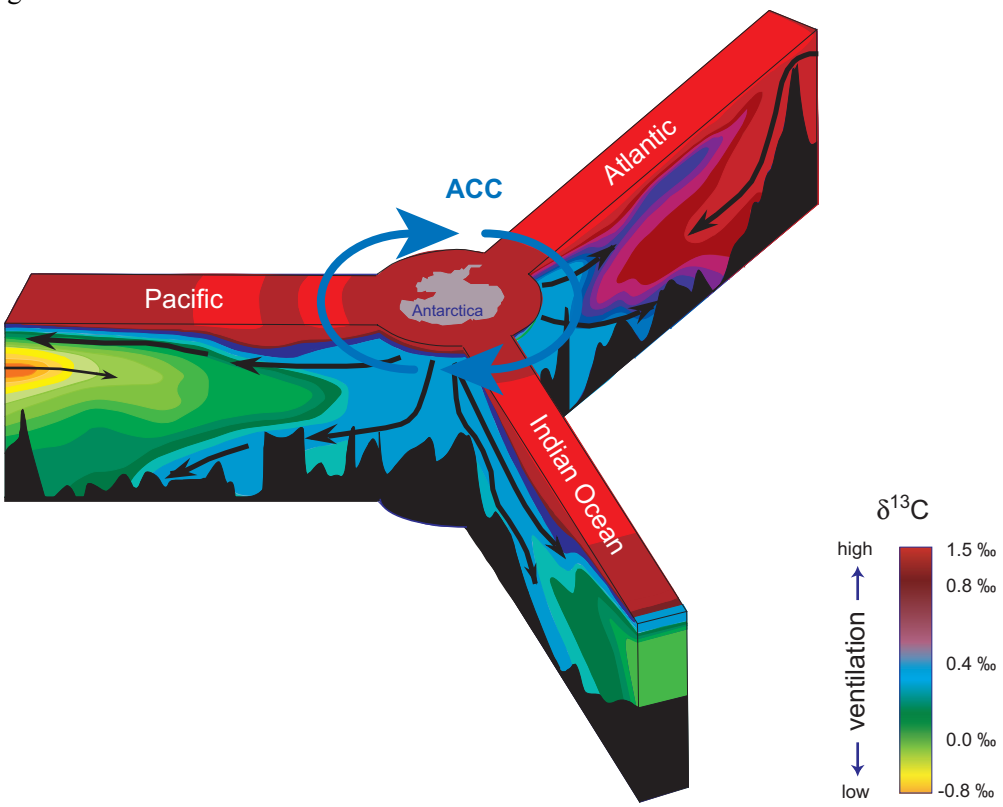

Figure 2-1. General distribution of $\delta^{13}C$ values in the ocean (Charles & Fairbanks, 1990) reflecting deep-water ventilation. High $\delta^{13}C$ values distinguish young, well-oxygenated and low nutrient water masses whereas low $\delta^{13}C$ values characterize older CO_2- and nutrient-rich water masses. The deep-reaching Antarctic Circumpolar Current connects the three major ocean basins.

2.2 SURFACE WATER MASSES AND FRONTAL SYSTEMS

In general, three different surface water masses can be distinguished from north to south separated by frontal systems (Table 2-1, Fig. 2-1 & 2-2). These fronts are the Subtropical Front, the Subantarctic Front and the Antarctic Polarfront. These zones of uniform water properties between the fronts are commonly referred to as the Subantarctic Zone between Subtropical Front and Subantarctic Front, the Polarfront Zone between the Subantarctic Front and the Antarctic Polarfront, and the Antarctic Zone between the Antarctic Polarfront and the Antarctic continent (e.g. Gordon *et al*., 1977; Orsi *et al.*, 1995; Belkin & Gordon, 1996).

The Subtropical Front separates warm, saline and nutrient-poor Subtropical Surface Water to the north from the nutrient-rich Subantarctic Surface Water with lower temperature and salinity. The Subtropical Front also represents the southern boundary of the subtropical gyre and is marked by a pronounced north-south salinity and temperature decrease approximated by the 34.7–34.8 surface isohalines and the ~10°C winter and ~15°C surface summer isotherms. Due to the influence of the convergent wind fields, the Subtropical Front is not stationary and more

often considered as a zone with seasonal shifts. Meanders, convolutions and eddies are integral parts of the structure. Although this front passes Tasmania and New Zealand south of 45°S, its latitudinal position occurs north of 40°S throughout most of the Indian and Pacific oceans.

Table 2-1. Characteristics of major water masses and fronts (shaded in grey) of the study area (derived from Gordon & Molinelli, 1986).

Water mass	Abbrev.	Depth (m)	Density	Salinity	Temp. (°C)	Oxygen	Silica
Subtropical Surface Water	STSW	surface	<26.4	>35.1	>15	<6	
Subtropical Front (convergence)	STF				separates STSW from SASW at15°C summer surface isotherm		
Subantarctic Surface Water	SASW	surface	<26.9	<34.0	8–15	>6.5	
Subantarctic Front (convergence)	SAF				at 8°C summer surface isotherm		
Subantarctic Surface Water	SASW	surface			5–8		
Antarctic Polarfront (divergence)	APF				separates SASW from AASW, with icebergs		
Antarctic Surface Water	AASW	surface	<27.4	33.8	<5°C	>7.0	
Thermocline Water		0–400		34.42–34.90	2.25	2.25	2.25
Subantarctic Mode Water	SAMW	400–600	26.80–27.20	34.0–34.2	6–10	very high	very low
Antarctic Intermediate Water	AAIW	600–1,400	27.20–27.35	34.36–34.50	3.20–7.00	3.20–4.70	
Upper Circumpolar Deep Water	UCPDW	1,400–3,000	36.50–37.00	34.67–34.71	1.60–1.80	3.03–3.45	high
Lower Circumpolar Deep Water	LCPDW	3,000–4,000	37.00–46.00	34.71–34.73	0.50–1.60	3.45–4.80	high
Antarctic Bottom Water	AABW	>4,000	>46.00	34.71–34.73	-0.50–0.00	>5	high

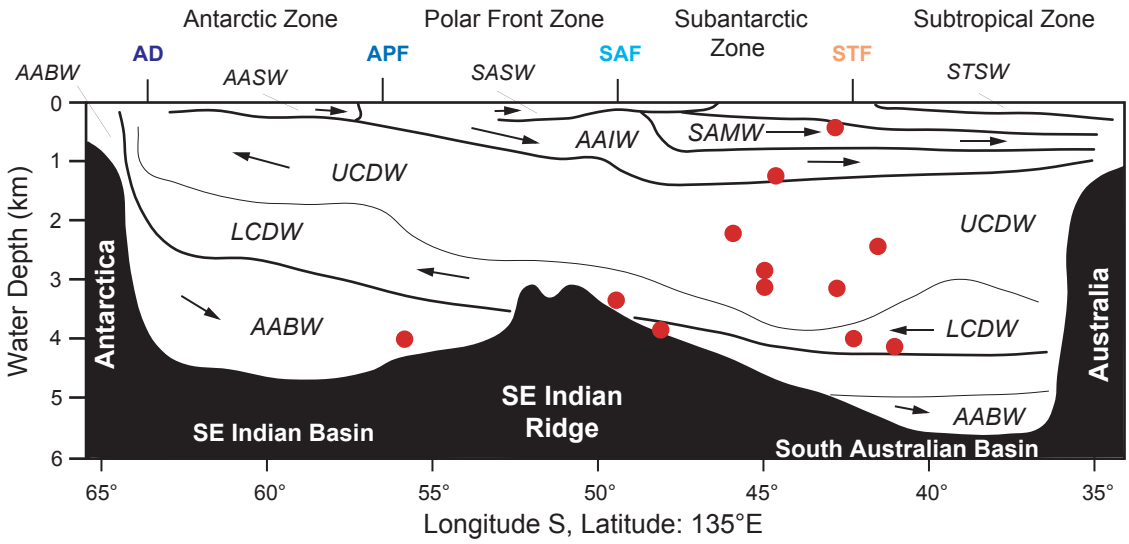

Figure 2-2. North–south transect along 135°E to sketch the modern distribution of water masses and position of oceanic fronts (from Gordon & Molinelli, 1986). Note: the latitudinal position of sediment cores (red points) is slightly modified to display them in relation to their position to the oceanic fronts. Abbreviations are explained in Table 2-1.

The Subantarctic Surface Water driven eastward by the prevailing westerly winds represents the northern part of the Antarctic Circumpolar Current. Subantarctic Surface Water is bounded to the south at ~54°S by the Antarctic Polarfront with fresh, cool Antarctic Surface Water occurring south of it. Within the Subantarctic Surface Water, the Subantarctic Front at ~50°S is characterized by a decrease in surface salinity (<34.5) and temperature (<8°C). The Subantarctic Front accounts for the main part of the eastward transport and is associated to a very deep (>500 m) winter mixed layer to the north, which defines the origin of Subantarctic Mode Water. Further south, Antarctic Surface Water with lowest salinities (33.8) and temperatures (reaching -1.9°C) characterize the area between the Antarctic Polarfront and Antarctica.

The Antarctic Zone is characterized by seasonal formation of sea-ice, mainly controlled by winds, temperature, precipitation and solar radiation, whereas ocean currents primarily affect the lateral extent. Modern interannual variations in Antarctic sea-ice are derived from satellite images (e.g. Gloersen *et al*., 1991; Zwally *et al*., 2002). The minimum in sea-ice extent occurs during February. March and May are the months of maximum sea-ice production. The maximum extension of sea-ice is generally reached in September with the ice edge situated at ~61°S in the study area. The decay of Antarctic sea-ice during October–January is considerably faster than the growth of sea-ice in the autumn–winter period (Zwally *et al*., 2002).

2.2 INTERMEDIATE WATER MASSES

Antarctic Intermediate Water formed by sinking along the Antarctic Polarfront is the most extensive and important water mass at intermediate depths in the world oceans (Emery & Meinke, 1986). The northward spreading Antarctic Intermediate Water (600–1,400 m) expands into the North Atlantic (Caribbean), northern Indian Ocean and equatorial Pacific and can be distinguished from other water masses by its salinity minimum (<34.5). It is further characterized by a temperature range of 3.2–7°C and has a high content of dissolved oxygen (Fig. 2-3). At the Subantarctic Front, deep-reaching convection during austral winter favors the formation of well-oxygenated Subantarctic Mode Water, which is situated above the Antarctic Intermediate Water at ~400–600 m water depth and is almost isothermal (7–10°C). The Subantarctic Mode Water is of special interest because it to ventilates the lower thermocline of the Southern Hemisphere subtropical gyres (e.g. McCartney, 1982). The region south of Tasmania and across the Campbell Plateau is considered as an area of active mode water formation, with partially slightly different properties (see Rintoul & Bullister, 1999).

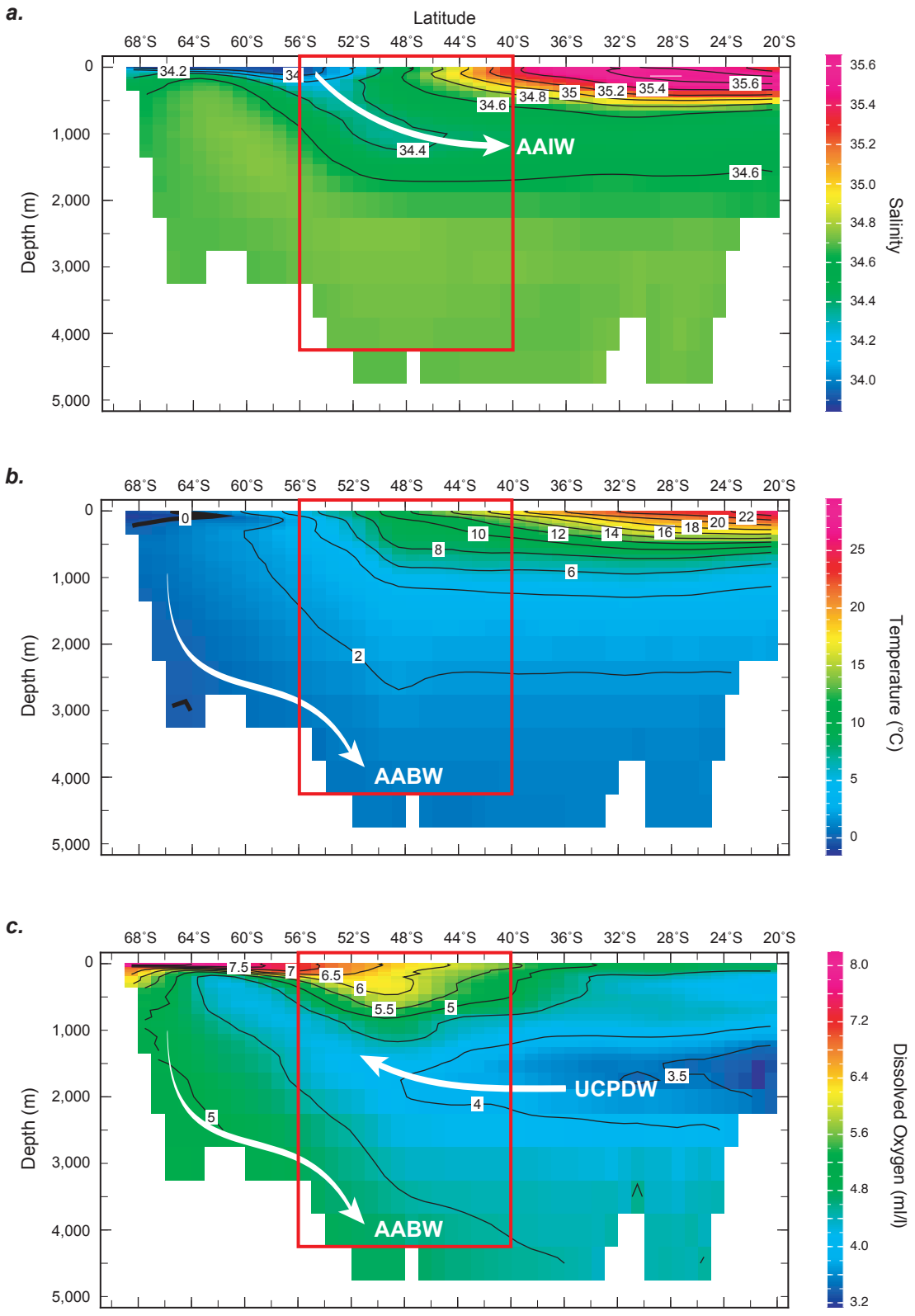

Figure 2-3. Modern distribution of (a) salinity, (b) temperature and (c) dissolved oxygen concentrations at a north–south transect across the western Tasman Sea to the Antarctic continent along 157°E, data are from LEVITUS World Ocean Atlas 1994 (Conkright *et al.*, 1994; Levitus *et al.*, 1994a, b, c; illustrated with http://iridl.ldeo.columbia.edu/). The descending salinity minimum at ~52°S (b) displays the formation of intermediate waters, the oxygen minimum ~2,000 m (c) represents the return flow of older, nutrient-rich Pacific deep-waters in the Upper Circumpolar Deep Water. Antarctic Bottom Water is characterized by the lowest temperatures (b) and high oxygen content (c). The red box indicates the investigated area.

2.3 DEEP WATER MASSES AND POSITION OF THE LYSOCLINE

Below Antarctic Intermediate Water, the Circumpolar Deep Water can be divided into the Upper and Lower Circumpolar Deep Water. The southward return flow of older, nutrient-rich deep-water masses from the Indian Ocean and the Pacific contributes to the Upper Circumpolar Deep Water between ~1,400 and ~3,000 m water depth, which is characterized by an oxygen minimum in the core layer (Fig. 2-3). Younger and well-oxygenated North Atlantic Deep Water, defined by a salinity maximum in the core layer, contributes to the Lower Circumpolar Deep Water, which is located between ~3,000 and ~4,000 m in the study area. This is in contrast to the Atlantic sector where Lower Circumpolar Deep Water dominates the water column between ~1,500 and ~4,000 m. South of the Antarctic Polarfront, Circumpolar Deep Water ascends towards the surface and mixes with Antarctic Surface Water, while releasing heat and becoming more oxygenated and less saline. These water masses contribute to the formation of Antarctic Bottom Water and intermediate water masses.

Antarctic Bottom Water is defined by its low temperature (-0.5–0.4°C) and salinity (~34.7) as well as by its high dissolved oxygen concentrations (5.0–5.6 ml/l). Its origin lies in deep convection at or near continental shelf regions of the Weddell Sea, along the Adelie Coast and the Ross Sea driven by freezing of sea-ice, but its final properties are shaped during intense mixing with the water from the Antarctic Circumpolar Current (Circumpolar Deep Water) while sinking to the bottom (Tomczak & Godfrey, 2003). Northward extensions of low bottom potential temperatures indicate the movement into the deep North Atlantic (up to ~45°N), the Indian and Pacific oceans below ~4,000 m as well as into the Tasman Basin and the South Australian Basin in the study area (Fig. 2-4).

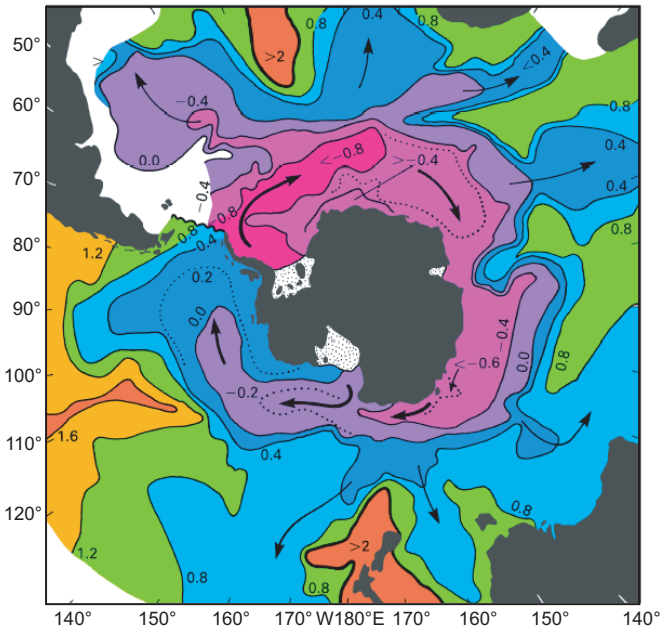

Figure 2-4. Bottom potential temperature in the Southern Ocean. The arrows show inferred movement of Antarctic Bottom Water. From Tomczak & Godfrey (2003).

Concerning today's position of the carbonate lysocline it must be noted, that the modern basin asymmetry between the carbonate-rich Atlantic with a deep lysocline (~4,900 m at 45°N; ~4,200 m at 3°N) and the Pacific with a much shallower lysocline (~3,700–4,000 m at 15°N–15°S; ~500 m at 53°N) is closely related to formation rate of North Atlantic Deep Water. While flowing from their origin in the North Atlantic via the Southern Ocean into the North Pacific, these initially oxygen-rich water masses accumulate nutrients and get progressively enriched in CO_2 by the decay of organic matter (ageing effect). As a result the $[CO_3^{2-}]$-concentration lowers and alkalinity increases making the water masses more carbonate-aggressive. South of ~45°S, the modern carbonate lysocline lies at ~3,400 m water depth (GEOSECS data, Takahashi *et al.*, 1981) and is therefore shallower than in the South Atlantic and equatorial Pacific. This is possibly related to the inflow of older, recirculated, and more CO_2-rich deep-water masses from the Pacific and Indian oceans into the Circumpolar Deep Water and Antarctic Bottom Water (Fig. 2-2 & 2-3). On the other hand, variations in surface productivity can account for regional changes in the lysocline level by changing the overall productivity or the $C_{org}/CaCO_3$ rain ratio (see Chapter 3). Martínez (1994) reconstructed the modern lysocline level in the western Tasman Basin using fragmentation ratios of planktonic foraminifers and suggested that the lysocline depth at ~3,600 m is marked by a fragmentation ratio of 40 %, which is confirmed by results from this study (Fig. 2-5).

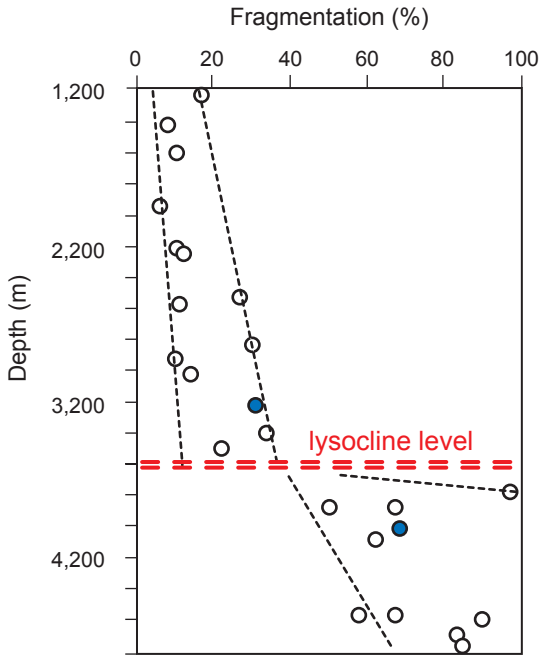

Figure 2-5. Reconstruction of the modern lysocline level in the western Tasman Basin based on fragmentation ratios of planktonic foraminifers counted on 22 core top samples (Martínez, 1994). Blue circles indicate core top values from SO136-163 and SO136-164 (this study). Fragmentation percentages above the lysocline at ~3,600 m water depth vary between 5–30 %. Below the lysocline level fragmentation values are widely scattered between 50–100 % due to enhanced carbonate dissolution that causes foraminiferal shell break down.

CHAPTER 3

PROXIES AND METHODS

To achieve the objectives of this study, ~2,500 samples of 15 sediment cores have been processed with a sampling resolution varying between 4–10 cm corresponding to a time resolution better than 4,000 years. Figure 3-1 summarizes the individual steps of the sample processing. The original samples (10–15 cm^3) were split into a sub-sample (~1 cm^3) and a main sample. The main samples were freeze-dried and washed through a 63-µm sieve. The coarse material was fractionated (63–125 µm, 125–250 µm, 250–315 µm and >315 µm) and foraminiferal specimens were collected for stable isotope analyses and radiocarbon (^{14}C) datings, and the fragmentation index of planktonic foraminifers was determined. The oven-dried (50°C) and homogenized sub-samples were analyzed for total and organic carbon to calculate the carbonate contents. The following paragraphs describe the applied methods and give a more detailed introduction into the different proxies.

3.1 OXYGEN AND CARBON ISOTOPE RATIOS, RADIOCARBON DATING

Stable isotopes analyses

The determination of oxygen and carbon isotopes on planktonic and epibenthic foraminifers were routinely carried out at GEOMAR, using a FINNIGAN 252 Mass Spectrometer with Kiel CARBO II device. About 1–4 specimens of epifaunal benthic foraminifers (*Cibicidoides wuellerstorfi:* >250 µm) and 5–20 specimens of planktonic foraminifers (*Globigerinoides bulloides:* 250–315 µm, *Globorotalia truncatulinoides:* >315 µm, *Neogloboquadrina pachyderma* sin.*:* 125–250 µm) were picked for the measurements. The ratios of $^{18}O/^{16}O$ and $^{13}C/^{12}C$ are reported as relative deviations (δ notation) from a laboratory standard, here with reference to the PeeDeeBelemnite (PDB) standard (Craig, 1957). The calibration to the PDB standard is calculated via the **N**ational **B**ureau of **S**tandards NBS 19 and an internal laboratory standard of Solnhofen Limestone (Tiedemann, pers. comm). Analytical reproducibility is ±0.06 ‰ for $\delta^{18}O$ and ±0.03 ‰ for $\delta^{13}C$.

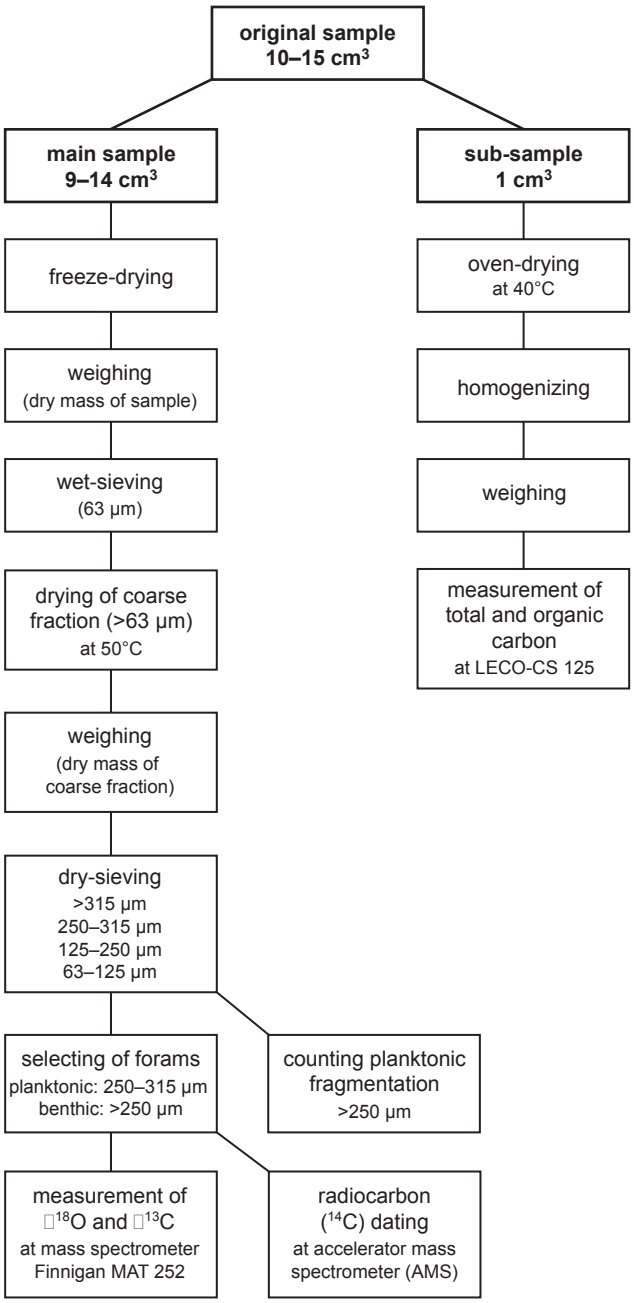

Figure 3-1. Summary of individual steps of sample preparation.

Radiocarbon dating

Accelerator mass spectrometer (AMS) ^{14}C radiocarbon dates were measured on specimens of *G. bulloides* and *N. pachyderma* (s) at the Leibniz Laboratory of Kiel University to define the sediment surface age of selected cores (see Table 4-1). AMS ^{14}C ages have been converted into calendar ages using the software CALIB 4.1.2 (Stuiver & Reimer, 1993).

Stratigraphic development

Benthic oxygen isotope records provide the primary stratigraphic control for the sediment records covering the time interval of the last 500,000 years. Isotope records of planktonic foraminifers were considered if the stratigraphic assignment of epibenthic $\delta^{18}O$ records was

uncertain. The oxygen isotope records were calibrated to the oxygen isotope time scale of Bassinot *et al*. (1994) developed for the late Pleistocene. A more detailed stratigraphy of the last 40,000 years is provided by radiocarbon (^{14}C) datings.

Reconstruction of changes in deep- and intermediate-water ventilation and circulation using benthic $\delta^{18}O$ and $\delta^{13}C$ values

Benthic foraminiferal $\delta^{18}O$ data provide a record of change in ice volume (global effect) and deep-water temperature and/or salinity (local effects). Differences in vertical and spatial $\delta^{18}O$ gradients reflect local differences in the water mass signatures. As the benthic $\Delta\delta^{18}O$ record (the difference between $\delta^{18}O$ records) eliminates the global isotopic signal (ice volume), the isotopic differences reflect local changes in the temperature and/or salinity histories at different core positions. For depth transects one can assume that seawater density (a function of temperature and salinity) of a shallower water mass is not higher than that of an underlying water mass, because density constraints to maintain seawater stability must be satisfied. This provides the opportunity to approximate temperature-salinity signals from overlaying water masses from benthic $\delta^{18}O$ values, using temperature, salinity, density relationships as illustrated in sigma-*t* diagrams with $\delta^{18}O$ isopleths of equilibrium calcite (e.g. Billups *et al*., 1998).

More useful for reconstructing changes in deep-water circulation are $\delta^{13}C$ values from the epifaunal benthic foraminifer *Cibicidoides wuellerstorfi*. Several studies have demonstrated that the $\delta^{13}C$ values of *C. wuellerstorfi* are approximately equal to bottom water $\delta^{13}C$ (dissolved inorganic carbon), and thus, are a good tool for reconstructions of deep-water ventilation (e.g. Belanger *et al*., 1981; Zahn *et al*., 1986; McCorkle & Keigwin, 1994). High $\delta^{13}C$ values indicate low nutrient- and CO_2-concentrations and well ventilated (O_2-rich) water masses (Kroopnick, 1985). This signature is typical for young intermediate- and deep-water masses that are close to their source regions. With increasing distance to their source region the $\delta^{13}C$ values continually decrease due to the persistent oxidation of ^{12}C-rich organic matter during the journey of the water mass away from its source (ageing effect). Low-$\delta^{13}C$ organic matter, formed in surface water, is oxidized and remineralized in the deeper ocean, which lowers the $\delta^{13}C$ values. Thus, deep- and intermediate-water masses from different sources are characterized by their $\delta^{13}C$-signature, which is a good proxy for reconstructing changes in deep-water circulation (e.g. Sarnthein *et al*., 1994).

Moreover, the $\delta^{13}C$ signal is also controlled by global changes in the carbon budget. Short-term global changes much shorter than the 200–300 kyr residence time of carbon in the oceans are thought to result from variations in ocean productivity and from changes in the mass of organic matter stored in forests, soils, and shallow-marine sediments, presumably related to

glacial-interglacial climate change (Shackleton, 1977). Long-term changes in oceanic $\delta^{13}C$ could reflect either the $\delta^{13}C$ of the mean river flux, the $\delta^{13}C$ of buried carbonate and organic carbon, or the fraction of carbon buried as organic matter in combination with changes in the $\delta^{13}C$ of biomass from C_3 to C_4 dominated ecosystems (Mix *et al*., 1995; Cerling *et al*., 1997). The benthic $\delta^{13}C$ record of east equatorial Pacific ODP Site 849 is thought to reflect the Pleistocene shifts in the whole ocean carbon budget (Mix *et al*., 1995) and can be used for comparisons. However, because global changes will affect all $\delta^{13}C$ records similarly, the difference between $\delta^{13}C$ records ($\Delta\delta^{13}C$) eliminates the global effect and indicates local changes in deep-water ventilation and nutrient concentrations.

3.2 CARBONATE, COARSE FRACTION, PLANKTONIC FRAGMENTATION

Determination of carbonate and organic carbon content, and planktonic fragmentation ratio

Weight percent carbonate and organic carbon were determined using a LECO CS-200 analyser at GEOMAR. Total carbon was derived from bulk sediments, whereas total organic carbon content is measured on de-calcified sediment samples. The carbonate content was then calculated from the difference between total and organic carbon.

For the determination of the fragmentation index, approximately 400 planktonic foraminifers of the fraction >250 µm were obtained with a micro splitter and examined under a microscope. The fragmentation index in percent was calculated by dividing the number of shell-fragments by the sum of whole planktonic foraminifers and fragments. Higher fragmentation ratios indicate stronger carbonate dissolution (e.g. Martínez, 1994a).

Reconstruction of variations in carbonate preservation

Understanding temporal and spatial changes in carbonate preservation is of key importance for testing numerous models that seek to explain past changes in atmospheric CO_2-concentrations through changes in the oceanic carbon cycle, as outlined in Chapter 1. In this context, records of carbonate dissolution in ocean sediments can provide constraints to these geochemical models. Thunell (1976) showed that dissolution can be estimated in a variety of ways using (1) the ratio of fragmented to whole foraminiferal tests, (2) the ratio of benthic to planktonic foraminifers and (3) the calcium carbonate content of the sediment sample.

The *calcium carbonate contents* in sediment records are difficult to interpret in terms of carbonate dissolution, because the deposition of carbonates is also influenced by changes in surface productivity and by dilution of other sediment components. In addition to the carbonate concentrations, the *sand content* (>63 µm) *of the total carbonate fraction* was determined to avoid these problems. It has been shown that the sand content of deep-sea carbonates decreases

as dissolution progresses (e.g. Wu *et al*., 1990; Bickert *et al*., 1997, Broecker & Clark, 1999). In pelagic sediment records the sand fraction usually consists of nearly 100 % of foraminiferal shells. These shells are weakened by dissolution and tend to break down in small fragments. As a result, material moves from the coarse fraction into finer fractions (Berger *et al*., 1982; Yasuda *et al*., 1993). However, changes in the ratio between nannofossil placoliths and foraminiferal shells could bias the relative portion of the coarse fraction without any changes in carbonate dissolution (Bickert & Wefer, 1996) and therefore, another dissolution proxy in addition to carbonate contents and sand fraction is required for interpretations.

Within the coarse fraction mainly planktonic foraminifers are affected by dissolution-controlled shell breakdown, compared to the more dissolution-resistant benthic foraminifers. Therefore, the *planktonic foraminiferal fragmentation percentage* was choosen as another sensitive indicator of carbonate dissolution. Berger (1970) and more recent studies (e.g. Keigwin, 1976; Le & Shackleton, 1992; Martínez, 1994a, 1994b) have suggested the fragmentation of planktonic foraminifers to be a more reliable indicator of dissolution opposed to other dissolution proxies. This indicator has been found to be independent of climatic effects, or other ecological influences that bias e.g. the foraminiferal dissolution index (solution-susceptible versus solution-resistant planktonic foraminifer species) as well as the benthic foraminiferal content. Both indicators are highly dependent on the composition of the original assemblage (Berger, 1978). However, fragmentation percentages can be altered by winnowing and reworking. Together, variations in fragmentation of planktonic foraminifers and changes in the carbonate sand fraction of deep-water cores served as a proxy to monitor vertical fluctuations of the carbonate lysocline.

It must be pointed out that deep-water mass properties are not the only controlling factor of carbonate dissolution. Various studies (Emerson & Bender, 1981; Jahnke *et al*., 1994; Bickert *et al*., 1997) have shown that even in supralysoclinal waters, which are supersaturated with respect to calcite, sediments undergo significant carbonate dissolution. The dissolution results from the decay of organic matter, which reduces the carbonate ion concentration in the pore water and enhances alkalinity. This process can affect the shallower cores, which are positioned above the lysocline.

In general, variations in the depth of the lysocline (and thus carbonate dissolution or preservation at the sea-floor) are controlled by changes in ocean's alkalinity (summary in Sigman & Boyle, 2000). Changes in the lysocline depth mainly result from imbalances between $CaCO_3$ input into the ocean and the $CaCO_3$ burial at the sea-floor (Fig. 3-2). If the input exceeds the burial (for example due to an increase in weathering of carbonate-bearing rocks on land or a decrease in coral reef growth in the shallow ocean), then the alkalinity (ALK) and dissolved

inorganic carbon (DIC) increases in a ratio of 2:1. This leads to both, a decrease in surface water CO_2-concentrations (extracting CO_2 from the atmosphere into the ocean) and a deepening of the lysocline. The opposite scenario occurs if the $CaCO_3$ input exceeds the $CaCO_3$ burial. The biological pump also affects the dissolved inorganic carbon and alkalinity of the ocean. The formation of organic tissues consumes carbon and lowers the dissolved inorganic carbon of the water (has no effect on alkalinity). The modest alkalinity increase associated with organic carbon export only (typical for high nutrient polar surface ocean ecosystems) is due to the associated uptake of nitrate by phytoplankton. When carbonate shells are formed, calcium ions are removed from the water, which reduces alkalinity by twice the amount that it changes the carbon content. On average, export production in warm low-latitude oceans removes carbon from surface waters at a molar ratio of 4:1 (C_{org} : $CaCO_3$), which lowers alkalinity and dissolved inorganic carbon. Both processes lead to a drop in surface pCO_2, but also affect the dissolved inorganic carbon and the alkalinity of the deep ocean. Organic carbon produced in the surface ocean and oxidized by bacteria in the ocean interior releases dissolved inorganic carbon and lowers the carbonate ion concentration of deep-water, which in turn affects the burial rate of $CaCO_3$ in the sea-floor sediments (Sigman & Boyle, 2000).

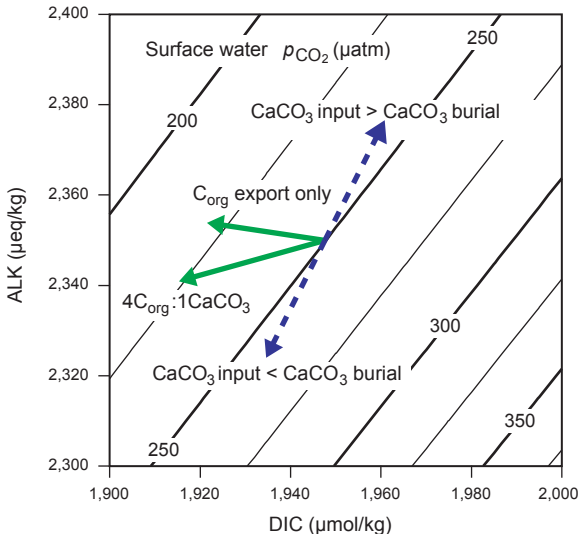

Figure 3-2. The pCO_2 of surface water at 20°C and a salinity of 35, as set by dissolved inorganic carbon (DIC) content and alkalinity (ALK) (Sigman & Boyle, 2000).

CHAPTER 4

STRATIGRAPHY AND SEDIMENTATION RATES

An accurate time calibration of the sediment sequences is essential because it provides the basis for all interpretations about ocean and climate history especially for quantitative estimates. The age control points and their degree of reliance determine the sedimentation rates, which are necessary for estimating and comparing paleo-fluxes of different sediment components and between sites.

The age models of the sediment records are mainly based on oxygen isotope stratigraphy (Fig. 4-1). In addition, 8 AMS ^{14}C dates (*G. bulloides* or *N. pachyderma* sin.) were determined at the Leibniz Laboratory in Kiel to refine the age control within the time interval of the last ~10,000 years (Table 4-1). Dr. Tim Barrows (National University of Australia, Canberra) kindly provided unpublished AMS ^{14}C dates from sediment surfaces from cores SO136-003 and SO136-011 that were used for the age model, too.

The establishment of the oxygen isotope stratigraphy is primarily based on benthic isotope records (Fig. 4-1). Planktonic isotope records were used if benthic foraminifers were not available in a sufficient number of specimens to generate an isotope record of high quality. In the Southern Ocean, benthic foraminiferal $\delta^{18}O$ records are more reliable for stratigraphic purposes because regional variability in deep-water temperature is lower than in near-surface waters as registered by planktonic foraminiferal $\delta^{18}O$ records.

The chronology of the isotope curves was generally obtained from graphic correlation of oxygen isotope events with the Bassinot *et al*. standard $\delta^{18}O$ stack (Bassinot *et al.*, 1994), which is an improvement of the SPECMAP standard time scale (Imbrie *et al.*, 1984). This target record was obtained by tuning cyclic variations in oxygen isotope records to the astronomical solution - a method that has been applied and constantly refined during the past decades. This method is based on the fact that cyclic changes in $\delta^{18}O$ climate records are linked to variations in insolation caused by cyclic variations in earth orbital parameters (eccentricity, obliquity and precession). The application of this tuning procedure makes a high-precision time-calibration possible, because the "astronomical" clock is very accurate (Berger & Loutre, 1991; Laskar *et al.*, 1993) and cyclic changes in orbital parameters give very small-scale time markers on geological time scales. The assumption of a time lag between the change in earth orbital parameters and their $\delta^{18}O$ climate

response of about 8 kyr (Imbrie & Imbrie, 1980; not accurately determined) may result in a constant error of less than 2 kyr (Bassinot *et al.*, 1994).

The marine oxygen isotope stages (MIS 1–13) and sub-stages of the last 500 ka were identified by visual graphic correlation using the isotope nomenclature defined by Martinson *et al.* (1987) and Bassinot *et al.* (1994). According to the stratigraphic classification, four sediment cores allow a comparison of different proxy records over the last ~500 kyr. The stratigraphic adjustment between the dated isotope records from the study area and the Bassinot *et al.* (1994) standard $\delta^{18}O$ stack was verified by obtaining the highest correlation coefficient and with aid of spectral analyses. An example for the spectral comparison is shown in Figure 4-2 for core SO136-163 indicating the excellent match of the dominant cyclicities (23, 41, 100 kyr) between the target record and sediment record from the South Tasman Rise. To keep the isotope records in phase with the target record, as few as possible age control points were used. Based on these age control points linear sedimentation rates (LSR) have been estimated for each core (Fig. 4-1). To avoid abrupt changes in sedimentation rates between age control points, the sedimentation rate was interpolated for samples that lie between age control points.

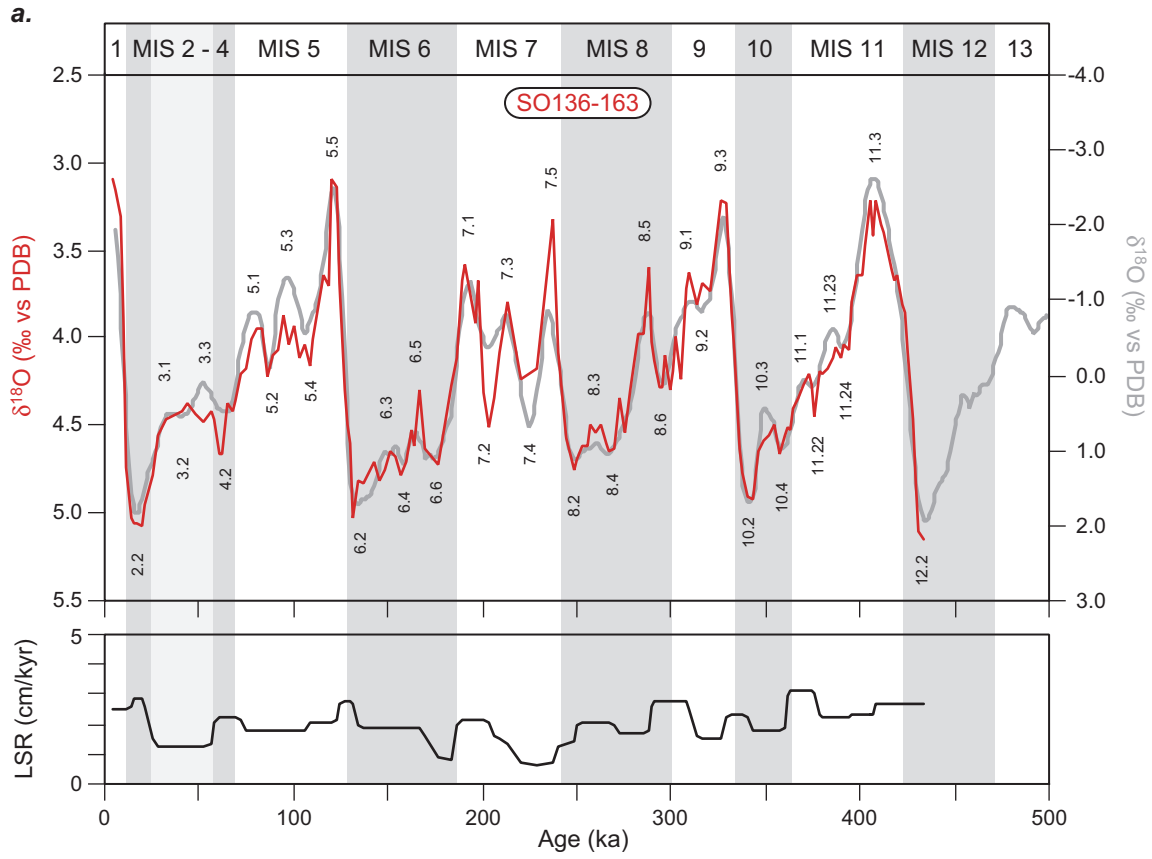

Figure 4-1a–o (continued on the following pages). Stratigraphy (upper panel) and linear sedimentation rates (LSR, lower panel) of sediment cores versus age. Epibenthic (red) and planktonic (blue) isotope records are shown in comparison to the Bassinot *et al.* (1994) standard $\delta^{18}O$ stack (grey line). Oxygen isotope stages and sub-stages are indicated, grey shaded intervals mark glacials.

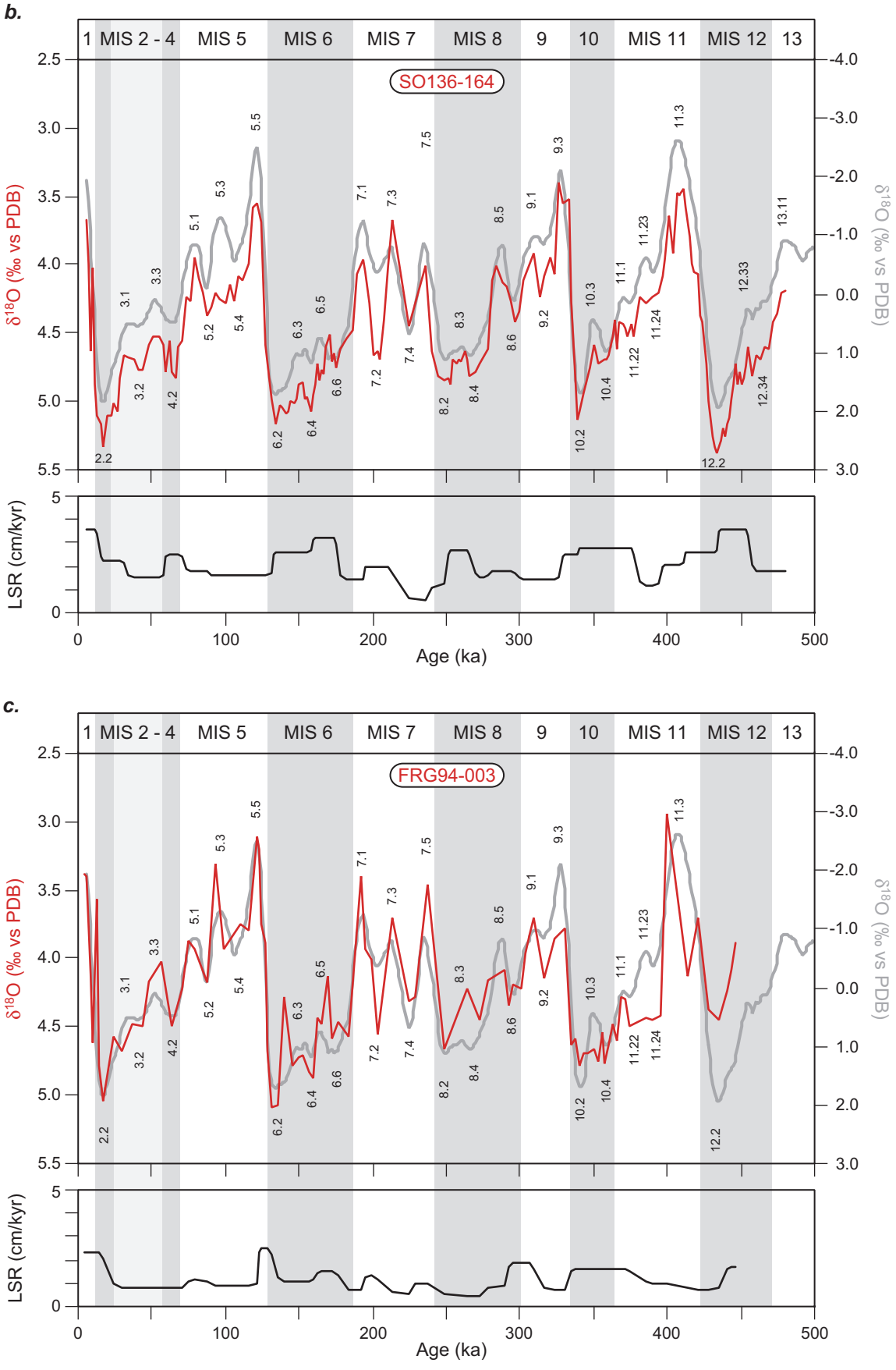

Figure 4-1a–o. Continued.

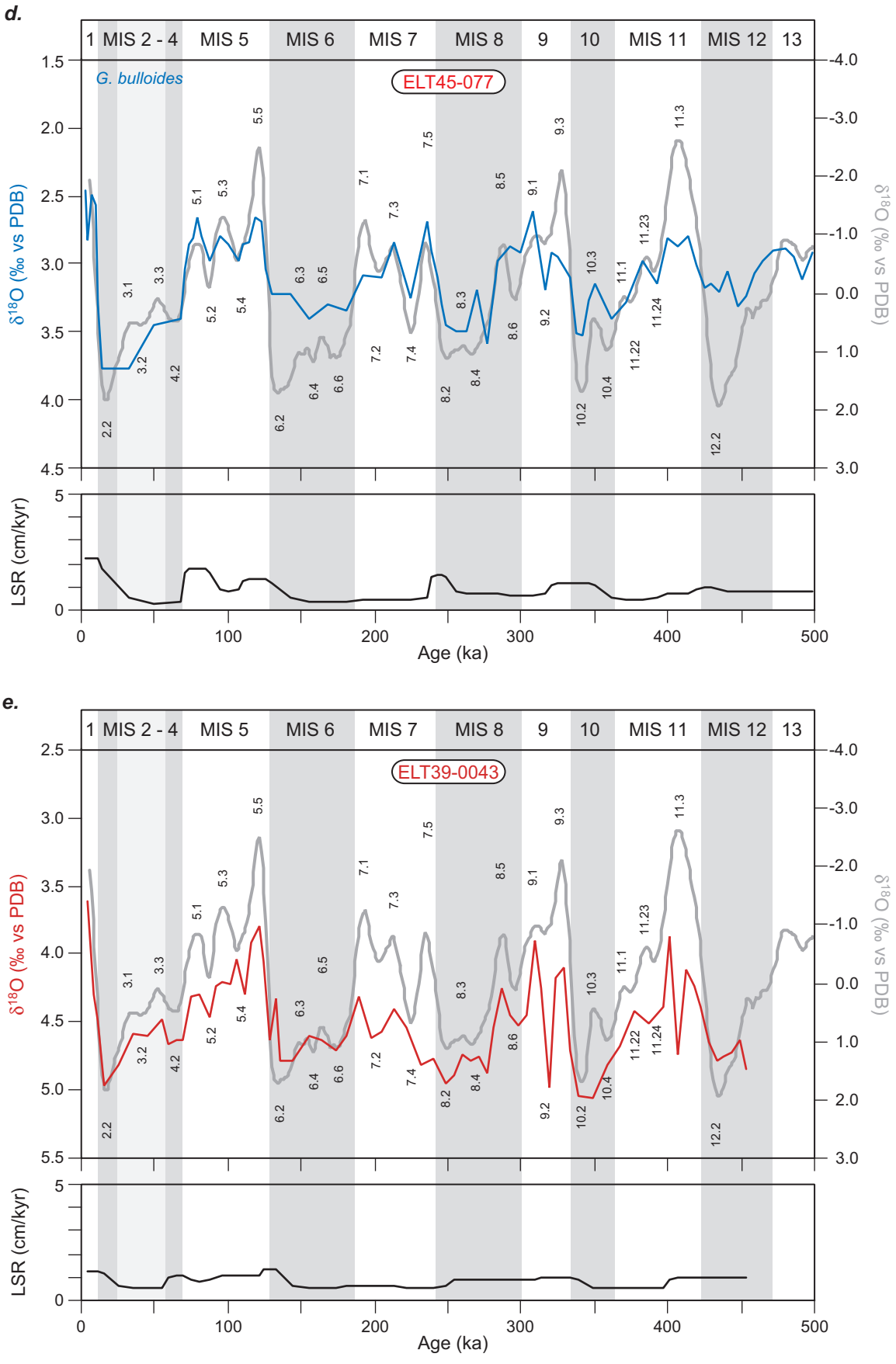

Figure 4-1a–o. Continued.

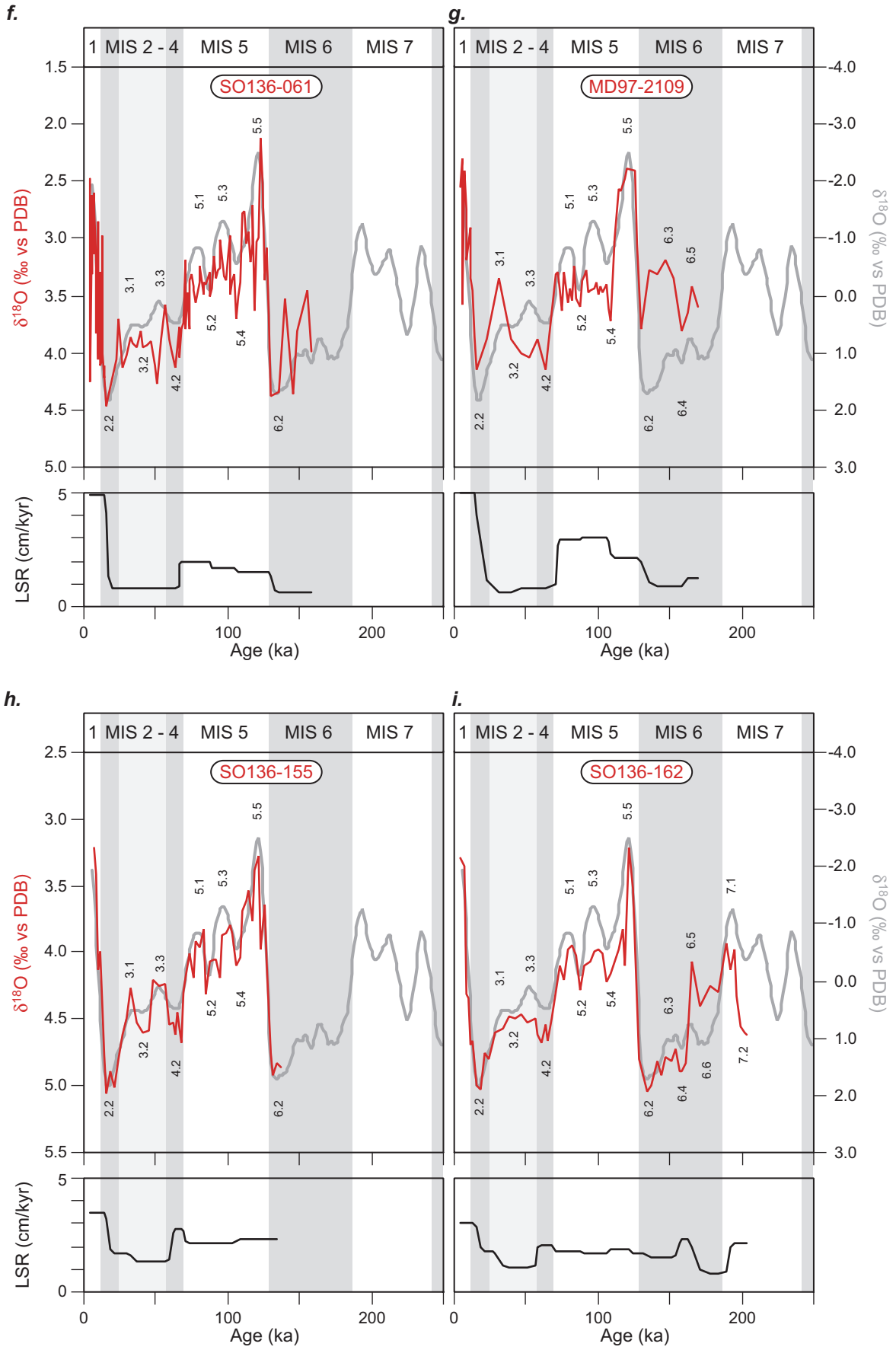

Figure 4-1a–o. Continued.

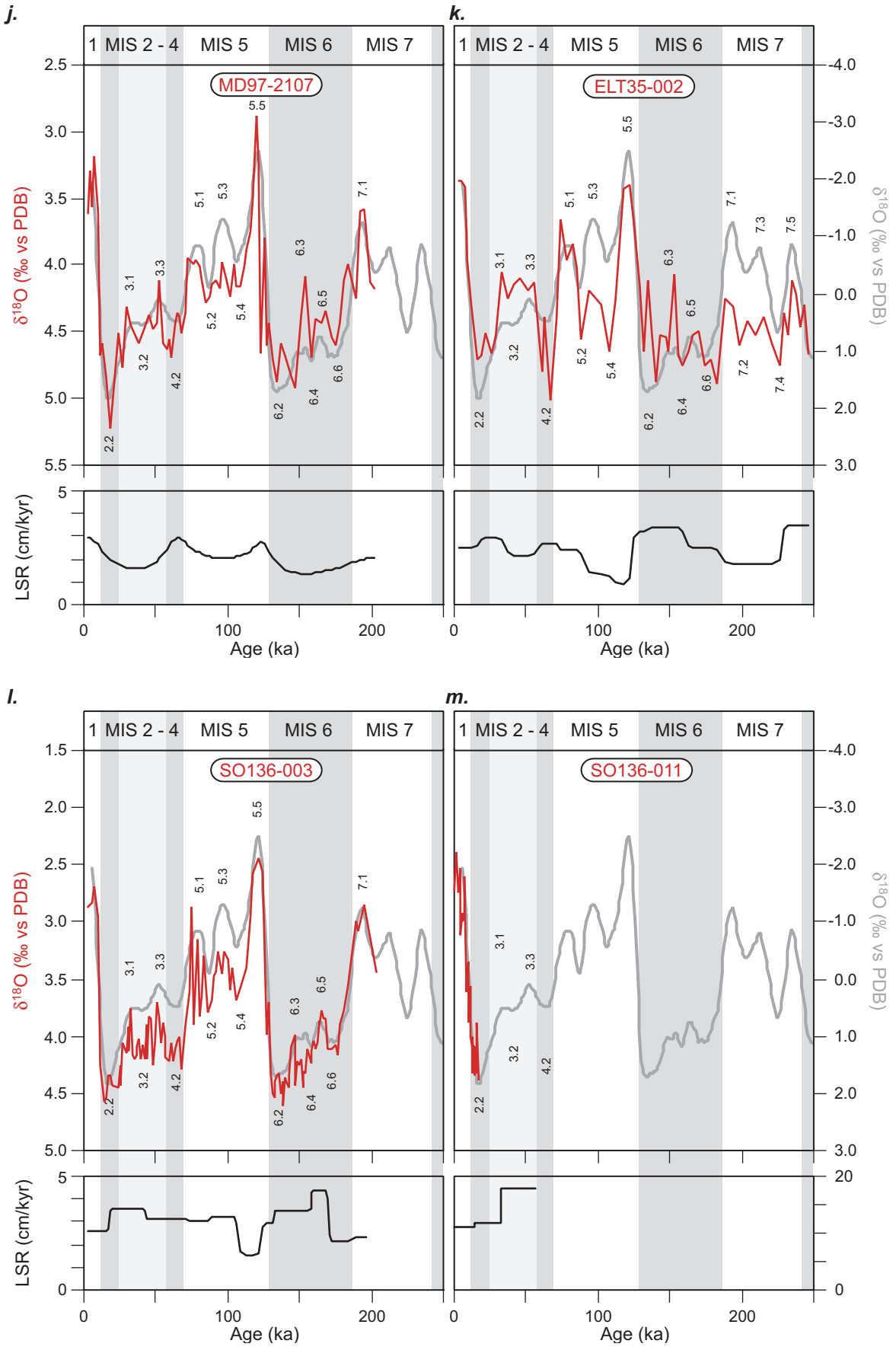

Figure 4-1a–o. Continued.

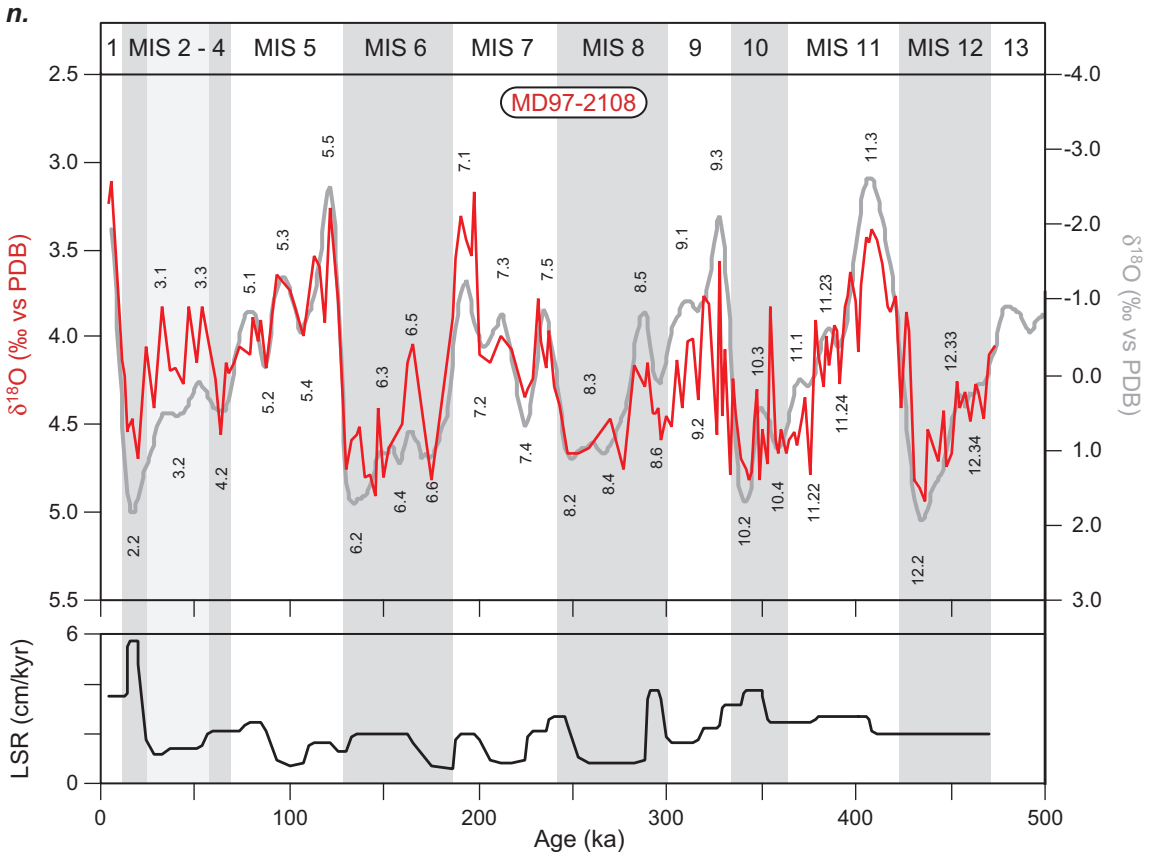

Figure 13a–o. Continued.

In the study area, pelagic sedimentation rates are generally low and vary from ~1–3 cm/kyr. Higher sedimentation rates of up to ~5–10 cm/kyr characterize the hemipelagic sediment records off the coast of New Zealand (SO136-003, SO136-011) as a result of increased terrigenous sediment supply. In general, minima in sedimentation rates are associated with glacial stages, whereas higher sedimentation rates occurred during carbonate enriched warm stages. Processes of erosion or non-deposition of sediments may have affected time intervals that are marked by extremely low sedimentation rates. This is indicated by AMS ^{14}C dates of surface sediments ranging between 3,300 and 7,500 years. The absence of upper Holocene sediment sequences may have occurred in response to strong bottom currents reducing or preventing sediment deposition. In this context it should be mentioned that some records are marked by very low sedimentation rates over longer time intervals, sometimes dropping below 1 cm/kyr (e.g. FRG94-003, SO136-111, SO136-061, MD97-2109). Here, the possibility of stratigraphic gaps due to erosion or non-deposition cannot be excluded. For example, core SO136-111 at the Antarctic Polarfront may include a hiatus within MIS 8 (sedimentation rates of ~0.5 cm/kyr). This interval is barren of foraminifers and lacks isotope stratigraphy. However, the structure of the magnetic susceptibility record reflects the structure of the planktonic isotope record over the last 240 kyr and thus, was used for the stratigraphic alignment between MIS 7.5 and 9.3. Core FRG94-003 on the East

Tasman Plateau with generally low sedimentation rates also reveals very low sedimentation rates during MIS 8. The northern flank of the South Tasman Rise is marked by extremely low sedimentation rates during MIS 7 as indicated in cores SO136-163 and SO136-164 and may also represent an interval of non-deposition.

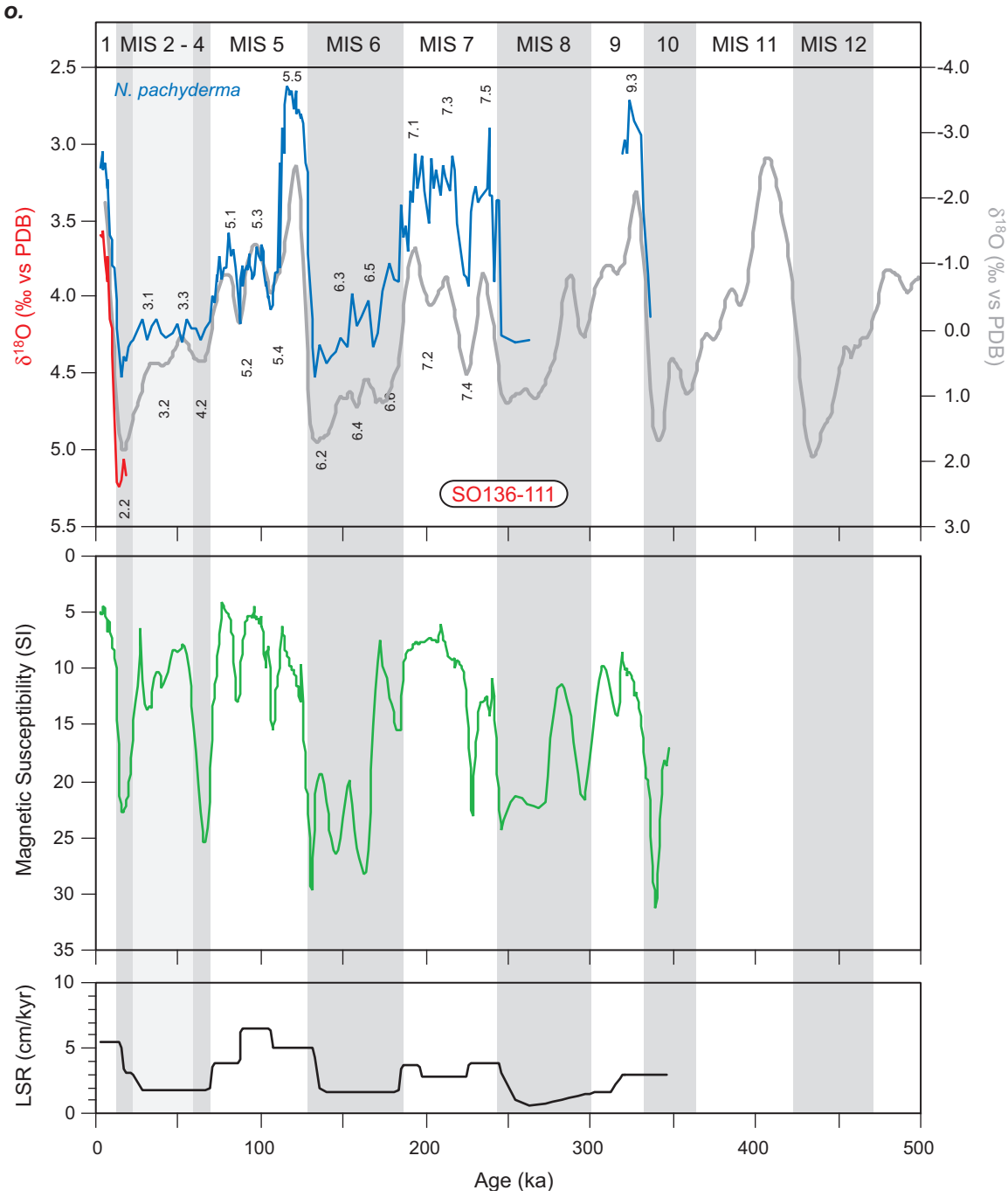

Figure 13a-o. Continued.

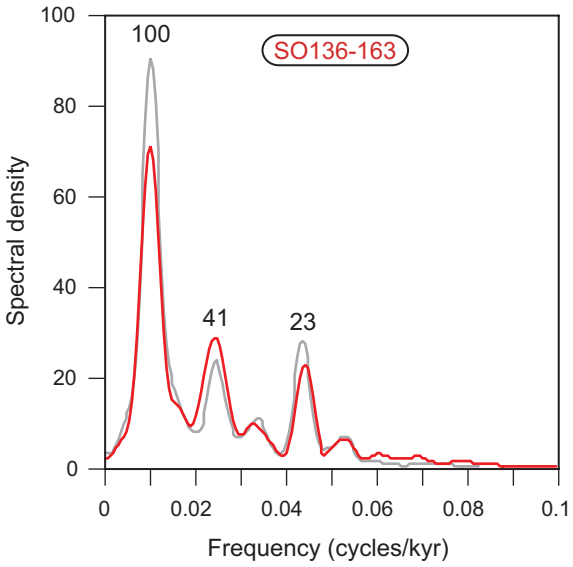

Figure 14. Spectral comparison of cyclic variations in oxygen isotope records between core SO136-163 (red) and the Bassinot *et al.* (1994) standard $\delta^{18}O$ stack (grey; Bassinot *et al.*, 1994). Such spectra have been used to prove the match between the target record and the isotope records.

The temporal resolution of the sediment records depends on the sedimentation rates and the sampling distance of ~4–5 cm. On average, the time resolution of the proxy records equals ~2,000 years. In regions of high sediment deposition (cores SO136-003 and SO136-011 from Challenger Plateau), the sampling resolution is better than 1,000 years, providing detailed insights into millennial scale links between ocean chemistry and climate variability.

Table 3. Summary of AMS ^{14}C dates and corrections (documented in years).

Core	Depth (cm)	Material	^{14}C age (planktonic)	±	Reservoir corrected ^{14}C age	Calendar age	Age range Area of highest probability
SO136-003	5-6 cm	*G. bulloides*	3,860	35	3,060	3,339	3,301–3,377
SO136-011	20-22 cm	*G. inflata*	2,840	40	2,040	2,071	2,020–2,121
SO136-111	1-2 cm	*N. pachyderma*	3,715	50	2,915	3,158	3,085–3,231
SO136-162	1-2 cm	*G. bulloides*	4,825	35	4,025	4,570	4,517–4,623
SO136-163	1-2 cm	*G. bulloides*	4,175	35	3,375	3,699	3,646–3,751
SO136-164	1-2 cm	*G. bulloides*	6,140	35	5,340	6,151	6,105–6,197
MD97-2108	1-2 cm	*G. bulloides*	7,410	40	6,610	7,505	7,466–7,544
MD97-2109	1-2 cm	*G. bulloides*	4,565	35	3,765	4,229	4,171–4,286

CHAPTER 5

CARBONATE CHEMISTRY AND DEEP-WATER CIRCULATION DURING THE LAST 500 KYR

The following chapter presents results from different proxy records to discuss changes in carbonate chemistry and deep-water circulation in the Australian sector of the Southern Ocean with respect to global climatic change and the globally linked oceanic circulation. The results concerning changes in carbonate dissolution are summarized for two latitudinal transects, the South Tasman Rise transect and the South Australian Basin transect, because productivity and carbonate flux as well as carbonate dissolution are different between those regions. Moreover, variations in carbonate dissolution at the South Tasman Rise transect are characterized by the "Pacific-type" pattern of carbonate preservation (enhanced dissolution during interglacials, increased preservation during glacials). This is in contrast to the reversed "Atlantic-type" pattern that has been documented for the Indian Ocean sector of the Southern Ocean, west of 100°E (Howard & Prell, 1994). The South Australian Basin transect is situated in between these areas and will indicate the westward expansion of the "Pacific-type" pattern that is observed at the South Tasman Rise.

In detail, records of carbonate concentrations and accumulation rates (AR), coarse carbonate fraction (>63 µm) and fragmentation ratios of planktonic foraminifers as well as epifaunal benthic foraminiferal $\delta^{13}C$ are presented. These records provide insights into regional and water depth related variations in carbonate dissolution that are associated with changes in deep-water alkalinity and ventilation.

5.1 RESULTS

5.1.1 DISSOLUTION PROXIES AT THE SOUTH TASMAN RISE TRANSECT

Carbonate concentrations and accumulation rates

In general, the carbonate content of sediments from the South Tasman Rise is a function of surface productivity, dilution effects mainly caused by terrigeneous sediment input from the Australian continent and carbonate dissolution controlled by water depth and changing deep-water alkalinity. At the South Tasman Rise, the carbonate fraction mainly consists of foraminiferal shells and calcareous nannoplankton (Thiede *et al.*, 1999).

The sediment records from the South Tasman Rise are characterized by high carbonate concentrations of >75 % (Fig. 5-1a). Carbonate concentrations vary on glacial/interglacial cycles with lower carbonate concentrations during glacial periods.

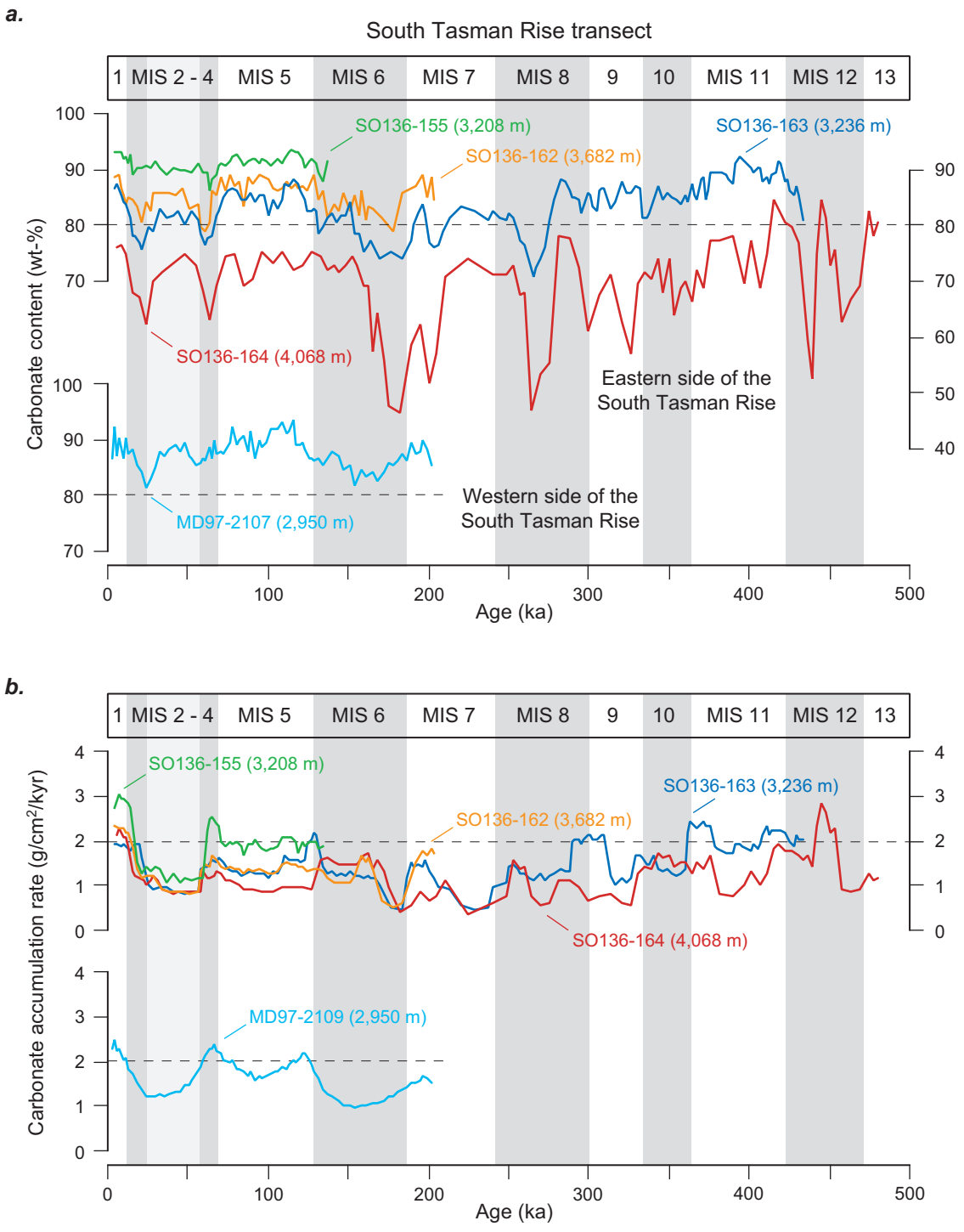

Figure 5-1. Carbonate records from the South Tasman Rise transect as a function of age: (a) carbonate concentrations expressed in weight percentage and (b) carbonate accumulation rates in g/cm^2/kyr.

Because carbonate preservation is generally enhanced during glacials, this pattern most likely results from both, dilution by higher terrigeneous input and regional changes in productivity. The carbonate content increases from north to south, most likely due to the decreasing influence of terrigeneous matter supply from Australia and Tasmania and increasing productivity towards the south. These two factors overprint the general relationship of decreasing carbonate concentrations with increasing water depth, which is related to carbonate dissolution in response to the position of the lysocline (today at ~3,600 m). A comparison of sediment records SO136-155, SO136-163 and MD97-2107 at ~3,000 m water depth and deep core SO136-164 at a water depth of 4,068 m clearly reflects the typical link between carbonate dissolution and water depth. The shallow cores above the modern lysocline show high carbonate concentrations with very small glacial/interglacial variations between 75–95 % (Fig. 5-1a). The deepest core SO136-164, distinctly below the modern lysocline, reveals the lowest carbonate concentrations and larger fluctuations ranging between 45–85 %.

An example for a reversed relationship between carbonate dissolution and water depth is provided by the comparison of core SO136-162 (3,682 m) and core SO136-163 (3,236 m). SO136-162 shows generally higher carbonate contents than the shallower core SO136-163. This reversed pattern most likely results from regional differences in productivity and siliciclastic sediment supply. In comparison to core SO136-163, core SO136-162 is positioned further south and thus less influenced by the supply of terrigeneous sediment from the continent but stronger affected by the higher productivity of the Subantarctic Zone.

Hence, any information on changes in the lysocline depth is regionally restricted to sediment records within the same oceanic environment, e.g. areas, where surface productivity and carbonate flux to each core could be assumed to be approximately equal. Accordingly, the differences in carbonate concentrations between shallow core SO136-163 and deep core SO136-164 is a qualitative indicator of the amount of carbonate lost to dissolution because both cores are located close together. The time interval of the last 170 kyr shows relatively small differences in carbonate concentrations of 8–15 % (= carbonate loss) reflecting only small-scale variations of the lysocline depth around its modern position (Fig. 5-2). Before 170 ka the difference in carbonate concentrations indicates strong fluctuations between 7–30 %. These large differences relate to enhanced carbonate dissolution and a distinct shoaling of the lysocline. Such events occurred during MIS 6.5/7.1, 8.4/8.5, 9 and 11. This is in agreement with other carbonate dissolution proxies discussed below. Additional information on changes in the lysocline depth is also provided by the comparison between cores SO136-155 (3,208 m) and SO136-162 (3,685 m) located at a more southern position below the zone of higher productivity. Over the last 140 kyr, the difference in carbonate concentrations between

3,200–3,700 m water depth is distinctly smaller than between 3,240–4,070 m water depth and varies from 3–9 % in contrast to 8–15 % (Fig. 5-2). During this time interval the southern depth-transect shows the largest differences in MIS 4 suggesting a paleo-position of the lysocline between 3,200–3,600 m water depths. This also indicates that the lysocline must have been distinctly shallower (above 3,240 m) during the strong dissolution events characterizing the time interval between 170–420 ka.

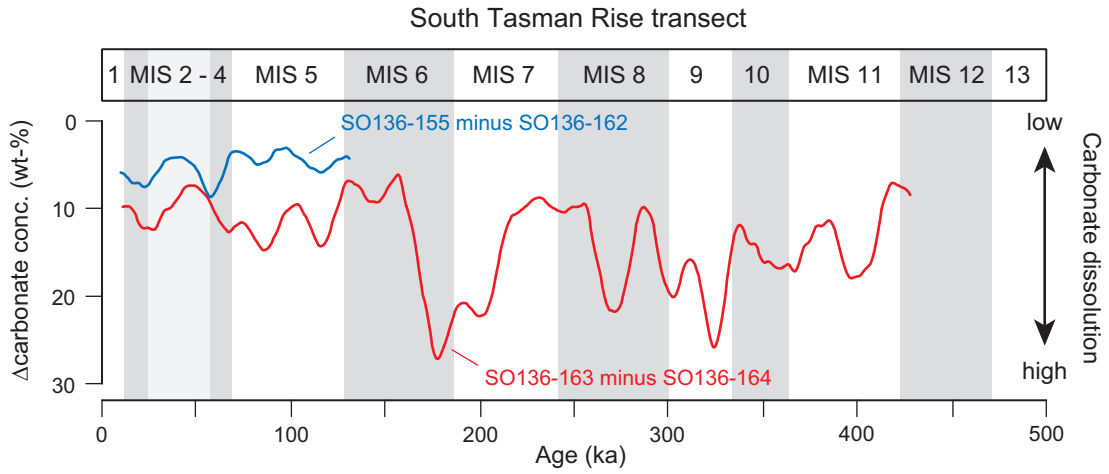

Figure 5-2. Differences in carbonate concentrations (Δcarbonate conc.) at the northern (SO136-163 minus SO136-164) and southern transect (SO136-155 minus SO136-162) as a function of age. Higher differences relate to stronger carbonate dissolution and indicate an increased amount of carbonate loss by dissolution.

Although located several degrees southeast of the South Tasman Rise, the southernmost deep-water core SO136-111 (3,912 m) from the Emerald Basin expands the results further to the south. However, this core is located close to the modern position of the Antarctic Polarfront where the supply of ice-rafted debris and the production of biogenic silica becomes important especially during glacial intervals and thus, direct comparisons with the other cores is not possible. The carbonate content varies between 0–53 % reflecting considerable glacial/ interglacial fluctuations with distinct maxima of 40–53 % at climatic optima MIS 1, 5.5, 7.5 and 9.3 that are most likely associated with an increase in carbonate production as indicated by carbonate accumulation rates (Fig. 5-3). The distinct minimum in biogenic silica concentrations during MIS 5.5 is possibly related to the southernmost position of the Antarctic Polarfront. Carbonate concentrations below 15 % characterize the glacial periods MIS 10, 8 and 6, followed by a continuous increase in carbonate content since ~160 ka that can also be observed in the carbonate accumulation rates. These increases in carbonate concentrations and accumulation rates may indicate enhanced carbonate production related to a southward shift of the Antarctic Polarfront and/or a change to an increase in carbonate preservation caused by modified deep-water circulation. An increase in carbonate preservation since ~160 kyr would be in agreement with the results from the South Tasman Rise. The extreme minima in carbonate

concentrations (0–5 %) during MIS 6 and MIS 8 suggest strong carbonate dissolution during glacial times. Enhanced carbonate dissolution during glacial times is in contrast to the results from the South Tasman Rise transect.

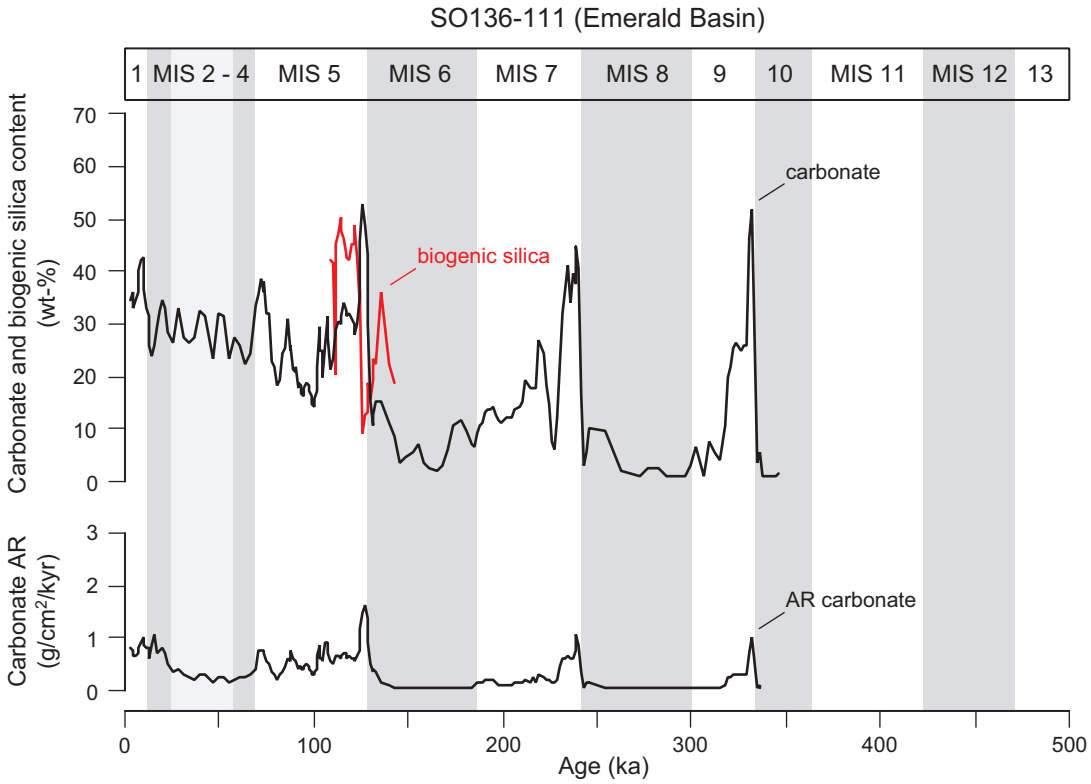

Figure 5-3. Carbonate records and biogenic silica concentrations (100–150 ka) at sediment core SO136-111 from the Emerald Basin as a function of age. High biogenic silica concentrations relate to the core location close to the Antarctic Polarfront and the high-productivity belt.

Compared to carbonate concentrations, carbonate accumulation rates largely reduce dilution effects caused by terrigeneous sediment input and thus, provide a better estimate for changes in carbonate dissolution and productivity. Over the last 170 kyr, the carbonate accumulation rates and concentrations along the South Tasman Rise transect are positively correlated except during MIS 4, where carbonate concentrations are low but accumulation rates are high (Fig. 5-1b). This is interpreted as an interval of enhanced productivity. The correlation between carbonate concentrations and accumulation rates is low between 170–450 ka. The shallower core SO136-163 is less affected by carbonate dissolution than the deeper core SO136-164 and thus, maxima in carbonate accumulation rates primarily indicate maxima in productivity (MIS 5.5, 7.1, transition 8/9, 11). The deeper core SO136-164 is characterized by larger fluctuations between 170–500 ka and with lower values during interglacial periods. The large differences between SO136-163 and SO136-164 are most prominent during MIS 9 and MIS 11 and coincide with the results of the carbonate concentrations. They imply enhanced carbonate dissolution during most of the older interglacial periods, which is in good agreement with other carbonate dissolution proxies (see below).

Coarse carbonate fraction and planktonic fragmentation

In general, the coarse carbonate fraction, calculated as percentage sand-sized material (>63 μm) of the total carbonate component, varies mainly as a function of the foraminifer–nannofossil proportion influenced by changes in productivity or winnowing and carbonate dissolution causing a breakdown of foraminiferal shells to smaller size fractions. The fragmentation index of planktonic foraminifers, however, is predominantly controlled by changes in carbonate dissolution.

In agreement with the results from the carbonate concentrations, the fluctuations in both, coarse carbonate fraction and planktonic fragmentation ratios confirm the suggested paleo-changes in lysocline depth and carbonate dissolution patterns.

At the South Tasman Rise transect, coarse carbonate concentrations range between 2–64 % (Fig. 5-4a) and indicate a similar water depth dependent carbonate dissolution that is overprinted by regional variations in surface productivity. Along the southern depth-transect (SO136-155 and SO136-162) the coarse carbonate fraction is higher than along the northern depth-transect (SO136-163 and SO136-164). This general difference may reflect variations in the ratio of foraminifer/nannoplankton at the southern transect due to higher productivity and cooler sea-surface temperatures, and/or selective dissolution altering the foraminifer/nannofossil ratio in the sediments. Alternatively a gradient of enhanced carbonate preservation towards the south might explain the observed pattern as well but is rather speculative due to the lack of sediment records below 4,000 m water depth at the southern depth-transect. Fragmentation ratios analyzed at SO136-163 and SO136-164 range between 18–77 % (Fig. 5-4b). Both records display higher fragmentation during interglacial intervals with generally higher fragmentation ratios at the deep core SO136-164 and therefore indicate stronger interglacial carbonate dissolution corroborating the results of the coarse carbonate concentrations.

Neglecting the regional overprints, coarse carbonate fraction and planktonic fragmentation index reveal a simple pattern of long- and short-term changes in carbonate preservation. The time interval of the last 250 kyr is characterized by enhanced carbonate preservation in contrast to the time interval from 250–500 ka that is marked by stronger carbonate dissolution. Superimposed on this long-term trend are glacial/interglacial variations with enhanced carbonate dissolution during interglacial periods and better preservation during the glacials. This pattern of short-term fluctuations corresponds to the “Pacific type” of carbonate preservation/dissolution.

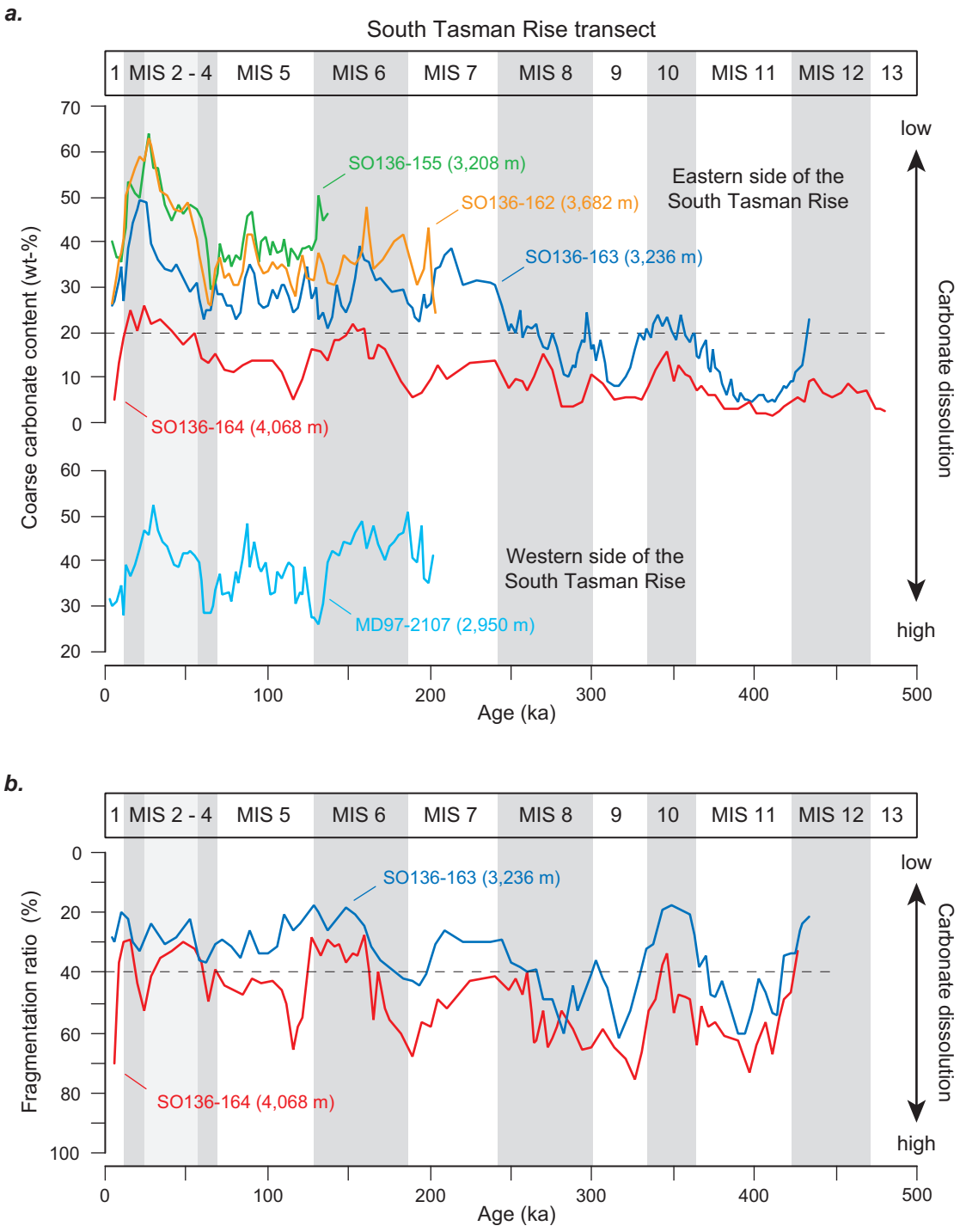

Figure 5-4. Coarse carbonate and planktonic fragmentation records from the South Tasman Rise transect as a function of age: (a) coarse carbonate fraction shown as weight percentage and (b) fragmentation ratio expressed as percentage shell-fragments of the sum of both, planktonic shell-fragments and whole planktonic tests. Both, low coarse carbonate concentrations and high fragmentation ratios indicate increased carbonate dissolution.

According to Martínez (1994b), planktonic fragmentation ratios may serve to reconstruct the fluctuations of the lysocline depth. Using surface sediments from the Tasman Sea, Martínez (1994b) suggested that the 40 %-fragmentation value of sediment-surface samples characterizes the modern lysocline level (see Fig. 2-4). Assuming the same relationship for the late

Pleistocene, changes in the fragmentation index at cores SO136-163 and SO136-164 can be used to assess the paleo-position of the lysocline by interpolating the 40 %-fragmentation contour line between ~3,200–4,100 m. If the fragmentation at both cores is above or below the 40 %-line (Fig. 5-4b) then the position of the lysocline can be assumed to have been above 3,200 m (MIS 7.1, 8.5, 9, 11) or below 4,100 m (MIS 2, 3, 6, 10, 12), respectively.

5.1.2 DISSOLUTION PROXIES AT THE SOUTH AUSTRALIAN BASIN TRANSECT

The primary goal of investigating the South Australian Basin was to examine whether the "Pacific-type" pattern of carbonate preservation expands farther to the west of the South Tasman Rise or if the "Atlantic-type" pattern expands from the Indian sector of the Southern Ocean farther to the east. The depth transect of cores ELT35-002 and ELT39-043 (3,365–3,945 m) at the northern flank of the Southeast Indian Ridge at ~131°E complemented by the westernmost core ELT45-077 (3,850 m) at 114°E, was used to approximate the boundary between both dissolution patterns.

Carbonate concentrations and accumulation rates

The sediment records ELT35-002 and ELT39-043 are generally characterized by high carbonate concentrations and small glacial/interglacial variations between ~80–95 % (Fig. 5-5a). Carbonate concentrations at 3,945 m water depth are slightly higher than at 3,365 m indicating a reversed relationship of higher carbonate concentrations at greater water depth similar to the South Tasman Rise. However, distinctly lower carbonate accumulation rates at the deeper core ELT39-043 document the expected carbonate loss due to enhanced dissolution with increasing water depth (Fig. 5-5b), but might also be attributed to higher productivity in the vicinity of the Antarctic Polarfront at the southern and shallower core ELT35-002. With respect to other dissolution proxies presented below, lower carbonate accumulation rates during MIS 1, 5 and 7 correspond to enhanced carbonate dissolution and therefore display a "Pacific-type" pattern at cores ELT35-002 and ELT39-043.

In contrast to the more eastern cores, sediment record ELT45-077 at 114°E shows larger glacial/interglacial fluctuations in carbonate concentrations between ~35–90 % with generally higher values during interglacial periods, except MIS 5.3 and 7. This pattern coincides with higher carbonate accumulation rates during MIS 1, 5.1, 5.5 and 9.3. On the one hand this may reflect enhanced carbonate dissolution during glacial intervals consistent with an "Atlantic-type" pattern of carbonate dissolution, although such changes in carbonate dissolution cannot be inferred from the carbonate record alone. On the other hand, higher carbonate accumulation during indicated interglacial periods may result from increased productivity, which was documented for the Indian sector of the Southern Ocean west of 105°E (Howard & Prell, 1994).

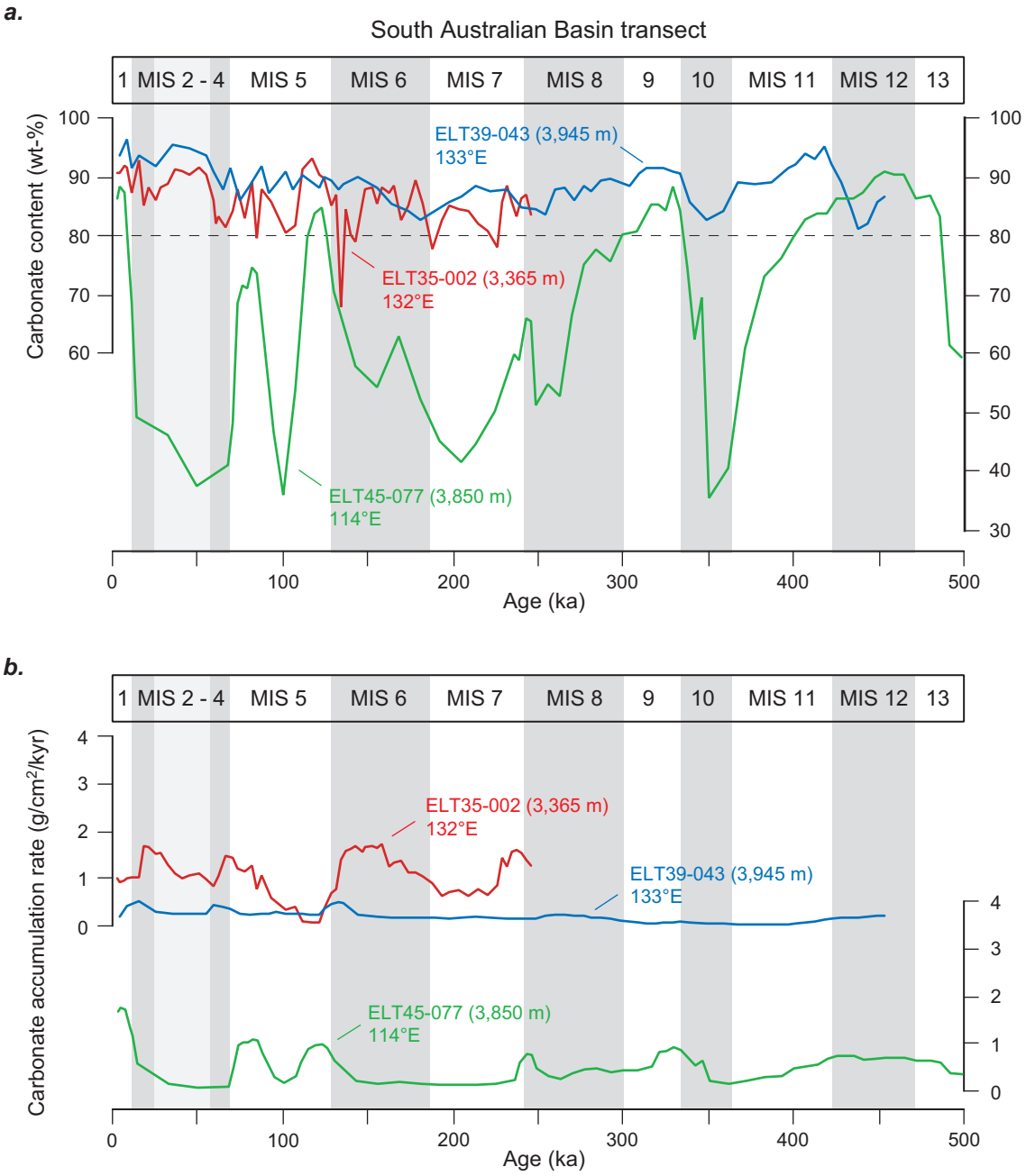

Figure 5-5. Carbonate records from the South Australian Basin transect as a function of age: (a) carbonate concentrations expressed in weight percentage and (b) carbonate accumulation rates in g/cm^2/kyr.

Coarse carbonate fraction and planktonic fragmentation

At the South Australian Basin transect, coarse carbonate concentrations (>63 µm) and planktonic fragmentation ratios range between 10–80 % and 3–47 %, respectively (Fig. 5-6). The sediment records generally show lower coarse carbonate concentrations and increased fragmentation ratios during most interglacial periods indicating enhanced dissolution with pronounced maxima during MIS 1, 5.5 and 9–11. This suggests the westward expansion of the "Pacific-type" pattern of carbonate preservation to 114°E. Thus, one explanation for the

negative correlation between carbonate accumulation rates and carbonate dissolution at westernmost core ELT45-077 is, that the "Atlantic-type" pattern of the carbonate record was rather driven by changes in productivity than by carbonate dissolution. Another significant feature of the carbonate dissolution records is a pronounced maximum in carbonate dissolution from 420–300 ka (MIS 11–9) and the long-term increase in carbonate preservation from 300–130 ka (MIS 8–6/5). These trends are observed at the records from the South Tasman Rise transect as well.

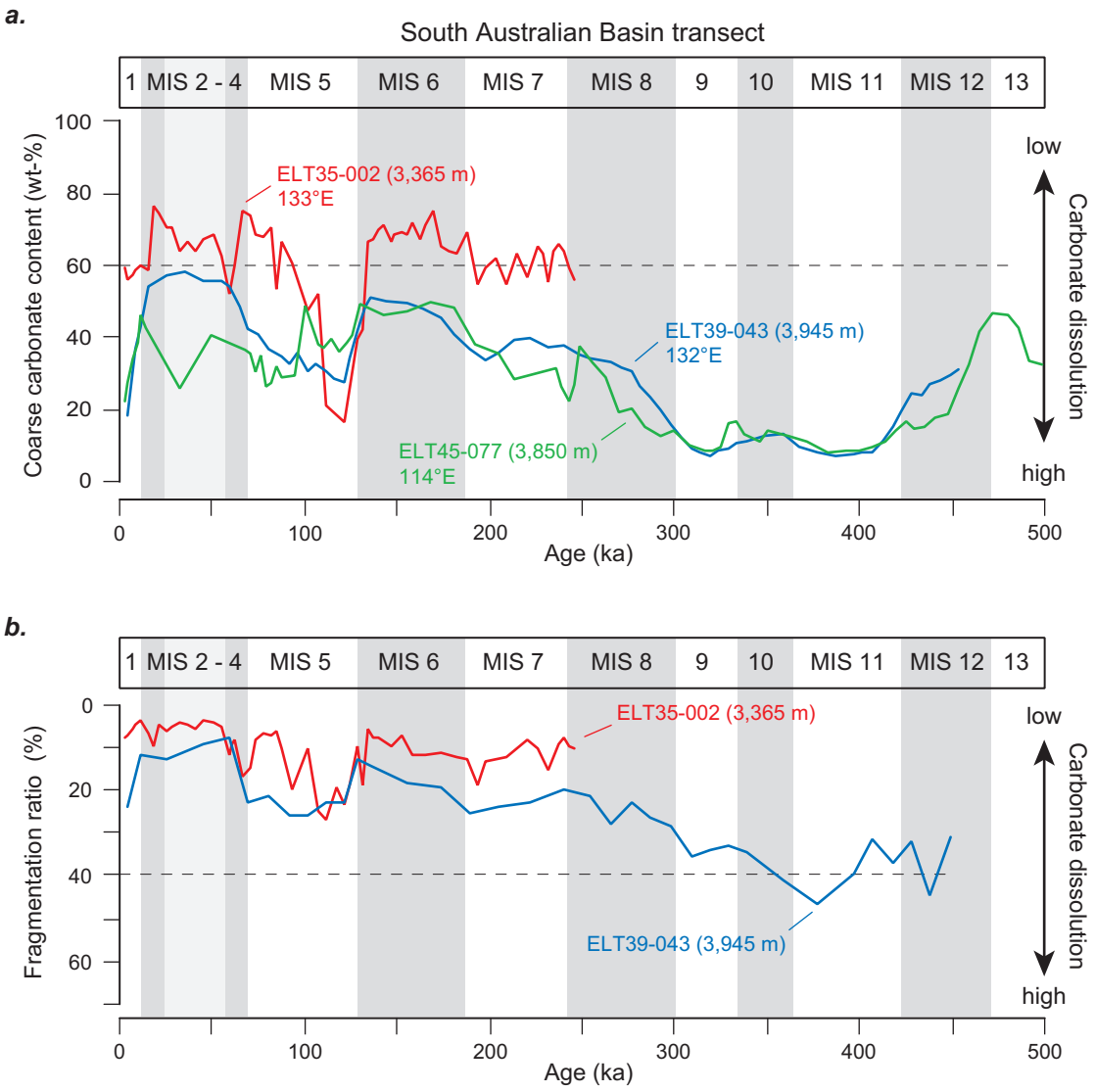

Figure 5-6. Coarse carbonate and planktonic fragmentation records from the South Australian Basin transect as a function of age: (a) coarse carbonate fraction shown as weight percentage and (b) fragmentation index expressed as percentage shell-fragments of the sum of planktonic shell-fragments and whole planktonic tests. Both, low coarse carbonate concentrations and high fragmentation ratios indicate increased carbonate dissolution.

However, the comparison between the eastern and western transects also reveal a significant difference in carbonate dissolution. At similar water depth, the South Tasman Rise transect shows higher coarse carbonate concentrations and fragmentation ratios than the South

Australian Basin transect. This implies generally better carbonate preservation at the westernmost depth transect if the relationship between carbonate ion concentration and fragmentation index according to Martínez (1994b) can be assumed to be similar between both regions. These trends along with the longitudinal change in the patterns of carbonate concentrations and accumulation rates (maxima in interglacials vs. maxima in glacials) and the dominating "Pacific-type" pattern of carbonate preservation raises a substantial question. If carbonate dissolution is strong enough during interglacials it may modulate or blur the productivity-controlled primary signal of carbonate percentages and accumulation rates. However, at South Australian Basin transect carbonate dissolution is similar at cores ELT45-077 and ELT39-043 (~3,900 m) and implies a distinct change in carbonate productivity from 114°E to 131°E.

5.1.3 EPIBENTHIC FORAMINIFERAL $\delta^{13}C$

The epifaunal benthic $\delta^{13}C$ profiles serve as a major tracer to reconstruct the ventilation (O_2) of past deep-water masses flooding the Australian Sector of the Southern Ocean. High benthic $\delta^{13}C$ values are indicative of relatively good ventilated deep-waters with low nutrient and low CO_2 concentrations. Low benthic $\delta^{13}C$ values identify poorly ventilated deep-water masses. Figures 5-7 to 5-9 illustrate short and long-term trends in benthic $\delta^{13}C$ along the two deep-water transects and their relationship to glacial/interglacial climate variability and carbonate dissolution patterns. In addition, benthic $\delta^{13}C$ records of the New Zealand sector (Campbell Plateau and Challenger Plateau) are shown to extend the $\delta^{13}C$ deep-water profiles into intermediate-water depth (Fig. 5-10).

At the South Tasman Rise transect, benthic $\delta^{13}C$ values vary between 1.0 and -1.3 ‰ and generally decrease with increasing water depth (Fig. 5-7) coinciding with an increase in carbonate dissolution. High $\delta^{13}C$ values of relatively better ventilated deep-water masses predominantly mark interglacials periods. Glacial intervals are characterized by reduced deep-water ventilation especially prior to 130 ka with pronounced minima in ventilation during MIS 6, 8, 10 and 12. A comparison between carbonate dissolution and deep-water ventilation would initially suggest that poorly ventilated water masses, relatively enriched in CO_2 and hence carbonate aggressive are associated with periods of enhanced carbonate preservation. However, the benthic $\delta^{13}C$ signal may have a strong overprint from global changes in the carbon budget and may also be affected by $\delta^{13}C_{\sum CO2}$ variations of the source waters, i.e., by variations of preformed $\delta^{13}C_{\sum CO2}$ (see Chapter 3.1). Thus, the difference of $\delta^{13}C$ profiles from different water depths is a more reliable indicator for regional and water depth dependent changes in nutrients and CO_2 because it eliminates the global background signal.

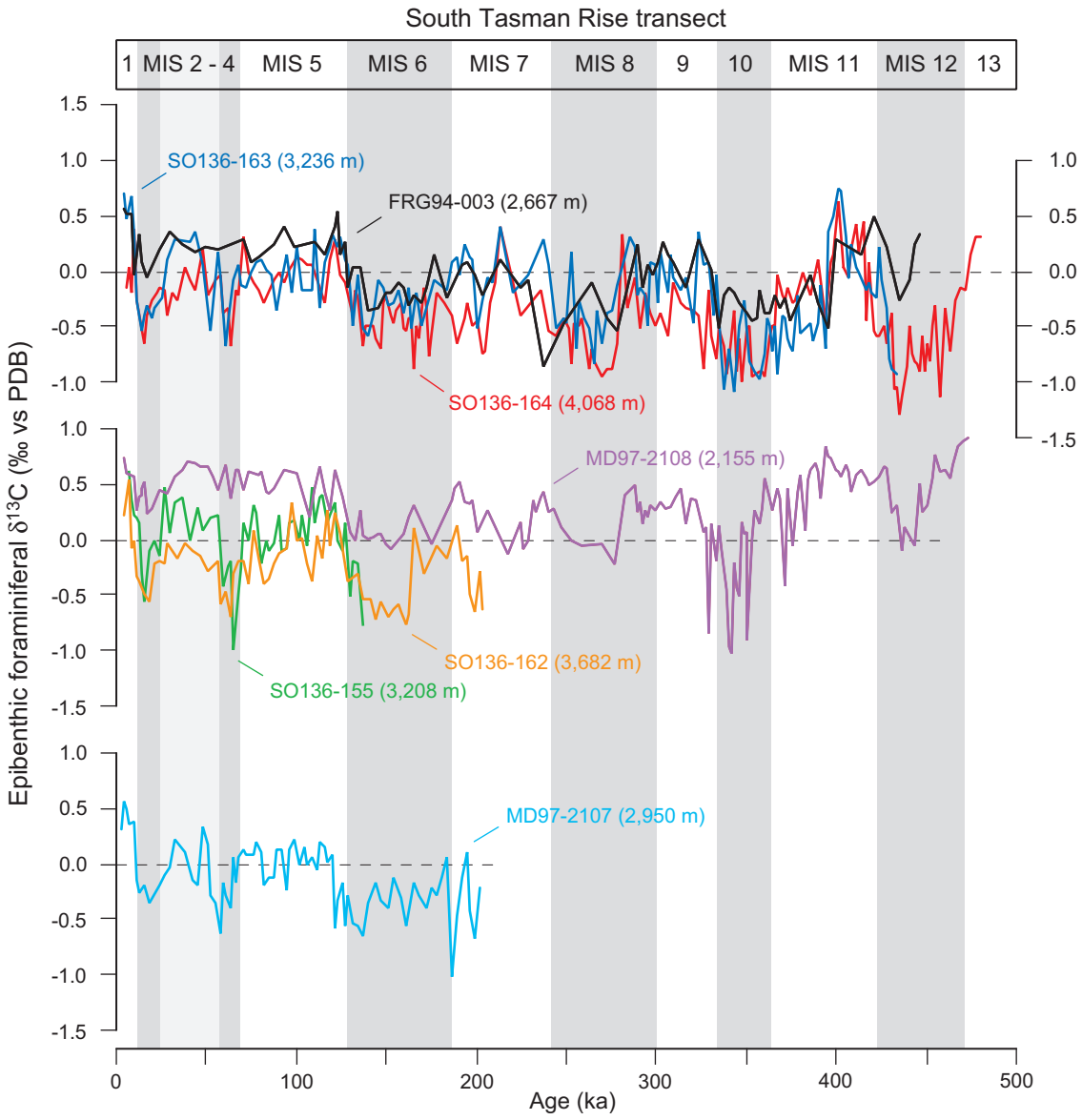

Figure 5-7. Benthic foraminiferal $\delta^{13}C$ records from the South Tasman Rise transect as a function of age.

Figure 5-8 compares the differences in $\delta^{13}C$ between cores SO136-163 and SO136-164 with the fragmentation ratios of core SO13-164 and the differences in carbonate concentrations between cores SO136-163 and SO136-164, that cover the time interval of the last 450 kyr. The relative increase in nutrient concentration and CO_2 ($\Delta\delta^{13}C = \delta^{13}C_{SO136\text{-}163}$ minus $\delta^{13}C_{SO136\text{-}164}$) is positively correlated with increased fragmentation and loss of carbonate (Δcarbonate = % $carbonate_{SO136\text{-}163}$ minus % $carbonate_{SO136\text{-}164}$). The small displacement between $\Delta\delta^{13}C$ and Δcarbonate within the interval from 175–230 ka may result from a small error in the age model due to the relatively weak stratigraphic time resolution at SO136-164.

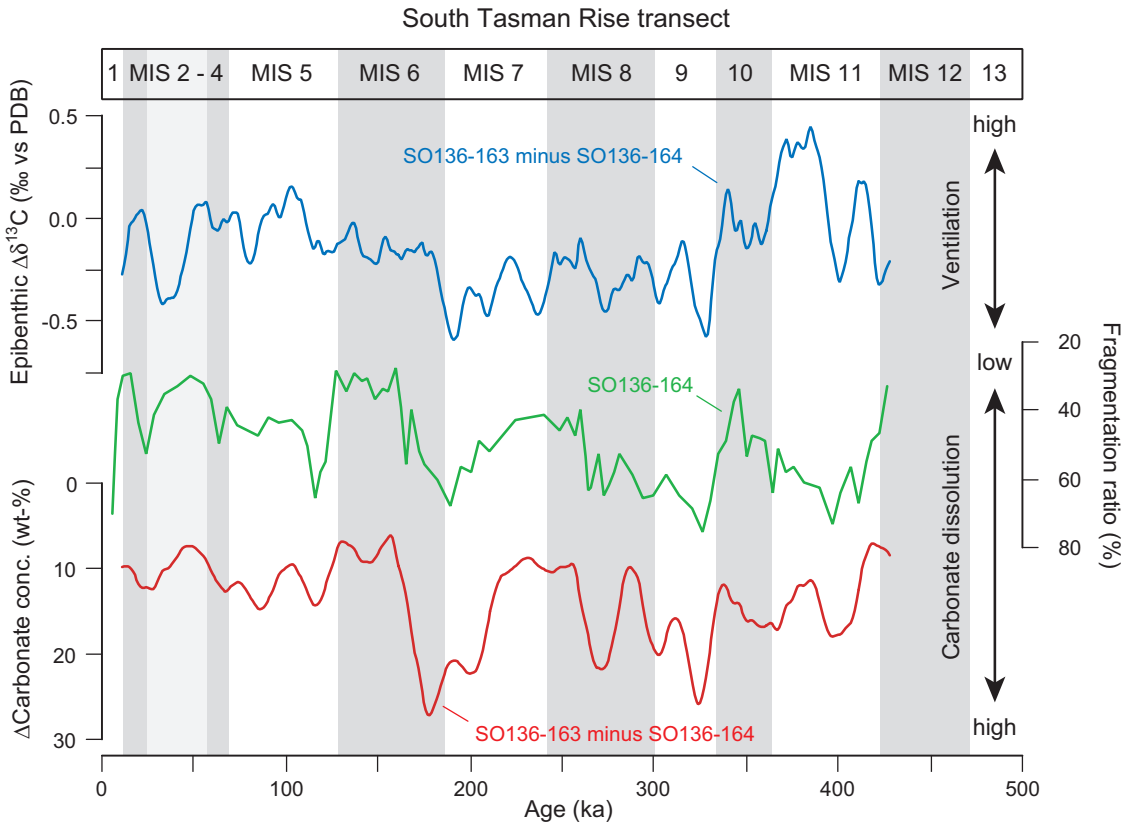

Figure 5-8. Comparison between benthic $\Delta\delta^{13}C$ records (SO136-163 minus SO136-164), indicating deep-water ventilation changes, and dissolution records from the South Tasman Rise transect. High fragmentation ratios of sediment core SO136-164 (green) and larger differences in carbonate concentrations between SO136-163 and SO136-164 (red) indicate stronger carbonate dissolution during interglacial intervals and correspond to relative increases in deep-water nutrient concentrations and CO_2 (blue).

At the South Australian Basin transect, benthic $\delta^{13}C$ values of cores ELT35-002 (3,365 m) and ELT39-043 (3,945 m) vary between 0.7 and -1.0 ‰ (Fig. 5-9a) and show similar variations as observed at South Tasman Rise with higher $\delta^{13}C$ values during interglacial intervals. Shallower core ELT35-002 is generally better ventilated than deeper core ELT39-043 as indicated by higher $\delta^{13}C$, except MIS 4 and 5.3. These exceptions are also reported by positive values in the $\delta^{13}C$ differences between both cores (Fig. 5-9b). The $\delta^{13}C$ differences for the last 250 kyr show slightly higher amplitudes compared to the $\delta^{13}C$ differences from the South Tasman Rise transect (SO136-163 minus SO136-164), but similar fluctuations. The displacement may relate to the weaker stratigraphic time resolution of the sediment cores from the South Australian Basin. The relation between $\delta^{13}C$ differences and fragmentation ratios at the South Australian Basin transect is weak probably due to the generally lower carbonate dissolution. However, the minima in $\delta^{13}C$ differences at MIS 5.5 and 6.5–7.1 correlate fairly well to maxima in planktonic fragmentation derived from the South Tasman Rise transect.

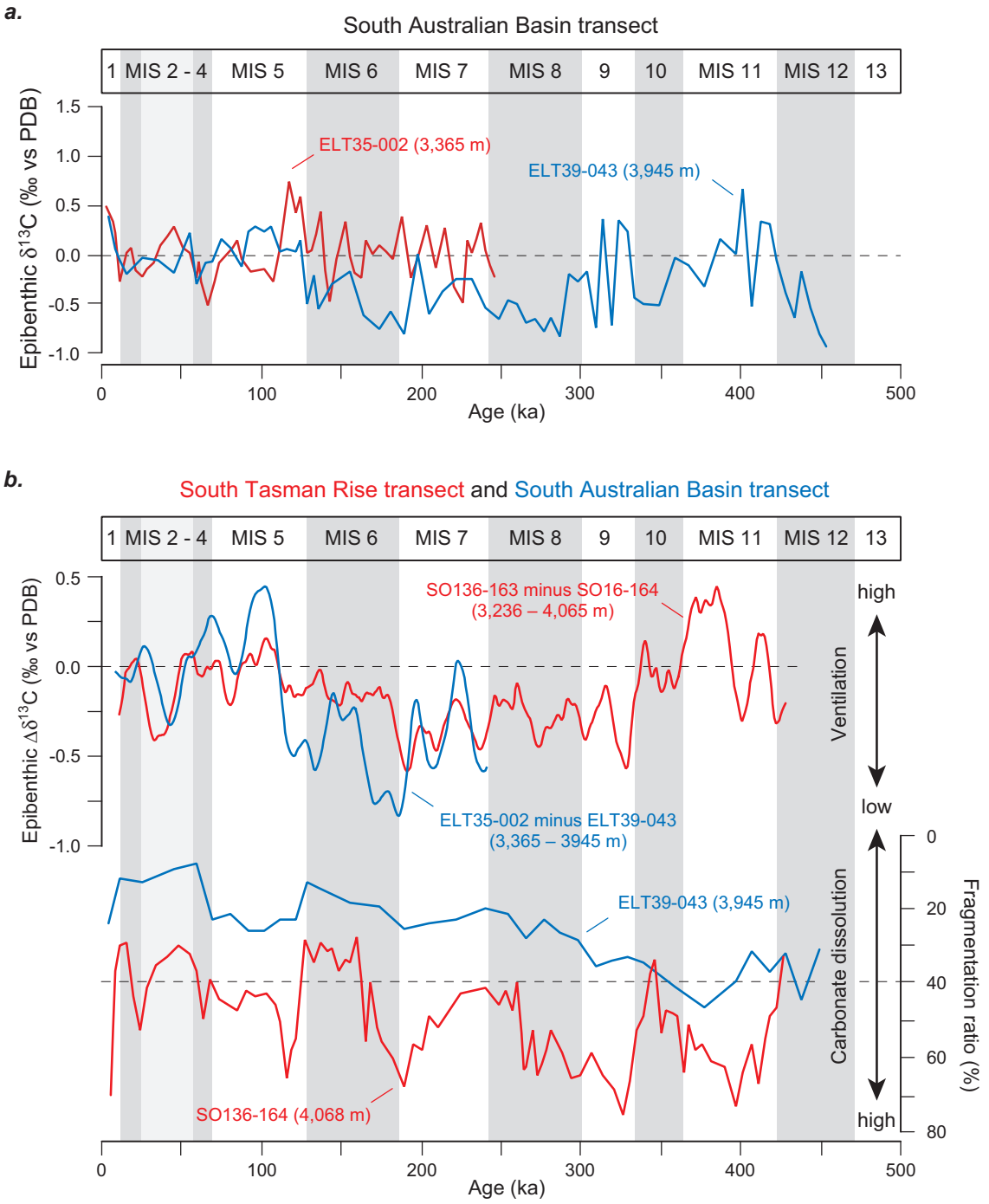

Figure 5-9. (a) Benthic foraminiferal $\delta^{13}C$ records from the South Australian Basin transect as a function of age. (b) Comparison of benthic $\Delta\delta^{13}C$ and fragmentation records from the South Australian Basin transect (blue) and South Tasman Rise transect (red) as a function of age.

At the intermediate-water transect, benthic $\delta^{13}C$ records between 600–2,155 m water depths reflect the general decrease in ventilation with increasing water depth. The shallowest core SO136-061 displays the highest $\delta^{13}C$ values (1.0–2.1 ‰) and only small variations during the 120 kyr. A distinct minimum occurs at the Termination II – MIS 5.5, which is not apparent at the deeper cores. This minimum at 600 m water depth may relate to strong $\delta^{13}C$ minima

observed in shallow- to deep-dwelling planktonic records from the South Tasman Rise transect, as the core is bathed today in Subantarctic Mode Water formed by deep convection during austral winter. This will be discussed in Chapter 6. The deeper cores show glacial/interglacial variations similar to the deep-water records with lower values during glacial intervals. During MIS 10, the lowest $\delta^{13}C$ values (-1.0 ‰) can be observed at MD97-2108.

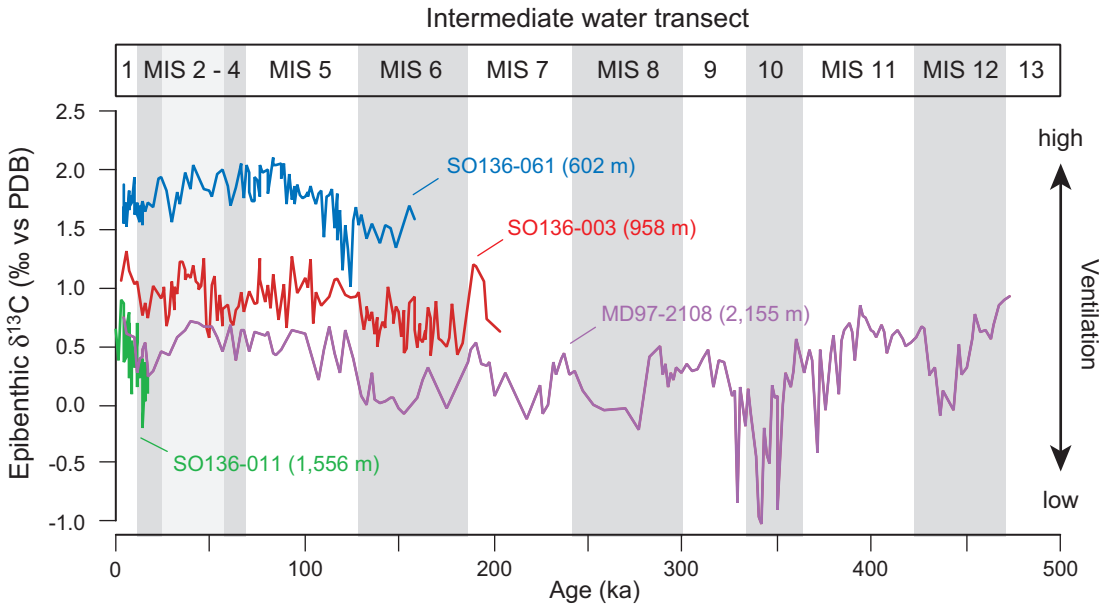

Figure 5-9. (a) Benthic foraminiferal $\delta^{13}C$ records from the Intermediate-water transect as a function of age, based on sediment cores from Campbell Plateau (SO136-061, MD97-2109) and Challenger Plateau (SO136-011). MD97-2108 from the South Tasman Rise is shown for comparison.

5.2 DISCUSSION

It is widely accepted that the "Atlantic-type" pattern of Pleistocene carbonate preservation (enhanced dissolution during glacials) is also characteristic of Southern Ocean deep-waters in general (e.g. Howard & Prell, 1994; Hodell *et al*., 2003), suggesting that the Atlantic Ocean and Southern Oceans may balance the opposite pattern of carbonate dissolution in the Indian and Pacific Ocean. The "Atlantic-type" pattern of carbonate preservation is interpreted in terms of rapid dissolution response signatures related to the strength of North Atlantic Deep Water production. Enhanced production of North Atlantic Deep Water (low concentrations of $\sum CO_2$, nutrients and alkalinity and high carbonate ion concentrations) during interglacials is thought to contribute to better carbonate preservation in the deep Atlantic as well as in the Southern Ocean because North Atlantic Deep Water is injected into the Lower Circumpolar Deep Water. In contrast, reduced glacial North Atlantic Deep Water production is associated with enhanced carbonate dissolution in the deep Atlantic Ocean as well as in the Atlantic and Indian sectors of the Southern Ocean.

The results presented here clearly document that the "Atlantic-type" of carbonate preservation did not expand into the Australian sector of the Southern Ocean. Here, the Pleistocene proxy records reveal the "Pacific-type" pattern characterized by enhanced interglacial carbonate dissolution. This type of pattern was first described by Arrhenius (1952) and extensively studied in the equatorial east and central Pacific by Farrell & Prell (1989) using carbonate records to monitor vertical changes in the carbonate compensation depth (CCD). The results from Farrell & Prell (1989) are based on Pleistocene changes in carbonate concentrations between 4,000–5,000 m water depth (Fig. 5-11a). Thus, variations in carbonate concentrations predominantly reflect vertical displacements of the CCD (10 % $CaCO_3$-isopleth). Over the last 500 kyr, the CCD remained at a relatively constant level of about 4,900 m water depth in the equatorial eastern and central Pacific. In general, the CCD was slightly shallower from 200–500 ka (~100 m) than during the last 200 kyr. The temporal fluctuations in carbonate concentrations above 10 % provide additional information on relative changes in the lysocline depth. Strong decreases in carbonate concentrations with increased water depth are typical for interglacial stages suggesting a shoaling of the lysocline of 400–800 m from glacial depths. The transition zone between the CCD and the lysocline appears to have thickened during interglacials because the CCD remained relatively constant. Le & Shackleton (1992) and Martínez (1994a) investigated Pleistocene fluctuations of the lysocline with similar results for the western equatorial Pacific. Both studies determined variations in the lysocline depth using planktonic fragmentation ratios, a more sensitive indicator for changes in carbonate dissolution.

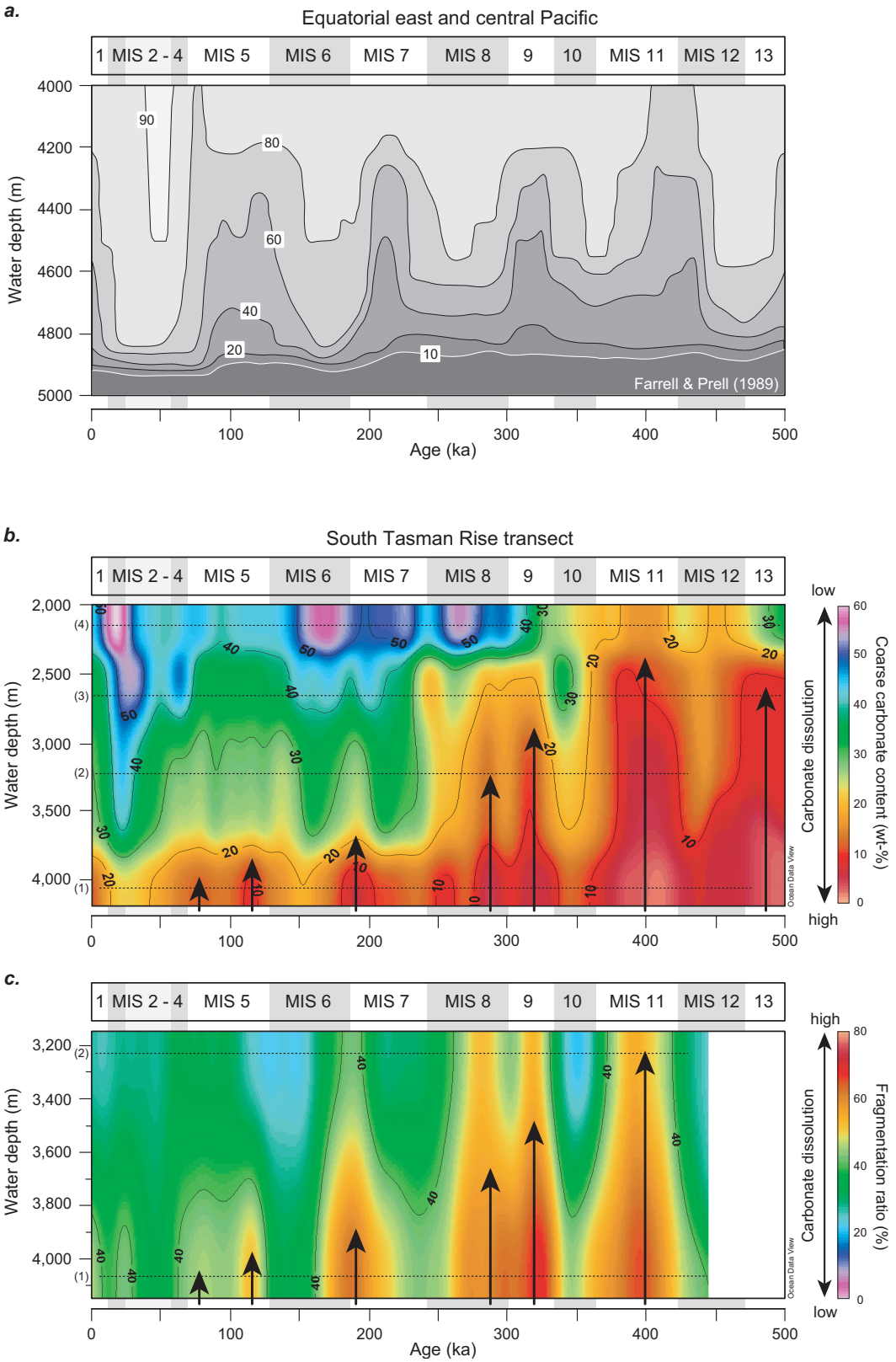

Figure 5-11. Bathymetric variations in carbonate preservation through time in the (a) equatorial Pacific (Farrell & Prell, 1989) in comparison to the (b & c) Australian sector of the Southern Ocean. Both regions are characterized by the "Pacific-type" preservation pattern with stronger carbonate dissolution during interglacial intervals as expressed by shallower isopleths. The coarse carbonate concentrations values and fragmentation ratios of sediment cores (1) SO136-164, (2) SO136-163, (3) FRG97-003 and (4) MD97-2108) are contoured using the program Ocean Data View (Schlitzer, 2003). Red colors indicate strong carbonate dissolution; arrows mark intervals of strongest dissolution.

Martínez (1994a & 1994b) used the 40 %-fragmentation value as a tracer of the lysocline level. Accordingly, the glacial lysocline was positioned on average at 3,100 m water depth and raised to levels between 2,500–3,000 m during interglacials. For the western Tasman Sea, Martínez (1994b) demonstrated that the modern lysocline depth at 3,600 m could be traced as well by the 40 % fragmentation level (see Fig. 2-4). Using the same approach as Martinez (1994b), the lysocline in the Australian sector of the Southern Ocean would have fluctuated from 4,100 m to less than 3,200 m water depth over the last 500 kyr. This suggests a larger total range of lysocline displacements on the order of 1,000 m and in general a deeper glacial position in comparison to the equatorial Pacific. These large fluctuations, however, are restricted to the time interval from ~250–500 ka, when carbonate dissolution was generally strong. These regional differences are probably due to the influence of different deep-water masses and carbonate fluxes characterizing the tropical Pacific and the Southern Ocean. Carbonate preservation improved over the last 250 kyr in the Southern Ocean as well as in the central Pacific and South Atlantic (Farrell & Prell, 1989; Bickert, 1992) and seems to represent a global feature driven by a decrease in oceans alkalinity. Whether this is due to an imbalance between the input of alkalinity from the continents and the removal of alkalinity by CaCO3 burial in the deep-sea or to changes in the biological pump or a reduced transfer of carbon from terrestrial sources remains speculative.

The extension of the “Pacific-type” pattern of carbonate preservation from the equatorial Pacific into the Australian sector of the Southern Ocean (114°E–150°E) is restricted towards the west by the “Atlantic-type” pattern characterizing the Atlantic and Indian sector of the Southern Ocean. Howard & Prell (1994) demonstrated that the Pleistocene “Atlantic-type” pattern (stronger dissolution during glacials) stretches to ~95°E (Fig. 5-12). Thus, the pattern of carbonate dissolution changes within a distance of ~1,500 km. A key position within this puzzle has sediment record ELT45-029 (3,863 m) at 106°31’E and 44°53’S investigated by Howard & Prell (1991). The record of planktonic fragmentation reveals an important change in carbonate dissolution at ~250 ka that was not considered in their discussion. Prior to ~250 ka, enhanced interglacial carbonate dissolution points to a “Pacific-type” pattern. After ~250 ka this record indicates an “Atlantic-type” pattern with enhanced interglacial carbonate preservation. This implies a change in deep-water circulation because different signals of alkalinity are transported to this core location. This suggests that the “Pacific-type” pattern of carbonate preservation before 250 ka may either result from enhanced inflow of Indian deep-waters or from Pacific deep-waters flowing westward into the South Australian Basin.

Modern hydrographic data from a latitudinal transect through the South Australian Basin at 115°E (Hufford & McCartney, 1997) indicate a westward deep-water flow below 3,500 m water

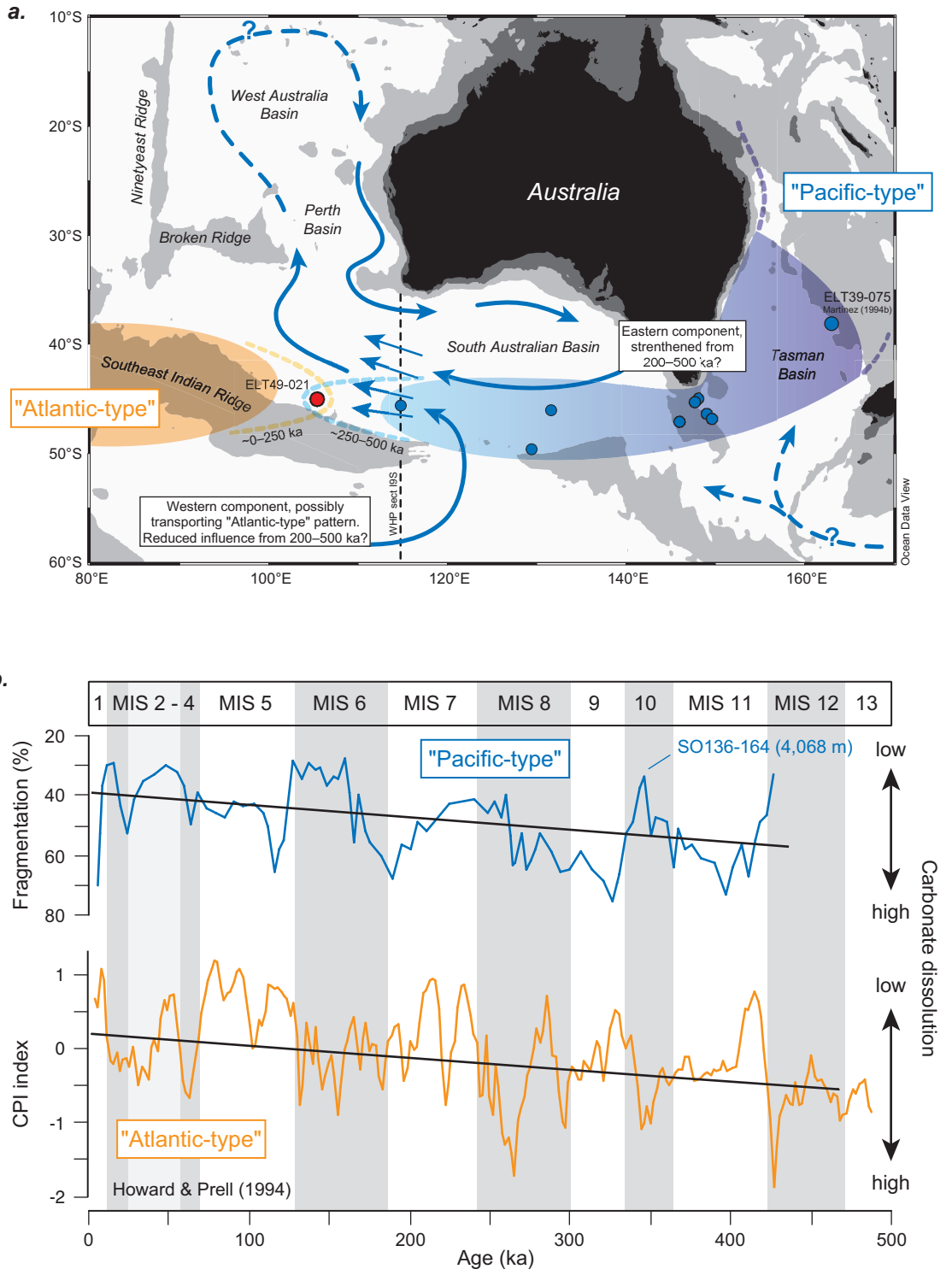

Figure 5-12. Contrasting carbonate preservation patterns in the southeast Indian Ocean and the Australian sector of the Southern Ocean. The map (a) illustrates the distribution of the "Atlantic-type" pattern (orange shaded) based on reconstructions from Howard & Prell (1994) and the "Pacific-type" pattern (blue shaded) based reconstruction from this study and Martínez (1994b). Arrows indicate the deep-water circulation scheme mainly deduced from hydrographic and velocity measurements along WHP section I9S along 115°E (redrawn from Hufford *et al*., 1997). Sediment core ELT49-021 (red, investigated by Howard & Prell, 1994) indicates the "Pacific-type" preservation patter prior to ~250 ka and the "Atlantic-type" pattern afterwards. The comparison of dissolution records from both regions (b) clearly reveals the contrasting patterns, but also the longer-term trend of increasing carbonate preservation during the last 500 kyr (black trendlines). The "Atlantic-type" pattern is presented by the composite preservation index (CPI) according to Howard & Prell (1994).

depth between 40°–45°S (Fig. 5-12a). This westward flow is possibly fed by both, an eastern component originating possibly in the Tasman Sea sector of the Southern Ocean and a southwestern component originating south of 50°S. At ~100°E, the westward flow turns to the north into the Perth Basin and forms the deep western boundary current flowing northward along Broken Ridge. This inflow is balanced by a southward deep-water outflow on the eastern side of the Perth Basin (>3,500 m). The outflow feeds the deep northern boundary current in the South Australian Basin that transports water of subtropical Indian Ocean origin towards the east.

This hydrographic pattern may serve as a model to explain the observed changes in carbonate preservation at 250 ka by changing the influence of eastern or southwestern components of the westward deep-water flow. This assumes, that the "Pacific-type" pattern is transported within the eastern component and the "Atlantic-type" pattern within the southwestern component. Prior to 250 ka, a strengthened westward transport of deep-water mainly originating from the Tasman Sea sector of the Southern Ocean (eastern component) may have caused the "Pacific-type" pattern of carbonate preservation farther westward up to the core location of ELT45-029 at 106°E. It is still an open question to what extend the deep northern boundary current supplied recirculated more nutrient-enriched water masses from the Indian Ocean via a loop into the eastern component (Hufford & McCartney, 1997). However, it seems more likely that the westward deep-water flow is fed by water masses originating in the vicinity of the South Tasman Rise where the "Pacific-type" pattern of carbonate preservation was most pronounced during the last 500 kyr. The assumption that changes in biogenic surface productivity may have triggered the observed longitudinal change from a "Pacific-type" to an "Atlantic-type" pattern can be largely excluded, because the sediment records from the Indian and Australian sectors of the Southern Ocean cover a latitudinal band between 40°–45°S, the Subantarctic Zone. Variations in productivity on glacial/interglacial cycles associated with latitudinal changes of oceanographic fronts would similarly affect both regions.

Cyclic variations in Atlantic carbonate preservation exhibit in-phase covariation between carbonate burial and deep-water circulation, whereas Pacific and Indian Ocean carbonate records significantly lags glacial ice volume (Le & Shackleton, 1992). Glacial carbonate burial outside of the Atlantic basin is related to enhanced preservation due to the temporary increase in mean ocean alkalinity levels (due to Atlantic carbonate dissolution) and due to the associated 5- to 10-kyr carbonate ion response time (e.g. de Menocal *et al*., 1997). In the Australian sector of the Southern Ocean, the preservation cycles are highly correlated with benthic $\delta^{18}O$ variations in the eccentricity and obliquity frequency bands (100 kyr^{-1} and 41 kyr^{-1}) and thus, allowed cross-spectral analyses to examine the time lag between carbonate preservation and changes in global

ice-volume. The results from cross-spectral analyses indicate that maxima in fragmentation (= dissolution maxima) lags $\delta^{18}O$ minima (ice-volume minima) on the order of 36.4° ±14.2° at the 100-kyr cycle and 45.0° ±19.6° at the 41-kyr cycle (Fig. 5-13). These phase differences correspond to temporal offsets of 5–10 ±4 kyr. This time lag is similar to the expected carbonate-ion response time (see above) and is in agreement with estimated phase differences from the western equatorial Pacific as well (Le & Shackleton, 1992). Le & Shackleton (1992) calculated that fragmentation lags behind ice-volume on the order of 6–20 kyr.

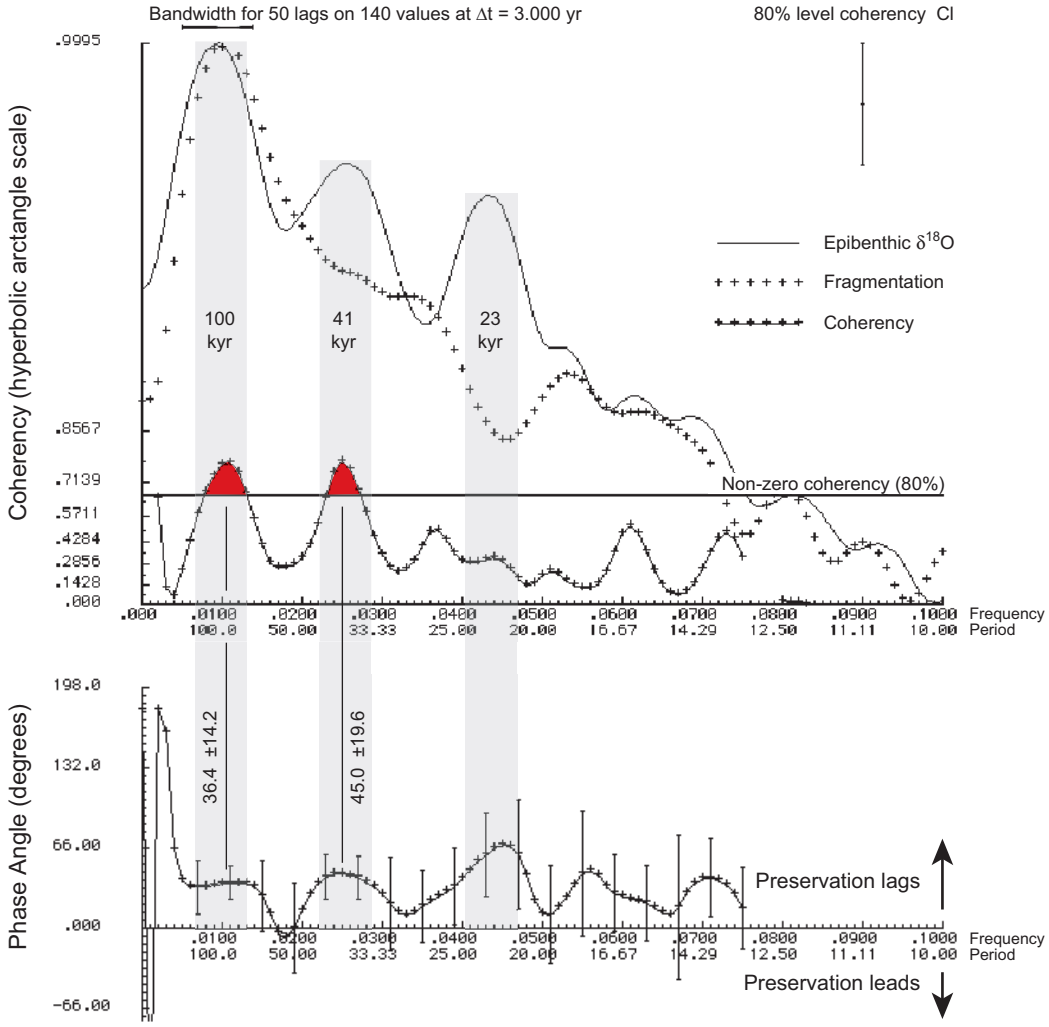

Figure 5-13. Cross-spectral analysis between benthic foraminiferal $\delta^{18}O$ and planktonic fragmentation of sediment core SO136-164. Red shaded areas indicate coherencies above the 80 %-level.

The glacial/interglacial cycles of carbonate preservation in the Australian sector of the Southern Ocean are superimposed on a longer-term trend of increasing carbonate preservation from 500 ka towards the present (Fig. 5-11). Apart from of different glacial/interglacial dissolution patterns, this trend corresponds to similar trends in carbonate preservation in the deep Atlantic, Indian and Pacific oceans (e.g. Bickert, 1992; Peterson & Prell, 1985; Farrell &

Prell, 1989) as well as in the Atlantic and Indian sectors of the Southern Ocean (Howard & Prell, 1994). This global evolution is also reflected in a long-term increase in benthic foraminiferal $\delta^{13}C$ (e.g. Mix et al., 1991) and suggests a change in the whole ocean carbon inventory, such as a long-term withdrawal of dissolved carbon of the ocean. This Pleistocene change is also clearly recognized in benthic $\delta^{13}C$ records from the Australian sector of the Southern Ocean summarized in Figure 5-14.

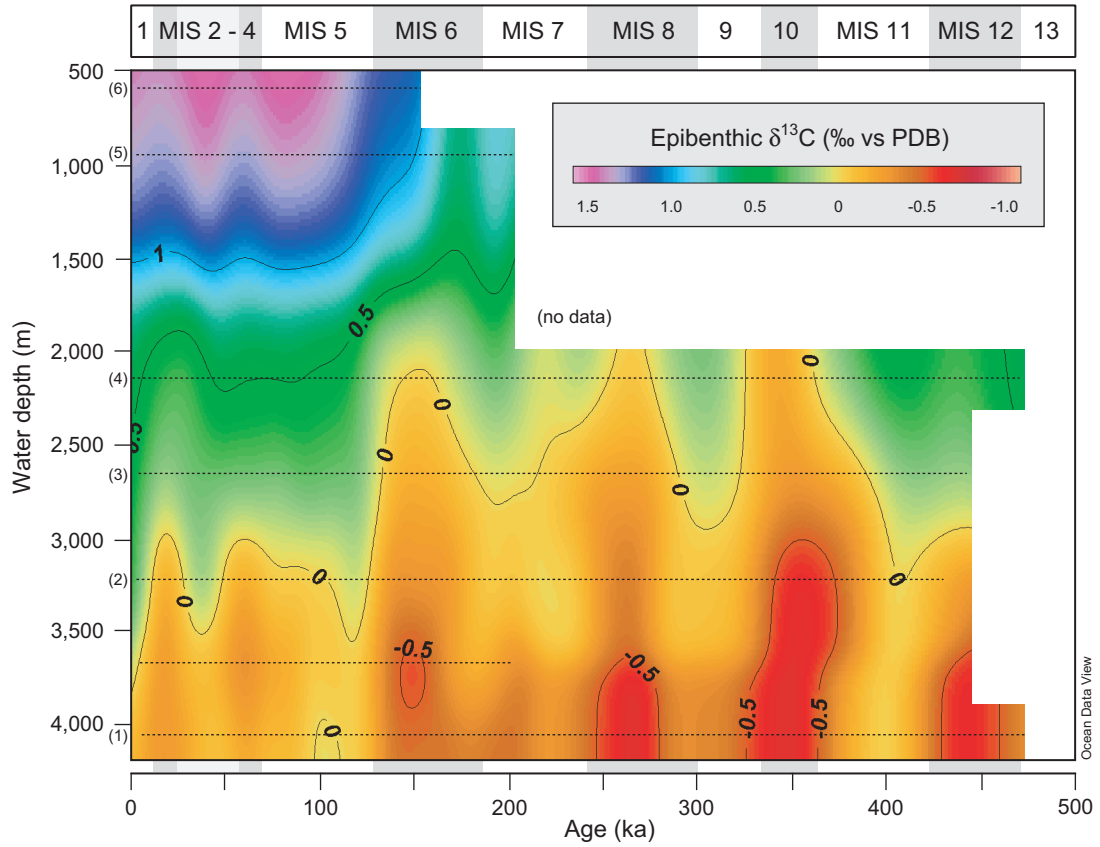

Figure 5-14. Bathymetric variations in intermediate- to deep-water ventilation through time in the Australian sector of the Southern Ocean. Benthic foraminiferal $\delta^{13}C$ records of (1) SO136-164, (2) SO136-162, (3) SO136-163, (4) FRG94-003, (5) MD97-2108, (6) SO136-003 and (7) SO136-061 between 600–4,100 m are contoured using the software Ocean Data View (Schlitzer, 2003); red colors indicate higher nutrient and CO_2 concentrations.

Based on the results from cross-spectral analyses between carbonate dissolution and ice-volume, changes in Atlantic deep-water circulation appear to be the dominant process responsible for the glacial-interglacial carbonate deposition patterns observed in the Pacific and Indian oceans. Benthic foraminiferal $\delta^{13}C$ and Cd/Ca data from the Atlantic and the Atlantic sector of the Southern Ocean indicated that deep (below 2,500 m water depth) North Atlantic Deep Water production was significantly reduced during glacial maxima, whereas upper North Atlantic Deep Water production was enhanced (also referred to as Glacial North Atlantic Intermediate Water; e.g. Oppo *et al.*, 1995; Boyle & Keigwin, 1987).

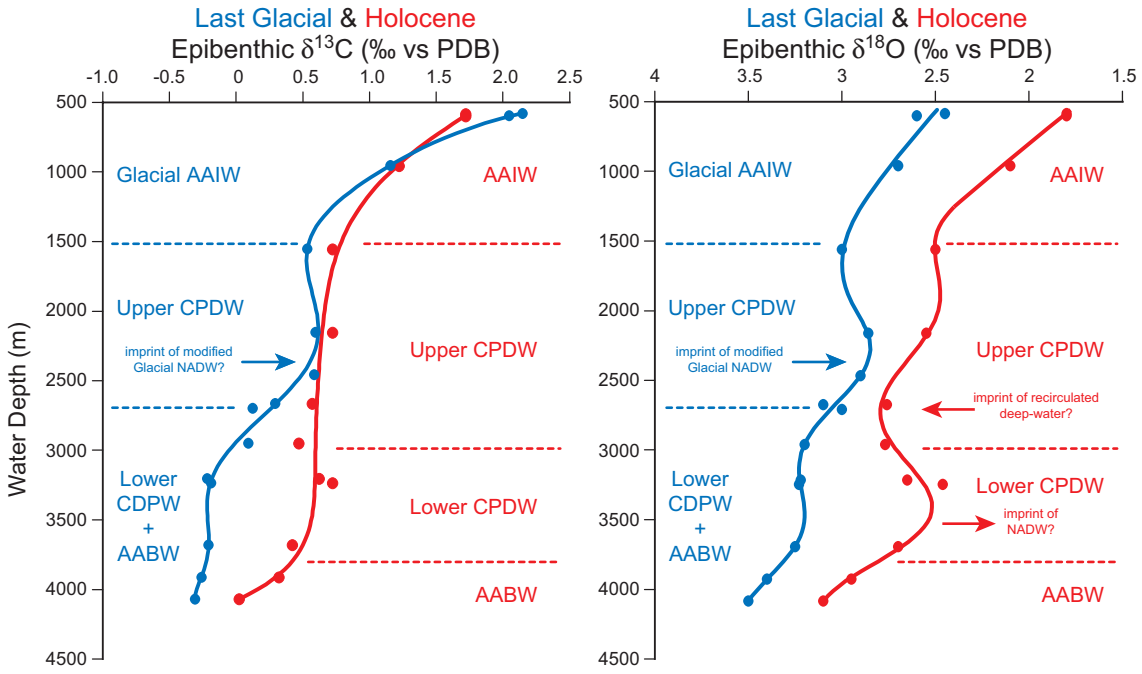

Figure 5-15. Reconstruction of vertical benthic foraminiferal $\delta^{13}C$ and $\delta^{18}O$ gradients in the Australian sector of the Southern Ocean for the Holocene (red) and last glacial maximum (blue). For direct comparison, glacial $\delta^{13}C$ values are corrected for the global ocean $\delta^{13}C$ decrease of 0.32 ‰ (Duplessy *et al.*, 1988) and glacial $\delta^{18}O$ values for the global ice-effect (1.2 ‰; Fairbanks, 1989). The Last Glacial Maximum values were selected on the basis of maximum $\delta^{18}O$ values between 15–20 ka.

Vertical $\delta^{13}C$ and $\delta^{18}O$ profiles for the Holocene and the last glacial maximum are used to reconstruct changes in intermediate- to deep-water circulation in the Australian sector of the Southern Ocean. For a direct comparison between the Holocene and the Last Glacial Maximum (Fig. 5-15), glacial $\delta^{18}O$ values were corrected for the increase in global ice-volume (-1.2 ‰; Fairbanks, 1989) and glacial $\delta^{13}C$ values for the global increase of 0.32 ‰ (Duplessy *et al.*, 1988). The vertical profiles from the Holocene coincide with the modern hydrographic pattern indicating relatively good ventilated Antarctic Intermediate Water above 1,400 m, nutrient enriched Upper Circumpolar Deep Water from 1,400–3,000 m, relatively good ventilated Lower Circumpolar Deep Water from 3,000–3,800 m, and nutrient-enriched Antarctic Bottom Water below. At about 2,700 m water depth maximum in $\delta^{18}O$ is revealed. Lower temperatures or higher salinities probably cause this maximum and may reflect an imprint of recirculated deep-waters from the Indian or Pacific oceans. The admixture of good ventilated and slightly warmer North Atlantic Deep Water to Lower Circumpolar Deep Water can be traced into the Australian sector of the Southern Ocean and is identified by a maximum in $\delta^{13}C$ and a minimum in $\delta^{18}O$ at about 3,300 m water depth. The distribution of $\delta^{18}O$ during the Last Glacial Maximum coincides with the distribution during the Holocene with an average offset of 0.5 ‰ towards higher values corresponding to a glacial temperature drop of about 2°C (assuming the salinity remained constant). The lowest offset occurred between 2,000–2,500 m water depths and

clearly indicates the imprint of warmer Glacial North Atlantic Intermediate Water. The comparison of epibenthic $\delta^{13}C$ profiles between the Holocene and the Last Glacial Maximum indicate only small changes in nutrient concentrations between 1,000–2,700 m water depth, but a decrease in nutrients above 1,000 m and an increase below 2,700 m during glacials. This clearly reflects the global shift of nutrients from intermediate depths into the deep ocean during glacials. In comparison to the $\delta^{18}O$ values, the glacial $\delta^{13}C$ profile is more suitable for identifying the major intermediate- to deep-water masses because it exhibits the strongest gradients (chemoclines):

- Antarctic Intermediate Water above 1,500 m that is marked by high $\delta^{13}C$ values >0.5 ‰.
- Upper Circumpolar Deep Water between 1,500–2,700 m that is strongly influenced by relatively good ventilated Upper North Atlantic Deep Water.
- Nutrient enriched Glacial Lower Circumpolar Deep Water below 2,700 m that may represent a mixture of Antarctic Bottom Water (Ross Sea) and deep-water masses originating from the Atlantic sector of the Southern Ocean.

To examine the spatial extension of deep-waters from the Atlantic sector into the Australian sector of the Southern Ocean, vertical $\delta^{13}C$ gradients for the Holocene and the Last Glacial Maximum are shown for both regions (Fig. 5-16). The mid-depth glacial chemocline at about 2,700 m water depth, separating well-ventilated water above from poorly-ventilated water below, was about 200 m shallower in the Atlantic sector of the Southern Ocean (Hodell *et al.*, 2003). The comparison demonstrates that glacial water masses above 2,000 m are consistently good ventilated as indicated by similar $\delta^{13}C$ values. However, glacial deep-water masses below 2,000 m were better ventilated in the Australian sector than in the Atlantic sector. Accordingly, the Holocene–Last Glacial Maximum $\delta^{13}C$ difference between Upper and Lower Circumpolar Deep Water is less pronounced in the Australian sector. The comparison with the vertical glacial $\delta^{13}C$ gradient from the equatorial Pacific suggests that water masses below 2,700 m are better ventilated than in the Australian sector of the Southern Ocean (Fig. 5-16). Between 1,500–2,500 m, glacial Pacific water masses are more nutrient enriched than in the Southern Ocean. Accordingly, the upper and lower deep-water masses are marked by different regional horizontal $\delta^{13}C$ gradients indicating their source areas. In upper deep-water masses, the degree of ventilation decreases from the South Atlantic via the Australian sector of the Southern Ocean towards the equatorial Pacific, suggesting Glacial Upper North Atlantic Deep Water as a major source. Deep-water masses below 2,700 m are marked by a reversed $\delta^{13}C$ gradient suggesting that glacial deep water in the Australian sector may represent a mixture of relatively good ventilated Pacific Deep Water and nutrient-enriched deep-water masses from the Atlantic sector of the Southern Ocean. This raises the question about the glacial source area of the relatively

good ventilated Pacific Deep Water. Today, the Southern Ocean is the principle source for Pacific deep and bottom water. This was probably also true in the glacial ocean, suggesting the Pacific sector of the Southern Ocean as a possible source.

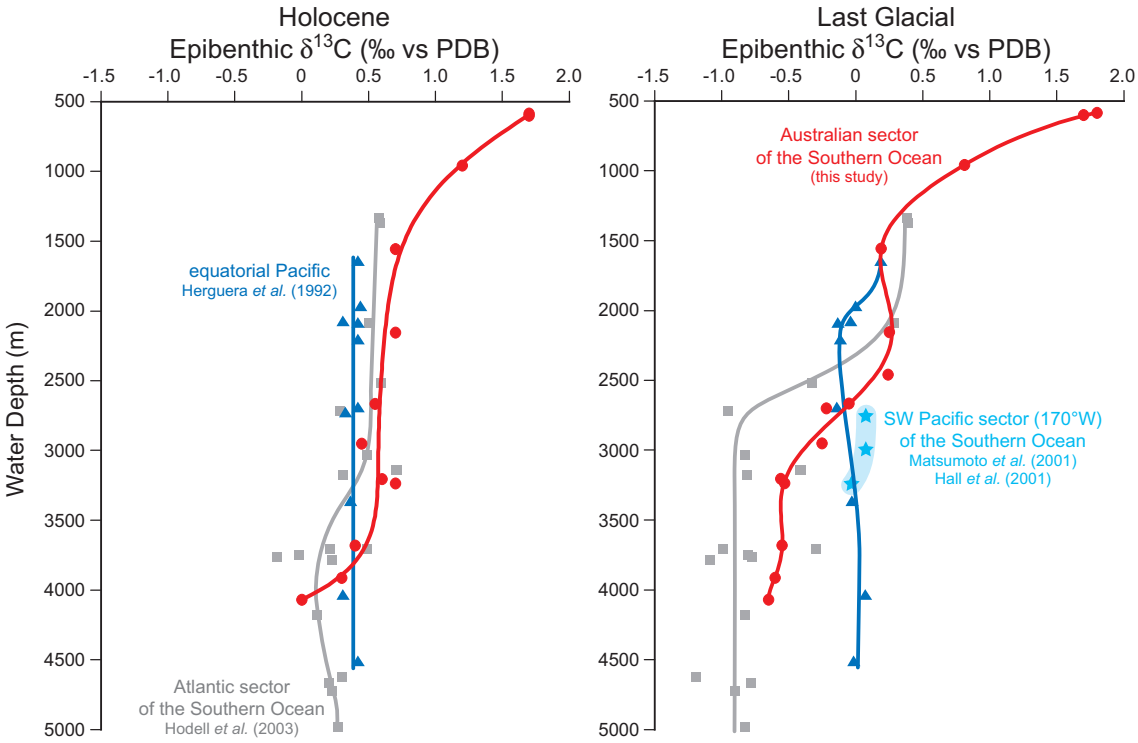

Figure 5-16. Comparison of vertical benthic $\delta^{13}C$ gradients from different sectors of the Southern Ocean and the equatorial Pacific for the Holocene (left) and Last Glacial Maximum (right).

Unfortunately, only few glacial benthic $\delta^{13}C$ data are available from the Pacific sector (Fig. 5-16), which are restricted to water depths between 2,700–3,200 m (Matsumoto *et al.*, 2001; Hall *et al.*, 2001). Below 3,000 m water depth, the $\delta^{13}C$ values are very similar to values from the central deep Pacific, especially those from the southwest Pacific sector. Hence, the Pacific sector of the Southern Ocean, possibly the Ross Sea, may have served as a source area for Pacific deep and bottom water. Today, the supply of deep-water to the Pacific is dominated by a single source, the Deep Western Boundary Current east of New Zealand. Grain size analyses and benthic $\delta^{13}C$ records from North Chatham Drift (ODP Site 1123, 3,300 m water depth) suggest a strengthened glacial deep-water flow into the Pacific probably related to increased production of Antarctic Bottom Water (Hall *et al.*, 2001). Glacial Upper North Atlantic Deep Water, modified during its route through the Southern Ocean, may have contributed as a significant component for the formation of Glacial Antarctic Bottom Water in the Ross Sea, because glacial $\delta^{13}C$ values of both water masses are very similar. This would also support the "Pacific-type" pattern of enhanced carbonate preservation during glacials. Towards the east, the sills of the Drake Passage block the direct inflow of relatively good ventilated

Pacific water masses below 3,200 m water depth into the South Atlantic, which is characterized by the lowest $\delta^{13}C$ values (Fig. 5-16). Above 3,200 m, the inflow of more nutrient-enriched Pacific water masses may have contributed to lower the $\delta^{13}C$ signature of Antarctic Bottom Water formed in the Weddell Sea. Although this hypothesis remains speculative due to the lack of $\delta^{13}C$ records in the vicinity of the Drake Passage, it is assumed that the modern Southeast Pacific comprises a major return route of nutrient enriched water masses from the North Pacific at about 2,500 m. Comparison of glacial $\delta^{13}C$ values from the equatorial Pacific indicate that the mid-depth eastern Pacific was more nutrient enriched (Mix *et al*., 1991; Matsumoto *et al*., 2002). This however, cannot fully explain the extremely low $\delta^{13}C$ values in the deep Atlantic sector of the Southern Ocean. On the one hand a productivity-related phytodetritus effect may have reduced glacial benthic $\delta^{13}C$ values in the Atlantic sector (Mackensen *et al*., 2001). On the other hand reduced air-sea gas exchange due to extended sea-ice coverage in the Weddell Sea may have contributed to low preformed Antarctic Bottom Water $\delta^{13}C_{DIC}$ values.

Further insights into endmember-signatures of glacial water masses are presented in Figure 5-17 showing the relationship between benthic $\delta^{13}C$ and $\delta^{18}O$ for water masses below 2,500 m water depth from different oceanic regions. This relationship clearly separates the water mass signatures of the Southern Ocean, the Pacific and the North Atlantic as first described by Duplessy *et al*. (2002). This comparison indicates that the Southern Ocean deep-waters were extremely cold and nutrient-enriched during the Last Glacial Maximum. The cluster of North Atlantic values exhibits a great variability, suggesting that the deep-waters in this basin were not homogenous probably due to sinking of different surface-waters at various locations during winter. The North Atlantic, however, is clearly separated from the Southern Ocean by its better-ventilated water masses. The Pacific and South Atlantic clusters can be distinguished from the North Atlantic and the Southern Ocean by medium deep-water ventilation and higher temperatures inferred from lighter $\delta^{18}O$ values. The cluster of the Australian sector of the Southern Ocean provides for the first time the missing link between the Southern Ocean and the Pacific. This strong link has already been demonstrated in Figures 5-15 & 5-16 and confirms the hypothesis of enhanced deep-water formation in the Ross Sea affecting both, the Australian sector of the Southern Ocean and the Pacific. The $\delta^{18}O$–$\delta^{13}C$ relationship for the Indian Ocean and from the South Australian Bight (continental margin) indicate deep-water masses that are medium ventilated but showing the lightest $\delta^{18}O$ values. The strong difference between the Australian sector of the Southern Ocean and the Australian Bight identifies the postulated return flow from the West Australia Basin that turns into the eastward-flowing deep northern boundary current that has been postulated to have played an important role also for explaining the observed regional change in glacial carbonate dissolution patterns.

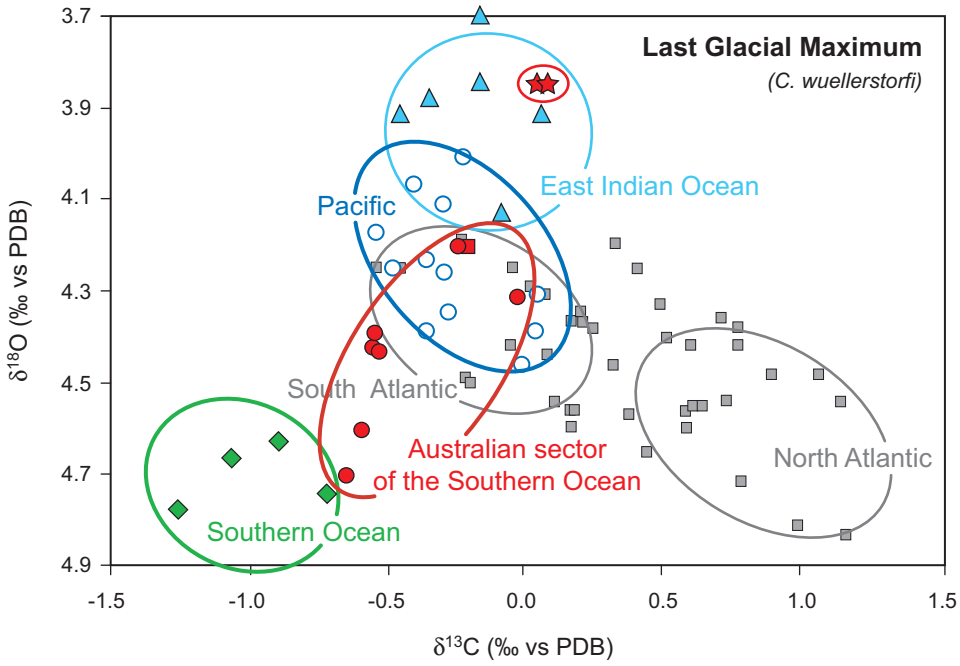

Figure 5-17. Relationship between benthic foraminiferal $\delta^{18}O$ (without correction for specific fractionation) and $\delta^{13}C$ in Last Glacial Maximum deep sediment cores (below 2,500 m) from different ocean Basins (modified from Duplessy *et al.*, 2002). In addition to the data collection from Duplessy *et al.* (2002), data from the East Indian Ocean (light blue; from Petersen, 1984), the continental slope off the South Australian Bight at ~130°E (red stars; from McCorkle et al., 1998) and from the Australian sector of the Southern Ocean (red; this study) have been plotted as well. The heaviest $\delta^{13}C$ values are found in the North Atlantic cores, whereas intermediate values between 0 ‰ and -0.5 ‰ are found in the South Atlantic, Pacific and Indian oceans. The lightest values lower than -0.5 ‰ are found only in the Southern Ocean. Values from the Australian sector lie in between the Southern Ocean and Indo-Pacific cluster and suggest some kind of mixing between deep-water masses.

The $\delta^{13}C$ pattern observed for the Last Glacial Maximum is reproduced for most glacial stages during the last 500 kyr indicating a contrasting response to upper and lower deep-water masses in the Australian sector. This is demonstrated in Figure 5-18, showing the change in deep-water ventilation from 2,000 m to 3,000 m and from 3,000 m to 4,000 m water depth. Both records are surprisingly good anti-correlated. During interglacial climate optima (MIS 11.3, 9.3, 7.5, 5.5, 1.1), the injection of North Atlantic Deep Water into the Circumpolar Deep Water results in relatively good ventilated water masses down to 3,200 m water depth. Hence, upper deep-water masses between 2,100 m and 3,200 m are equally good ventilated ($\Delta\delta^{13}C \approx 0$ ‰). During glacial maxima, North Atlantic Deep Water was converted to an intermediate water mass, ventilating the Southern Ocean above ~2,500 m. Accordingly, large gradients towards weaker ventilated water masses mark the $\delta^{13}C$ profiles from 2,100 m to 3,200 m water depth. An opposite glacial/interglacial pattern characterizes the deep Southern Ocean below 3,200 m. During glacial intervals, the difference in $\delta^{13}C$ is generally low between 3,200–4,100 m indicative of only small changes in deep-water ventilation. Differences in $\delta^{13}C$ increased during interglacial events when the influence of good ventilated North Atlantic Deep Water expanded

to depth greater than 3,200 m but shallower than 4,100 m. This pattern reflects the glacial shift of nutrient concentrations into the deeper ocean caused by reduced formation of Lower North Atlantic Deep Water.

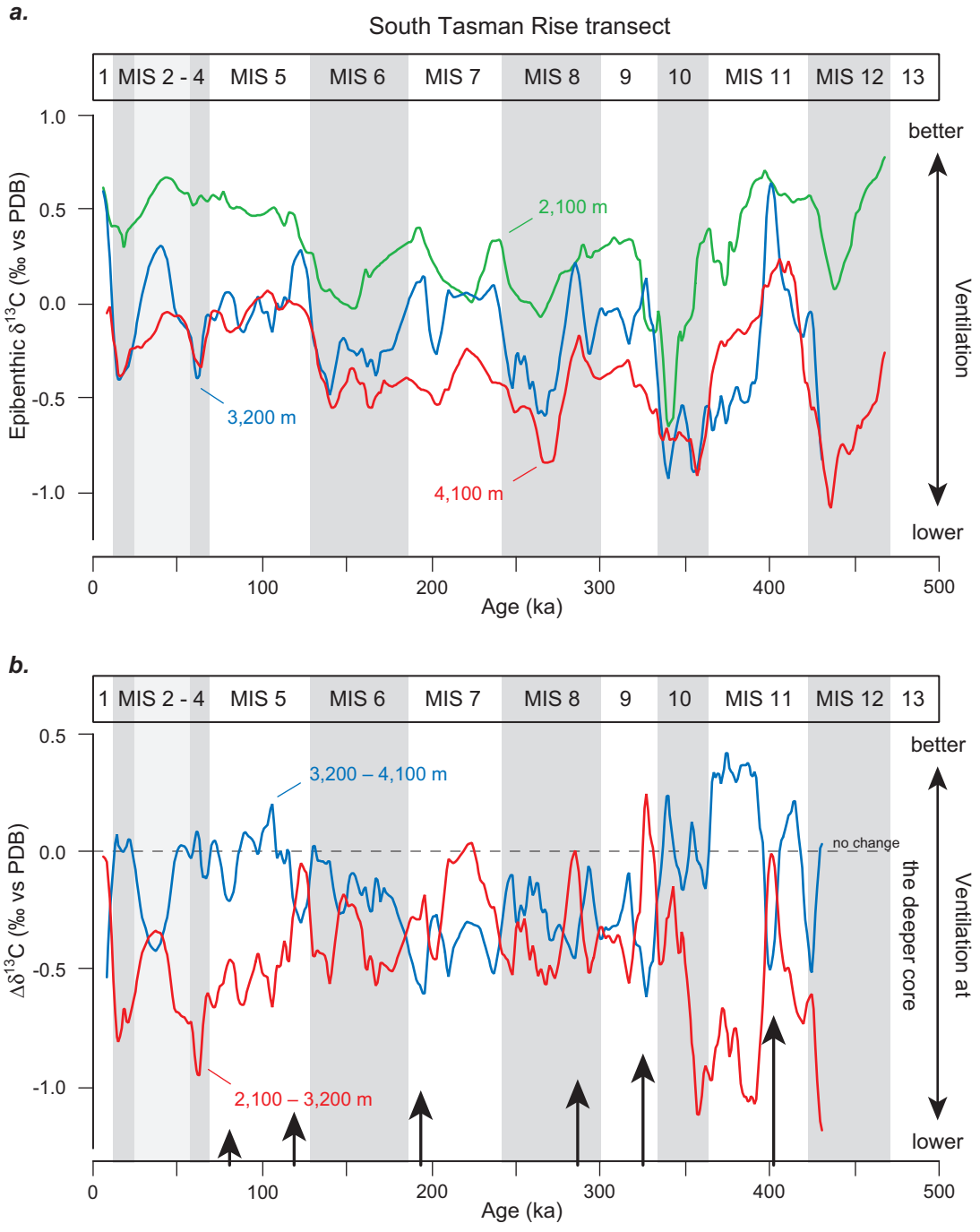

Figure 5-18. Changes in deep-water ventilation between 2,100–4,100 m water depths at the South Tasman Rise transect. (a) Averaged benthic foraminiferal $\delta^{13}C$ records (3-point running mean) from MD97-2108 (green), SO136-163 (blue) and SO136-164 (red) are shown for comparison. (b) Vertical benthic $\delta^{13}C$ gradients from 2,100–3,200 m (blue) and 3,200–4,100 m (red) reveals a strong anticorrelation in changes between both water levels. In general, more negative values indicate relatively less-ventilated water masses at the deeper core. Arrows mark interval of strongest carbonate dissolution.

The difference in $\delta^{13}C$ between 3,200–4,100 m is also positively correlated with changes in carbonate preservation. During interglacials, the relative increase in nutrients and CO_2 from 3,200–4,100 m corresponds to increased carbonate dissolution (Fig. 5-18). The glacial differences in $\delta^{13}C$ from 3,200–4,100 m are close to zero, because the signal of the glacial transfer of nutrients into the deep ocean is eliminated by the difference. This relative reduction in nutrients is associated with increased carbonate preservation. This also indicates that the glacial relationship between $\delta^{13}C$ and alkalinity was decoupled as the Pacific buffered the strong dissolution in the Atlantic.

On a longer-term scale, differences in $\delta^{13}C$ between 3,200-4,100 m are low during the last 120 kyr. This time interval comprises carbonate dissolution events that are less strong developed when compared to the interval from 120–500 ka (Fig. 5-18). Prior to 120 ka, strong carbonate dissolution events are associated with a reduction in deep-water ventilation as indicated by an increased difference in $\delta^{13}C$ between 3,200–4,100 m. An outstanding feature characterizes the time interval from 360–390 ka (late MIS 11 and transition to MIS 10). This interval is marked by largest differences in $\delta^{13}C$ from 3,200 m towards shallower and deeper water masses because deep-water ventilation is lowest at 3,200 m. This pattern is associated with low but increasing carbonate preservation probably associated with increased formation of relatively good ventilated Antarctic Bottom Water.

CHAPTER 6

SURFACE- TO INTERMEDIATE-WATER CIRCULATION DURING THE LAST 500 KYR

Four planktonic $\delta^{18}O$ records from the South Tasman Rise transect were examined to monitor Pleistocene changes in upper ocean water-mass signatures. These records form a latitudinal transect from 48.5°S to 44.5°S and provide evidence for glacial-interglacial shifts of the frontal system, especially for the Subtropical Front. This area is marked by strong gradients in sea-surface temperatures and salinities caused by the southward flowing East Australian Current, which transports relatively warm and saline water masses of tropical origin into the subantarctic sector, which is dominated by cooler and less saline surface water masses. Today, the East Australian Current dominates the water-mass signatures at sediment core FRG94-003 (44.5°S), whereas sediment cores MD97-2108 (48.5° S) is positioned in subantarctic waters. Sediment cores and SO136-163 (45.5° S) and SO136-162 (46°S) are located in the transition zone between subtropical and subantarctic waters. The comparison of $\delta^{13}C$ and $\delta^{18}O$ records of *G. bulloides* provide information about regional changes in the upper 50 m of the water column, accordingly to their preferential depth habitat (e.g. Niebler, 1999). Vertical changes in water-mass signatures are derived from isotopic comparisons between the shallow-dwelling planktonic foraminifer *G. bulloides* and the deeper-dwelling planktonic foraminifers *G. inflata* and *G. truncatulinoides* at sediment core SO136-163. The benthic $\delta^{18}O$ record from core SO136-061 at 600 m water depth complements the depth-transect, although located further southeast at Campbell Plateau. This vertical transect of isotope records has been generated in the hope to gain insights into the variability of glacial-interglacial formation and expansion of Subantarctic Mode Water that is strongly coupled to changes in the frontal system. This variability is of special interest, because Subantarctic Mode Water together with Antarctic Intermediate Water are hypothesized to ventilate thermocline waters in the tropical Pacific (Ninnemann *et al.*, 1997; Spero & Lea, 2002) and may have acted as a conduit for transferring $\delta^{13}C$ variability from high to low latitudes.

6.1 RESULTS

Latitudinal transect of Pleistocene changes in surface water signatures deduced from G. bulloides isotope records

The planktonic oxygen isotope records from the South Tasman Rise transect are marked by high amplitude fluctuations. In general, the $\delta^{18}O$ amplitudes at glacial terminations range between 2–2.5 ‰. As the global ice-volume effect at terminations was close to 1.2 ‰ (Fairbanks, 1989), a large part of isotope variability (0.8–1.3 ‰) has to be ascribed to changes in temperature and/or salinity. Cores SO136-162 and SO136-163 reveal the highest $\delta^{18}O$ amplitudes. Today, both cores are positioned close to the Subtropical Front, which separates subtropical and subantarctic surface-waters. During interglacial maxima, both cores show $\delta^{18}O$ values that are similar to the northernmost core FRG94-003. In contrast, glacial $\delta^{18}O$ values are similar to those from the southernmost core MD97-2108. This suggests an interglacial position of the Subtropical Front between 46.3°–48.3°S and a glacial position between 44.2–46.5°S. In total, the glacial-interglacial variability of the Subtropical Front south of Tasmania is relatively small and would correspond to a latitudinal northward shift of about 2 degrees during glacials.

Today, summer sea-surface temperatures and sea-surface salinities at the South Tasman Rise transect decrease southward from 16° to 11°C and from 35.1 to 34.6, respectively. This would approximate to a southward increase in $\delta^{18}O$ values of 0.85 ‰, which on average would match the Pleistocene difference in $\delta^{18}O$ of 0.5–1 ‰ across the transect (FRG94-003 to MD97-2108). An outstanding feature characterizes the glacial intervals of the last 200 kyr, when considering all $\delta^{18}O$ records across the transect. During MIS 2, 4 and 6, $\delta^{18}O$ values at the southernmost core MD97-2108 appear to be lower than those at the more northern cores SO136-163 and SO136-162. This is in conflict with a generally southward temperature decrease. The lighter glacial $\delta^{18}O$ values at core MD97-2108 thus clearly reflect a decrease in sea-surface salinities towards the south, which strongly overprints the $\delta^{18}O$ temperature signal. This glacial feature is not observed for the time-interval prior to 200 ka. During the last 200 kyr, the glacial presence of less saline surface-water at the position of core MD97-2108 may represent the northward expansion of Circumpolar Surface Water, which is today characterized by the lowest salinities in the Southern Ocean. On the other hand, enhanced summer melting of icebergs and sea-ice around Antarctica or changes in the precipitation/evaporation ratio may have lowered sea-surface salinities during glacial summers. In the absence of an additional independent temperature proxy (e.g. Mg/Ca paleo-thermometry) further derivations remain rather speculative.

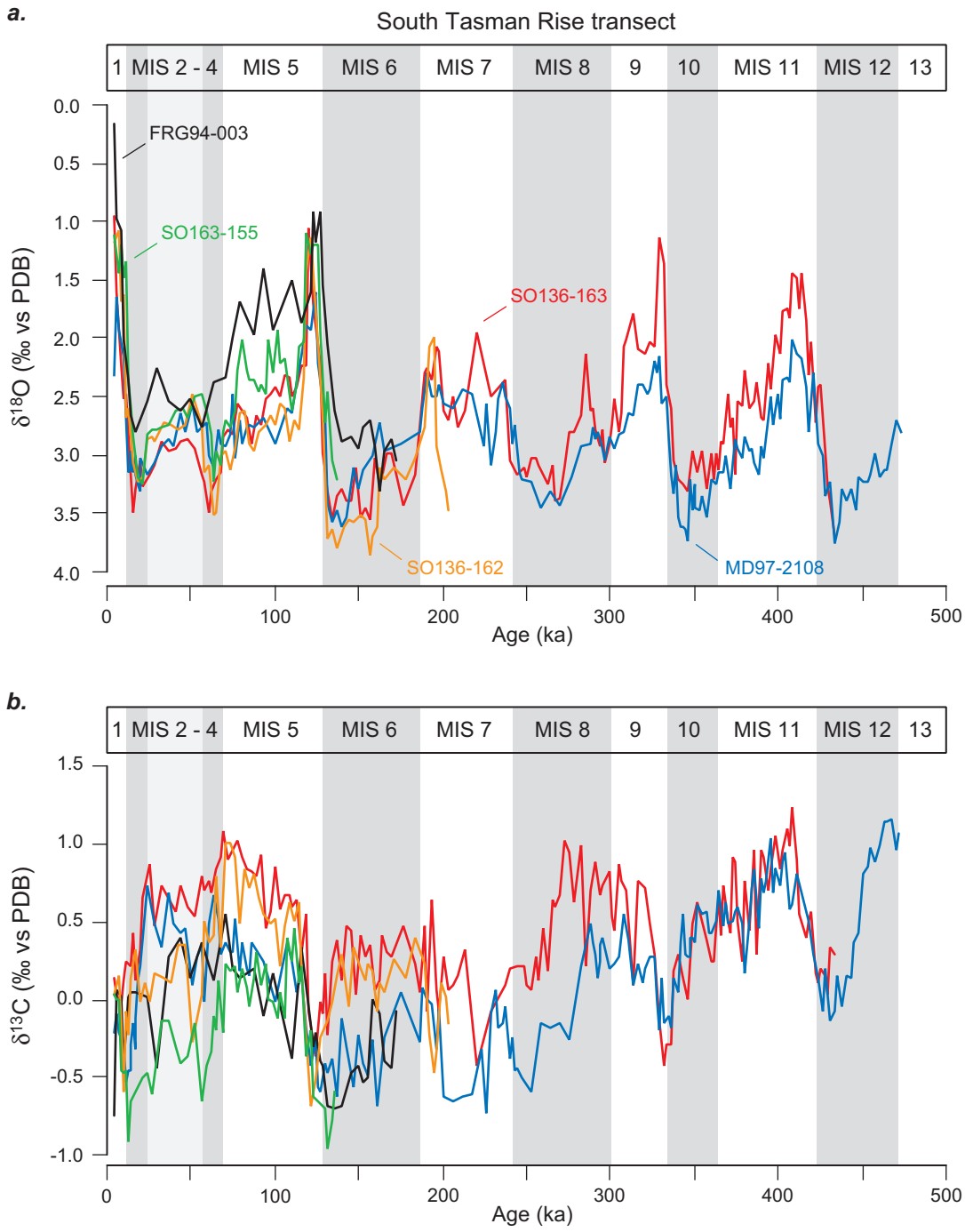

Figure 6-1. Planktonic oxygen (a) and carbon (b) isotope records (*G. bulloides*) from the South Tasman Rise transect as a function of age.

The $\delta^{13}C$ records are summarized in Figure 6-1b. In general, temporal fluctuations in $\delta^{13}C$ are generally good correlated across the latitudinal transect, although no clear relationship exists between climate change and $\delta^{13}C$. The southernmost and northernmost records of the latitudinal transect display the highest $\delta^{13}C$ values whereas the records from cores SO136-163 and SO136-162 are marked by lower $\delta^{13}C$ values. Thus, changes of Subtropical Front cannot be reconstructed from the $\delta^{13}C$ records, as $\delta^{13}C$ values are similar at the north and south. Moreover,

changes in productivity, nutrient utilization of the biological pump and air-sea gas-exchange may have altered $\delta^{13}C$ records of surface waters in different ways and thus will not be considered for further discussions. The only feature that is typical for all $\delta^{13}C$ records is the significant $\delta^{13}C$ minimum occurring at all glacial terminations persisting into the subsequent climate optima (e.g. Termination II – MIS 5.5). This drop has been suggested to be associated with the warming of around Antarctica whereas the increase is possibly related to enhanced North Atlantic Deep Water production at climatic optima, which will be discussed later.

Isotopic evidence for vertical changes in the water column (0–600 m)

Planktonic isotope records from *G. bulloides* and the deeper dwelling foraminifers *G. inflata* and *G. truncatulinoides* are used to reconstruct vertical changes in Pleistocene water mass signatures (sediment core SO136-163). *G. inflata* has been shown to calcify at water depth between 50–150 m (Niebler, 1999) and *G. truncatulinoides* at depth of ≥250 m. The benthic isotope record from SO136-061 (50°S) provides additional information about isotopic changes at 600 m water depth. The $\delta^{18}O$ records are summarized in Figure 6-2. Today, temperatures decrease from 14°C at the surface to 9°C at 600 m water depth. The decrease in salinity is relatively low and drops by about 0.2 PSU. This would correspond to an increase in $\delta^{18}O$ of about 0.8 ‰. The $\delta^{18}O$ difference between the shallow-dweller *G. bulloides* and the benthic foraminifer *C. wuellerstorfi* at 600 m water depth varied over the last 150 kyr between 0.6–1.0 ‰, roughly reflecting the modern $\delta^{18}O$ difference. The deep-dwelling foraminifers record the expected temperature decrease and show $\delta^{18}O$ values that are in general higher than *G. bulloides* values and lighter than benthic values from 600 m water depth. Unfortunately, the benthic isotope record only covers the last 150 kyr. More interesting, however, is the time-interval prior to 170 ka, where the deep-dweller *G. truncatulinoides* presents $\delta^{18}O$ values that are up to 0.5–0.8 ‰ lower than those from the shallower-dwelling foraminifers *G. bulloides* and *G. inflata*. This would be in conflict with a general vertical decrease in temperature and can be explained by a salinity decrease characterizing the depth habitat of *G. truncatulinoides* at ≥250 m. Assuming a vertical decrease in water temperatures similar to the last 170 kyr, the observed isotopic change prior to 170 ka would correspond to a salinity decrease on the order of 1 PSU. Such low salinity values suggest a stronger influence of Antarctic Intermediate Water possibly in response to a northward shift of the Antarctic Polarfront moving the source regions of Antarctic Intermediate Water closer to the core location.

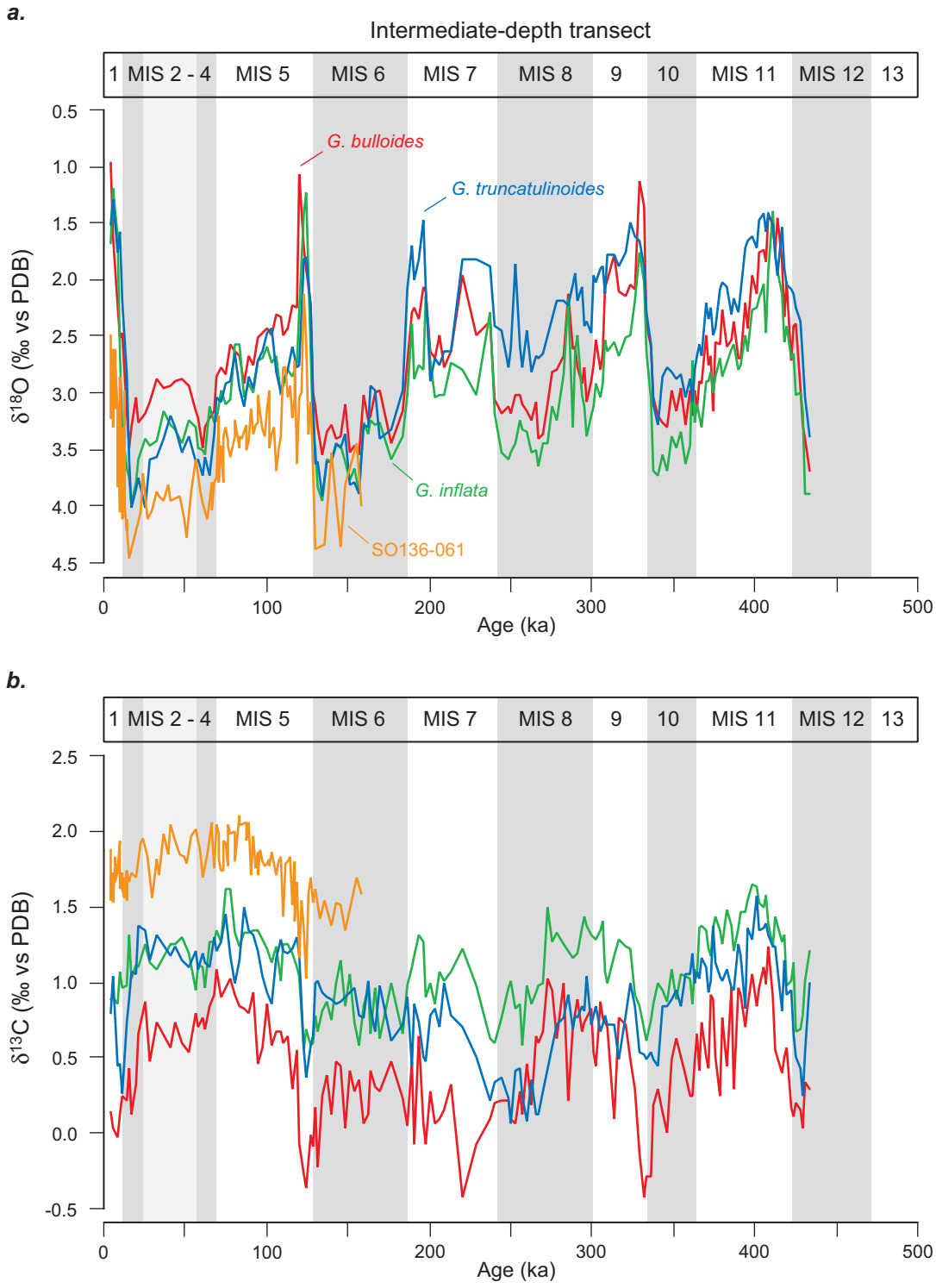

Figure 6-2. Intermediate-water depths transect based on planktonic isotope records from *G. bulloides* (red) and the deeper dwelling foraminifers *G. inflata* (green) and *G. truncatulinoides* (blue) from sediment core SO136-163, and the epibenthic isotope records from SO136-061 (602 m water depth): (a) oxygen isotope records and (b) carbon isotope records as a function of age.

6.2 DISCUSSION

The latitudinal transect of planktonic oxygen isotope records along South Tasman Rise suggests glacial/interglacial migrations of the Subtropical Front on the order of 2° indicating a Holocene position between 46.3°–48.3°S and a position between 44.2°–46.5°S for the Last Glacial Maximum. This is consistent with sea-surface temperature reconstructions from this region that were based on diatom and planktonic foraminifera assemblages (Armand, 1997; Passlow *et al*., 1997). Both studies suggest a glacial position close to 45°S and an interglacial position similar to the modern one at 47°S. Larger fluctuations have been reported for the Indian sector of the Southern Ocean and for the Australian sector west of Tasmania identifying a 5° northward shift of the Subtropical Front for the Last Glacial Maximum (Prell *et al*., 1980; Howard & Prell, 1992). The latitudinal transect of planktonic isotope records along the South Tasman Rise suggests a long-term southward migration of the Subtropical Front with a general more northern position during interglacial MIS 11 and 9 and a more southern position during MIS 1, 5 and 7. This is indicated by a decreasing difference in planktonic isotope records between MD97-2108 (48.3°S) and SO136-163 (46°S) over the last 250 kyr (Fig 6-1). This long-term interglacial southward displacement of the Subtropical Front is consistent with results from Nürnberg *et al*. (in press). These authors examined changes in surface-water productivity in the Tasmanian sector of the Southern Ocean. The southward displacement was recognized by a southward shift of the subantarctic high productivity belt. The latitudinal transect of sediment records along the South Tasman Rise is positioned within the elongated axis of the East Australian Current and thus is sensitive to changes in the strength. Hence, the southward expansion of subtropical surface-water masses associated with a southward shift of the Subtropical Front during interglacial MIS 1, 5 and 7 may have resulted from a strengthened East Australian Current. A similar effect may have occurred if the interglacial stages MIS 1, 5 and 7 were warmer on Antarctica than those prior to 250 ka (MIS 9 and 11), which however was not the case as indicated by the temperature record from the Vostok ice-core (Vimeux *et al*., 2001).

Comparisons of $\delta^{18}O$ records from shallow- and deep-dwelling planktonic foraminifers at sediment core SO136-163 suggest a long-term change in salinity at water depths >250 m. From 420–170 ka, salinities appeared to be lower than during the last 170 kyr. This suggests a stronger influence of Circumpolar Surface Water in response to a more northern position of the Antarctic Polarfront, moving the source regions of Antarctic Intermediate Water closer to the core location. This result agrees with the more northern position of the Subtropical Front prior to 250 ka as indicated by the latitudinal $\delta^{18}O$ transect from *G. bulloides*.

The most striking feature in $\delta^{13}C$ records from shallow- and deep-dwelling planktonic foraminifers is the presence of strong $\delta^{13}C$ minima at glacial terminations, which is of global

importance. Such minima in planktonic $\delta^{13}C$ are already known from the subantarctic Atlantic and Indian sectors of the Southern Ocean (Ninnemann *et al*., 1997). Spero & Lea (2002) demonstrated that the onset of $\delta^{13}C$ minimum events, the initiation of Southern Hemisphere warming and the $\delta^{13}C$ minimum in the Antarctic atmospheric record occurred simultaneously. This suggests that the deglacial events were a response to the breakdown of surface-water stratification, renewed circumpolar deep-water upwelling, and advection of low $\delta^{13}C$ waters to the convergence zone at the Subantarctic Front where intermediate waters are formed. As such minima at the beginning of glacial terminations are also documented in planktonic $\delta^{13}C$ from the equatorial Pacific, a close link between high- and low-latitude surface waters has been proposed. Ninnemann *et al*. (1997) assumed that Antarctic Intermediate Water acted as a conduit for transferring the subantarctic $\delta^{13}C$ signal into the low latitudes. So far, this link has not been documented due to the lack of subantarctic $\delta^{13}C$ records from intermediate water depth. The $\delta^{13}C$ record from the deep-dwelling planktic foraminifer *G. truncatulinoides* (SO136-163) and the epibenthic $\delta^{13}C$ record from Campbell Plateau at 600 m water depth (SO136-061) could trace these $\delta^{13}C$ minima for the first time into intermediate water depth. The epibenthic $\delta^{13}C$ record, however, reveals a clear and pronounced $\delta^{13}C$ minimum only at glacial Termination II. This would at least corroborate the hypothesis that Subantarctic Mode Water and Antarctic Intermediate Water ventilated the equatorial thermocline in the Pacific during glacial Termination II.

CHAPTER 7

CONCLUSIONS

Glacial/interglacial changes in surface, intermediate and deep-water circulation as well as variations in deep-water ventilation and carbonate chemistry were reconstructed for the last 500,000 years from 15 sediment records of the Australian sector of the Southern Ocean. These reconstructions are based on high-resolution stable isotope records and proxy records of carbonate dissolution and led to the following new insights:

- The Australian sector of the Southern Ocean has been identified to represent the southernmost expansion of the "Pacific-type" pattern of carbonate preservation characterized by increased dissolution during interglacials and enhanced preservation during glacials. This pattern persisted through glacial/interglacial stages and expanded westward up to ~110°E. West of 110°E, the Southern Ocean is marked by the reversed "Atlantic-type" pattern of carbonate preservation. This boundary marks the contrasting flow of water masses carrying opposite signs of alkalinity and mixing at ~110°E. In general, carbonate preservation improved during the last 250 kyr, which is consistent with an increase in deep-water ventilation as indicated by epibenthic $\delta^{13}C$ records. The increase in carbonate preservation over the last 250 kyr has been globally recognized and thus, seems to represent a general decrease in whole ocean alkalinity. This improvement was also associated with an eastward retreat of the "Pacific-type" carbonate preservation pattern to 114°E. The presence of the "Pacific-type" pattern suggests that deep-waters in the Australian sector flowed westwards against the predominant eastward drift in the Southern Ocean.
- Reconstructions of the Pleistocene lysocline depth are based on records of planktonic fragmentation ratios assuming that the 40 %-fragmentation value can be used to assess the lysocline level. The 40 %-fragmentation value characterizes the modern lysocline level at ~3,600 m water depth in the Western Tasman Basin. In general, the Pleistocene reconstructions (0–500 ka) suggest lysocline fluctuations between ≥4,100 m (glacial) and ≤3,200 m (interglacial) for the Australian sector of the Southern Ocean. During MIS 2 and 6 the lysocline was deeper than 4,100 m, while the lysocline was always shallower during earlier glacial isotope stages, e.g. above 3,800 m at MIS 8.4–7.2 and 10. Interglacial stages MIS 7.1, 8.5, 9 and 11 are marked by the strongest dissolution associated with lysocline levels shallower than 3,200 m.

- The comparison of carbonate dissolution and epifaunal benthic $\delta^{13}C$ suggests increased carbonate preservation during glacials when deep-water ventilation was reduced. However, the intermediate- to deep-water $\delta^{13}C$ gradient (eliminates the regional glacial/interglacial background) is positively correlated with changes in carbonate dissolution. Hence, increased carbonate dissolution during interglacials coincides with a depth-related net decrease in deep-water ventilation.
- The intermediate- to deep-water epifaunal benthic $\delta^{13}C$ profile identifies strong gradients during glacials and allows to separate 3 major glacial water masses in the Australian sector of the Southern Ocean:
  - Antarctic Intermediate Water above 1,500 m that is marked by high $\delta^{13}C$ values >0.5 ‰.
  - Upper Circumpolar Deep Water between 1,500–2700 m that is strongly influenced by modified, relatively good ventilated Upper North Atlantic Deep Water.
  - Nutrient enriched Lower Circumpolar Deep Water below 2,700 m that may represent a mixture of Antarctic Bottom Water from the Ross Sea and deep-water masses originating from the Atlantic sector of the Southern Ocean.
- The epifaunal benthic isotope records from the Australian sector provide the missing link in glacial deep-water circulation as $\delta^{18}O$ and $\delta^{13}C$ signatures below 2,500 m water depth occur on the mixing line between two deep-water endmembers: cold and poorly ventilated water masses from the Atlantic sector of the Southern Ocean, and warmer and relatively good ventilated deep-waters from the central Pacific. This suggests a westward deep-water flow south of Australia, which is consistent with the "Pacific-type" pattern of carbonate preservation.
- In a more global perspective, glacial $\delta^{13}C$ data suggest two major source regions for deep-waters below 2,500 m water depth (referenced here as Glacial Antarctic Bottom Water), the Weddell Sea in the Atlantic sector and the Ross Sea in the SW Pacific sector of the Southern Ocean. Glacial Antarctic Bottom Water formed in the Weddell Sea possibly suffered from strongly reduced air-sea gas exchange due to persistent sea-ice coverage and increased contribution of older, recirculated Pacific water with low preformed $\delta^{13}C$ masses via the Drake Passage. Deep-waters originating from the Weddell Sea were marked by the lowest $\delta^{13}C$ values in the glacial ocean. In contrast, Glacial Antarctic Bottom Water formed in the SW Pacific sector of the Southern Ocean was marked by higher $\delta^{13}C$ values and therefore depicts better-ventilated water masses. It is very likely that the well-ventilated water masses between 1,400–2,400 m (identified as modified Upper North Atlantic Deep Water) contributed via upwelling to the formation of Antarctic Bottom Water in the Ross Sea.

- The latitudinal transect of planktonic oxygen isotope records along South Tasman Rise suggests glacial/interglacial migrations of the Subtropical Front on the order of 2° indicating a position between 44.2° and 46.5°S for the Last Glacial Maximum. This is consistent with other reconstructions of this region.
- Comparisons of $\delta^{18}O$ records from shallow- and deep-dwelling planktonic foraminifers suggest a long-term change in salinity at a water depth of >250 m. From 420–170 ka, salinities appeared to be lower than during the last 170 kyr, which is paralleled by a long-term southward shift of the frontal system.
- Planktonic $\delta^{13}C$ records revealed strong $\delta^{13}C$ minima at glacial terminations. These $\delta^{13}C$ minima have been traced for the first time into the Antarctic Intermediate Water as indicated by an epifaunal benthic $\delta^{13}C$ record from the Campbell Plateau at 600 m water depth. This corroborates the recent hypothesis that the intermediate waters may have acted as a conduit for transferring the subantarctic $\delta^{13}C$ variability to low latitudes, because the timing of $\delta^{13}C$ changes are similar to those observed in the tropical Pacific.

8. REFERENCES

Adkins, J.F., McIntyre, K., and Schrag, D.P., 2002, The Salinity, Temperature, and $\delta^{18}O$ of the Glacial Deep Ocean: Science, v. 298, p. 1769-1773.

Alley, R.B., and Clark, P.U., 1999, The deglaciation of the northern hemisphere; a global perspective: Annual Review of Earth and Planetary Sciences, v. 27, p. 149-182.

Archer, D., and Maier, R.E., 1994, Effect of deep-sea sedimentary calcite preservation on atmospheric CO_2 concentration: Nature (London), v. 367, p. 260-263.

Armand, L.K., 1997, The use of diatom transfer functions in estimating sea-surface temperature and sea-ice in cores from the southeast Indian Ocean [PhD thesis]: Canberra, The Australian National University.

Arrhenius, G.O.S., 1952, Sediment cores from the east Pacific: Rep. Swed. Deep Sea Exped. 1947-1948, p. 1-228.

Bassinot, F.C., Labeyrie, L.D., Vincent, E., Quidelleur, X., Shackleton, N.J., and Lancelot, Y., 1994, The astronomical theory of climate and the age of the Brunhes-Matuyama magnetic reversal: Earth and Planetary Science Letters, v. 126, p. 91-108.

Belanger, P.E., Curry, W.B., and Matthews, R.K., 1981, Core-top evaluation of benthic foraminiferal isotopic ratios for paleo-oceanographic interpretations, *in* Berger, W.H., Be, A.W.H., and Vincent, E., eds., Oxygen and carbon isotopes in foraminifera: Palaeogeography, Palaeoclimatology, Palaeoecology, v. 33, p. 205-220.

Belkin, I.M., and Gordon, A.L., 1996, Southern Ocean fronts from the Greenwich meridian to Tasmania: Journal of Geophysical Research, v. 101, p. 3675-3696.

Berger, A., and Loutre, M.F., 1991, Insolation values for the climate of the last 10 million years: Quaternary Science Reviews, v. 10, p. 297-317.

Berger, W.H., 1970, Planktonic Foraminifera; selective solution and the lysocline: Marine Geology, v. 8, p. 111-138.

Berger, W.H., Bonneau, M.C., and Parker, F.L., 1982, Foraminifera on the deep-sea floor; lysocline and dissolution rate: Oceanologica Acta, v. 5, p. 249-258.

Berger, W.H., 1978, Sedimentation of deep-sea carbonate; maps and models of variations and fluctuations: Journal of Foraminiferal Research, v. 8, p. 286-302.

Bickert, T., 1992, Rekonstruktion der spätquartären Bodenwasserzirkulation im östlichen Südatlantik über stabile Isotope benthischer Foraminiferen [Ph.D. thesis]: Bremen, Universität Bremen.

Bickert, T., and Wefer, G., 1996, Late Quaternary deep water circulation in the South Atlantic: Reconstruction from carbonate dissolution and benthic stable isotopes, *in* Wefer, G., Berger, W.H., Siedler, G., and Webb, D.J., eds., The South Atlantic: Present and Past Circulation: Berlin Heidelberg New York, Springer, p. 599-620.

Bickert, T., Cordes, R., and Wefer, G., 1997, Late Pliocene to mid-Pleistocene (2.6-1.0 M.Y.) carbonate dissolution in the western Equatorial Atlantic; results of Leg 154, Ceara Rise, *in* Shackleton, N.J., Curry, W.B., Richter, and Bralower, T.J., eds., Proc. ODP, Sci. Results, 154: College Station, TX, Ocean Drilling Program, p. 229-237.

Billups, K., Ravelo, A.C., and Zachos, J.C., 1998, Early Pliocene deep water circulation in the western Equatorial Atlantic; implications for high-latitude climate change: Paleoceanography, v. 13, p. 84-95.

Blunier, T., Chappellaz, J., Schwander, J., Daellenbach, A., Stauffer, B., Stocker, T.F., Raynaud, D., Jouzel, J., Clausen, H.B., Hammer, C.U., and Johnson, S.J., 1998, Asynchrony of Antarctic and Greenland climate change during the last glacial period: Nature (London), v. 394, p. 739-743.

Blunier, T., and Brook, E.J., 2001, Timing of millennial-scale climate change in Antarctica and Greenland during the last glacial period: Science, v. 291, p. 109-112.

Boyle, E.A., and Keigwin, L.D., 1987, North Atlantic thermohaline circulation during the past 20,000 years linked to high-latitude surface temperature: Nature (London), v. 330, p. 35-40.

Boyle, E.A., 1988, Vertical oceanic nutrient fractionation and glacial/ interglacial CO_2 cycles: Nature (London), v. 331, p. 55-56.

Boyle, E.A., 2002, Oceanography: Oceanic Salt Switch: Science, v. 298, p. 1724-1725.

Brathauer, U., and Abelmann, A., 1999, Late Quaternary variations in sea surface temperatures and their relationship to orbital forcing recorded in the Southern Ocean (Atlantic sector): Paleoceanography, v. 14, p. 135-148.

Brix, H., and Gerdes, R., 2003, North Atlantic Deep Water and Antarctic Bottom Water: Their interaction and influence on the variability of the global ocean circulation: Journal of Geophysical Research, v. 108, p. doi:10.1029/2002JC001335.

Broecker, W.S., 1991, The Great Ocean Conveyor: Oceanography, v. 4, p. 79-89.

Broecker, W.S., and Maier, R.E., 1992, The influence of air and sea exchange on the carbon isotope distribution in the sea: Global Biogeochemical Cycles, v. 6, p. 315-320.

Broecker, W.S., 1997, Thermohaline circulation: the Achilles heel of our climate system: will man-made CO_2 upset the balance?: Science, v. 278, p. 1582-1588.

Broecker, W.S., and Clark, E., 1999, $CaCO_3$ size distribution; a paleocarbonate ion proxy?: Paleoceanography, v. 14, p. 596-604.

Catubig, N.R., Archer, D.E., Francois, R., de Menocal, P., Howard, W., and Yu, E.F., 1998, Global deep-sea burial rate of calcium carbonate during the last glacial maximum: Paleoceanography, v. 13, p. 298-310.

Cerling, T.E., Harris, J.M., MacFadden, B.J., Leakey, M.G., Quade, J., Eisenmann, V., and Ehleringer, J.R., 1997, Global vegetation change through the Miocene/ Pliocene boundary: Nature (London), v. 389, p. 153-158.

Charles, C.D., and Fairbanks, R.G., 1990, Glacial to interglacial changes in the isotopic gradients of Southern Ocean surface water, *in* Bleil, U., and Thiede, J., eds., Proceedings of the 1988 NATO advanced research workshop on Geological history of the polar oceans; Arctic versus Antarctic, NATO ASI Series. Series C: Mathematical and Physical Sciences: Dordrecht-Boston, D. Reidel Publishing Company: v. 308, p. 519-538.

Charles, C.D., Wright, J.D., and Fairbanks, R.G., 1993, Thermodynamic influences on the marine carbon isotope record: Paleoceanography, v. 8, p. 691-697.

Charles, C.D., Lynch, S.J., Ninnemann, U.S., and Fairbanks, R.G., 1996, Climate connections between the hemisphere revealed by deep sea sediment core/ ice core correlations: Earth and Planetary Science Letters, v. 142, p. 19-27.

Conkright, M.E., Levitus, S., and Boyer, T.P., 1994, World Ocean Atlas 1994 - Nutrients: NOAA Atlas NESDIS 1, v. 1, p. 162.

Craig, H., 1957, Isotopic standards for carbon and oxygen and correction factors for mass-spectrometric analysis of carbon dioxide: Geochimica et Cosmochimica Acta, v. 12, p. 133-149.

Crosta, X., Pichon, J.J., and Burckle, L.H., 1998, Application of modern analog technique to marine Antarctic diatoms; reconstruction of maximum sea-ice extent at the last glacial maximum: Paleoceanography, v. 13, p. 284-297.

Curry, W.B., Duplessy, J.C., Labeyrie, L.D., and Shackleton, N.J., 1988, Changes in the distribution of $\delta^{13}C$ of deep water Sigma CO_2 between the last glaciation and the Holocene: Paleoceanography, v. 3, p. 317-341.

de Menocal, P., Archer, D., and Leth, P., 1997, Pleistocene variations in deep Atlantic circulation and calcite burial between 1.2 and 0.6 Ma; a combined data-model approach, *in* Shackleton, N.J., Curry, W.B., Richter, and Bralower, T.J., eds., Proc. ODP, Sci. Results, 154: College Station, TX, Ocean Drilling Program, p. 285-297.

Duplessy, J.C., Shackleton, N.J., Fairbanks, R.G., Labeyrie, L.D., Oppo, D., and Kallel, N., 1988, Deepwater source variations during the last climatic cycle and their impact on the global deepwater circulation: Paleoceanography, v. 3, p. 343-360.

Duplessy, J.C., Labeyrie, L., and Waelbroeck, C., 2002, Constraints on the ocean oxygen isotopic enrichment between the last glacial maximum and the Holocene: paleoceanographic implications: Quaternary Science Reviews, v. 21, p. 315-338.

Elderfield, H., and Rickaby, R.E.M., 2000, Oceanic Cd/P ratio and nutrient utilization in the glacial Southern Ocean: Nature (London), v. 405, p. 305-310.

Emerson, S., and Bender, M., 1981, Carbon fluxes at the sediment-water interface of the deep-sea; calcium carbonate preservation: Journal of Marine Research, v. 39, p. 139-162.

Emery, W.J., and Meincke, J., 1986, Global water masses: summary and review: Oceanologica Acta, v. 9, p. 383-391.

Fairbanks, R.G., 1989, A 17,000-year glacio-eustatic sea level record; influence of glacial melting rates on the Younger Dryas event and deep-ocean circulation: Nature (London), v. 342, p. 637-642.

Farrell, J.W., and Prell, W.L., 1989, An 800,000-year bathymetric reconstruction from the central equatorial Pacific Ocean: Paleoceanography, v. 4, p. 447-466.

Frakes, L.A., 1973, USNS Eltanin Cruises 32–45, core desriptions.: Tallahassee, TX, Dept. of Geology, Florida State University, 105 p.

Francois, R., Altabet, M.A., Yu, E.F., Sigman, D.M., Bacon, M.P., Frank, M., Bohrmann, G., Bareille, G., and Labeyrie, L.D., 1997, Contribution of Southern Ocean surface-water stratification to low atmospheric CO_2 concentrations during the last glacial period: Nature (London), v. 389, p. 929-935.

Gildor, H., and Tziperman, E., 2001, Physical mechanisms behind biogeochemical glacial-interglacial CO_2 variations: Geophysical Research Letters, v. 28, p. 2421-2424.

Gildor, H., Tziperman, E., and Toggweiler, J.R., 2002, Sea ice switch mechanism and glacial-interglacial CO_2 variations: Global Biogeochemical Cycles, v. 16, p. 10.1029/2001GB001446.

Gloersen, P., and Campbell, W.J., 1991, Recent variations in Arctic and Antarctic sea-ice covers: Nature (London), v. 352, p. 33-36.

Gordon, A.L., Taylor, H.W., and Georgi, D.T., 1977, Antarctic oceanographic zonation, *in* Dunbar, M.J., ed., Polar Oceans, Arct. Inst. of North Am., Calgary, p. 45-76.

Gordon, A.L., and Molinelli, E.J., 1986, Southern Ocean Atlas: Rotterdam, Balkema.

Hall, I.R., McCave, N.I., Shackleton, N.J., Weedon, G.P., and Harris, S.E., 2001, Intensified deep Pacific inflow and ventilation in Pleistocene glacial times: Nature (London), v. 412, p. 809-812.

Herguera, J.C., Jansen, E., and Berger, W.H., 1992, Evidence for a bathyal front at 2000 m depth in the glacial Pacific, based on a depth transect on Ontong Java Plateau: Paleoceanography, v. 7, p. 273-288.

Hodell, D.A., Venz, K.A., Charles, C.D., and Ninnemann, U.S., 2003, Pleistocene vertical carbon isotope and carbonate gradients in the South Atlantic sector of the Southern Ocean: Geochem. Geophys. Geosyst., v. 4, p. 1004, doi:10.1029/2002GC000367.

Howard, W.R., and Prell, W.L., 1992, Late Quaternary surface circulation of the southern Indian Ocean and its relationship to orbital variations: Paleoceanography, v. 7, p. 79-117.

Howard, W.R., and Prell, W.L., 1994, Late Quaternary $CaCO_3$ production and preservation in the Southern Ocean; implications for oceanic and atmospheric carbon cycling: Paleoceanography, v. 9, p. 453-482.

Hufford, E.H., and McCartney, M.S., 1997, Northern boundary currents and adjacent recirculations of southwestern Australia: Geophysical Research Letters, v. 24, p. 2797-2800.

Imbrie, J., and Imbrie, J.Z., 1980, Modeling the climatic response to orbital variations: Science, v. 207, p. 943-953.

Imbrie, J., Hays, J.D., Martinson, D.G., McIntyre, A., Mix, A.C., Morley, J.J., Pisias, N.G., Prell, W.L., and Shackleton, N.J., 1984, The orbital theory of Pleistocene climate: support from a revised chronology of the marine $\delta^{18}O$ record, *in* Berger, A., Imbrie, J., Hays, J., Kukla, G., and Satzman, B., eds., Milankovitch and Climate, Volume C126(I), Reidel, NATO Series, Netherlands, p. 269-305.

Jahnke, R.A., Craven, D.B., and Gaillard, J.F., 1994, The influence of organic matter diagenesis on $CaCO_3$ dissolution at the deep-sea floor: Geochimica et Cosmochimica Acta, v. 58, p. 2799-2809.

Kanfoush, S.L., Hodell, D.A., Charles, C.D., Guilderson, T.P., Mortyn, P.G., and Ninnemann, U.S., 2000, Millennial-scale instability of the Antarctic ice sheet during the last glaciation: Science, v. 288, p. 1815-1818.

Keeling, R.F., and Stephens, B.B., 2001, Antarctic sea ice and the control of Pleistocene climate instability: Paleoceanography, v. 16, p. 112-131.

Keigwin, L.D., Jr., 1976, Late Cenozoic planktonic foraminiferal biostratigraphy and paleoceanography of the Panama Basin: Micropaleontology, v. 22, p. 419-442.

Keigwin, L.D., 1998, Glacial-age hydrography of the far Northwest Pacific Ocean: Paleoceanography, v. 13, p. 323-339.

Kroopnick, P.M., 1985, The distribution of ^{13}C of Sigma CO_2 in the world oceans: Deep-Sea Research. Part A: Oceanographic Research Papers, v. 32, p. 57-84.

Laskar, J., Joutel, F., and Robutel, P., 1993, Stabilization of the Earth's obliquity by the Moon: Nature (London), v. 361, p. 615-617.

Le, J., and Shackleton, N.J., 1992, Carbonate dissolution fluctuations in the western Equatorial Pacific during the late Quaternary: Paleoceanography, v. 7, p. 21-42.

Levitus, S., Boyer, T.P., and Antonov, J., 1994a, World Ocean Atlas 1994 - Temperature: NOAA Atlas NESDIS, v. 4, p. 129.

Levitus, S., Burgett, R., and Boyer, T.P., 1994b, World Ocean Atlas 1994 - Salinity: NOAA Atlas NESDIS, v. 3, p. 202.

Levitus, S., and Boyer, T.P., 1994c, World Ocean Atlas 1994 - Oxygen: NOAA Atlas NESDIS, v. 2, p. 202.

Mackensen, A., Rudolph, M., and Kuhn, G., 2001, Late Pleistocene deep-water circulation in the subantarctic eastern Atlantic: Global and Planetary Change, v. 30, p. 197-229.

Manabe, S., and Stouffer, R.J., 1999, Are two modes of thermohaline circulation stable?: Tellus, Ser. A., v. 51, p. 400-411.

Martínez, R.J.I., 1994a, Late Pleistocene dissolution cycles in the Vanuatu region, western Pacific Ocean, *in* Greene, H.G., Collot, J.Y., Stokking, L.B. and Fox, C., eds., Proc. ODP, Sci. Results, 134: College Station, TX, Ocean Drilling Program, p. 293-308.

Martínez, R.J.I., 1994b, Late Pleistocene carbonate dissolution patterns in the Tasman Sea, *in* van der Lingen, G.J., Swanson, K.M., and Muir, R.J., eds., Evolution of the Tasman Sea basin.: Rotterdam, Netherlands, A.A. Balkema, p. 215-228.

Martínez, R.J.I., 1994c, Late Pleistocene palaeoceanography of the Tasman Sea; implications for the dynamics of the warm pool in the Western Pacific: Palaeogeography, Palaeoclimatology, Palaeoecology, v. 112, p. 19-62.

Martinson, D.G., Pisias, N.G., Hays, J.D., Imbrie, J., Moore, T.C., Jr., and Shackleton, N.J., 1987, Age dating and the orbital theory of the ice ages; development of a high-resolution 0 to 300,000-year chronostratigraphy: Quaternary Research (New York), v. 27, p. 1-29.

Matsumoto, K., Lynch, S.J., and Anderson, R.F., 2001, Similar glacial and Holocene Southern Ocean hydrography: Paleoceanography, v. 16, p. 445-454.

Matsumoto, K., Oba, T., Lynch, S.J., and Yamamoto, H., 2002, Interior hydrography and circulation of the glacial Pacific Ocean: Quaternary Science Reviews, v. 21, p. 1693-1704.

McCartney, M.S., 1982, The subtropical recirculation of mode waters: Journal of Marine Research, v. 40, p. 427-464.

McCorkle, D.C., Heggie, D.T., and Veeh, H.H., 1998, Glacial and Holocene stable isotope distributions in the southeastern Indian Ocean: Paleoceanography, v. 13, p. 20-34.

McCorkle, D.C., and Keigwin, L.D., 1994, Depth profiles of delta ^{13}C in bottom water and core top C. wuellerstorfi on the Ontong Java Plateau and Emperor Seamounts: Paleoceanography, v. 9, p. 197-208.

Michel, E., Labeyrie, L.D., Duplessy, J.C., Gorfti, N., Labracherie, M., and Turon, J.L., 1995, Could deep subantarctic convection feed the world deep basins during the last glacial maximum?: Paleoceanography, v. 10, p. 927-941.

Mix, A.C., Pisias, N.G., Zahn, R., Rugh, W., Lopez, C., and Nelson, K., 1991, Carbon 13 in Pacific deep and intermediate waters, 0-370 ka; implications for ocean circulation and Pleistocene CO_2: Paleoceanography, v. 6, p. 205-226.

Mix, A.C., Le, J., and Shackleton, N.J., 1995, Benthic foraminiferal stable isotope stratigraphy of Site 846; 0-1.8 Ma, *in* Pisias, N.G., Mayer, L.A., Janecek, and Stewart, S.K., eds., Proc. ODP, Sci. Results, 134: College Station, TX, Ocean Drilling Program, p. 839-854.

Nees, S., Jellinek, T., Suhonen, J., Winkler, A., Helmke, J., Emmermann, P., and Shipboard Scientific Party, 1997, IMAGES III - iphis Indian and Pacific Ocean Pleistocene and Holocene History - Cruise MD106 - Leg 1.2 RV MARION DUFRESNE Hobart (Australia) - Christchurch (New Zealand), May 6 to May 21 1997, GEOMAR - Research Center for marine Geosciences.

Niebler, H.S., Hubberten, H.W., and Gersonde, R., 1999, Oxygen isotope values of planktic Foraminifera; a tool for the reconstruction of surface water stratification, *in* Fischer, G., and Wefer, G., eds., Use of proxies in paleoceanography; examples from the South Atlantic.: Berlin, Germany, Springer, p. 165-189.

Ninnemann, U.S., and Charles, C.D., 1997, Regional differences in Quaternary subantarctic nutrient cycling; link to intermediate and deep water ventilation: Paleoceanography, v. 12, p. 560-567.

Ninnemann, U.S., and Charles, C.D., 2002, Changes in the mode of Southern Ocean circulation over the last glacial cycle revealed by foraminiferal stable isotopic variability: Earth and Planetary Science Letters, v. 201, p. 383-396.

Nürnberg, D, Brughmans, N., Schönfeld, J., Ninnemann, U., and Dullo, W.-C., in press, Marine productivity, terrigenous flux and sea surface temperatures around Tasmania – Implications for glacial/interglacial changes in the Subtropical Convergence Zone (ODP Leg 189): AGU Geophysical Monograph Ser.

Opdyke, B.N., and Walker, J.C.G., 1992, Return of the coral reef hypothesis; basin to shelf partitioning of $CaCO_3$ and its effect on atmospheric CO_2: Geology (Boulder), v. 20, p. 733-736.

Oppo, D.W., Raymo, M.E., Lohmann, G.P., Mix, A.C., Wright, J.D., and Prell, W.L., 1995, A delta ^{13}C record of upper North Atlantic Deep Water during the past 2.6 million years: Paleoceanography, v. 10, p. 373-394.

Orsi, A.H., Whitworth, I.T., and Nowlin Jr., W.D., 1995, On the meridional extent and fronts of the Antarctic Circumpolar Current: Deep-Sea, Part I, v. 42, p. 641-673.

Passlow, V., Wang, P., and Chivas, A.R., 1997, Late Quaternary palaeoceanography near Tasmania, southern Australia, *in* De, D.P., ed., The late Quaternary palaeoceanography of the Australasian region., Volume 131: Palaeogeography, Palaeoclimatology, Palaeoecology: Amsterdam, Netherlands, Elsevier, p. 433-463.

Peterson, L.C., 1984, Late Quaternary deep-water paleoceanography of the eastern equatorial Indian Ocean: Evidence from benthic foraminifera, carbonate dissolution, and stable isotopes [Ph.D. thesis]: Providence, R.I., Brown Univ.

Peterson, L.C., and Prell, W.L., 1985, Carbonate dissolution in Recent sediments of the eastern equatorial Indian Ocean; preservation patterns and carbonate loss above the lysocline: Marine Geology, v. 64, p. 259-290.

Rintoul, S.R., and Bullister, J.L., 1999, A late winter hydrographic section from Tasmania to Antarctica: Deep-Sea Res. Part I, v. 46, p. 1417-1454.

Rintoul, S.R., 2000, Southern Ocean currents and climate: Papers and Proceedings of the Royal Society of Tasmania, v. 133, p. 41-50.

Sarmiento, J.L., and Toggweiler, J.R., 1984, A new model for the role of the oceans in determining atmospheric PCO_2: Nature (London), v. 308, p. 621-624.

Sarnthein, M., Winn, K., Jung, S.J.A., Duplessy, J.C., Labeyrie, L., Erlenkeuser, H., and Ganssen, G., 1994, Changes in East Atlantic deepwater circulation over the last 30,000 years; eight time slice reconstructions: Paleoceanography, v. 9, p. 209-267.

Schlitzer, R., 2003, Ocean Data View, http://www.awi-bremerhaven.de/GEO/ODV.

Seidov, D., Barron, E.J., and Haupt, B.J., 2001, Meltwater and the global ocean conveyor; northern versus southern connections: Global and Planetary Change, v. 30, p. 257-270.

Shackleton, N.J., 1977, Carbon-13 in Uvigerina; tropical rainforest history and the equatorial Pacific carbonate dissolution cycles, *in* Andersen, N.R., and Malahoff, A., eds., The fate of fossil fuel CO_2 in the oceans.: New York, N.Y., United States, Plenum Press, p. 401-427.

Siedler, G., Church, J., and Gould, J., 2001, Ocean circulation and climate; observing and modeling the global ocean., Academic Press. San Diego-San Francisco-New York.

Sigman, D.M., and Boyle, E.A., 2000, Glacial/ interglacial variations in atmospheric carbon dioxide: Nature (London), v. 407, p. 859-869.

Spero, H.J., and Lea, D.W., 2002, The cause of carbon isotope minimum events on glacial terminations: Science, v. 296, p. 522-525.

Stephens, B.B., and Keeling, R.F., 2000, The influence of Antarctic sea ice on glacial-interglacial CO_2 variations: Nature (London), v. 404, p. 171-174.

Stocker, T.F., 1998, The seesaw effect: Science, v. 281, p. 61-62.

Stuiver, M., and Reimer, P.J., 1993, Extended ^{14}C data base and revised CALIB 3.0 ^{14}C age calibration program, *in* Stuiver, M., and Long, A., eds., Calibration 1993., Volume 35: Radiocarbon: American Journal of Science, v. 35, p. 215-230.

Takahashi, T., Broecker, W.S., and Bainbridge, A.E., 1981, The alkalinity and total carbon dioxide concentration in the world oceans, *in* Bolin, B., ed., Carbon cycle modelling., Volume 16: SCOPE (Chichester): Pages: 271-286, Wiley & Sons. Chichester, United Kingdom.

Thiede, J., Nees, S., Altenbach, A., Andresen, N., Findlay, C., Hill, P., Howard, W., Jellinek, T., Jurkschat, T., Laurent, E., van der Lingen, G., Müller, A., Neil, H., Probert, I., Rehder, W., Reijmer, J., Rendle, R., Roth, S., Rueggeberg, A., Runze, O., Schulz, H., Schumann, M., Sturm, A., Swanson, K., and Willamowski, C., 1999, FS SONNE cruise report SO136, TASQWA; Quaternary variability of water masses in the Southern Tasman Sea and the Southern Ocean (SW Pacific sector), Wellington to Hobart, October 16-November 12, 1998: Kiel, GEOMAR Report, v. 78, p1-106.

Thunell, R.C., 1976, Optimum indices of calcium carbonate dissolution in deep-sea sediments: Geology (Boulder), v. 4, p. 525-528.

Toggweiler, J.R., and Samuels, B., 1993, Is the magnitude of the deep outflow from the Atlantic Ocean actually governed by Southern Hemisphere winds?, *in* M. Heinemann, ed., The Global Carbon Cycle, NATO ASI Ser. I, Volume 15: New York, Springer Verlag, p. 303-331.

Toggweiler, J.R., 1999, Variation of atmospheric CO_2 by ventilation of the ocean's deepest water: Paleoceanography, v. 14, p. 571-588.

Tomczak, M. and GodfreyJ.S., 2003: Regional Oceanography: an Introduction: 2nd Edition, 390 p.

Vidal, L., Schneider, R.R., Marchal, O., Bickert, T., Stocker, T.F., and Wefer, G., 1999, Link between North and South Atlantic during the Heinrich events of the last glacial period: Climate Dynamics, v. 15, p. 909-919.

Vimeux, F., Masson, V., Jouzel, J., Petit, J.R., and Stievenard, M., 2001, A 420,000 year deuterium excess record from East Antarctica: Information on past changes in the origin of precipitation at Vostok: J. Geophys. Res., v. 106, p. 683-873.

Watson, A.J., Bakker, D.C.E., Ridgwell, A.J., Boyd, P.W., and Law, C.S., 2000, Effect of iron supply on Southern Ocean CO_2 uptake and implications for glacial atmospheric CO_2: Nature (London), v. 407, p. 730-733.

Wu, G., Herguera, J.C., and Berger, W.H., 1990, Differential dissolution; modification of late Pleistocene oxygen isotope records in the western Equatorial Pacific: Paleoceanography, v. 5, p. 581-594.

Yasuda, M., Berger, W.H., Wu, G., Burke, S., and Schmidt, H., 1993, Foraminifer preservation record for the last million years; Site 805, Ontong Java Plateau, *in* Berger, W.H., Kroenke, L.W., Janecek, T.R., Backman, and Maddox, E.M., eds., Proc. ODP, Sci. Results: College Station, TX, Ocean Drilling Program, p. 491-508.

Zahn, R., Winn, K., and Sarnthein, M., 1986, Benthic foraminiferal $\delta^{13}C$ and accumulation rates of organic carbon; Uvigerina peregrina group and Cibicidoides wuellerstorfi: Paleoceanography, v. 1, p. 27-42.

Zahn, R., Pedersen, T.F., Bornhold, B.D., and Mix, A.C., 1991, Water mass conversion in the glacial subarctic Pacific (54°N, 148°W); physical constraints and the benthic-planktonic stable isotope record: Paleoceanography, v. 6, p. 543-560.

Zwally, H.J., Comiso, J.C., Parkinson, C.L., Cavalieri, D.J., and Gloersen, P., 2002, Variability of Antarctic sea ice 1979-1998: Journal of Geophysical Research, C, Oceans, v. 107.

APPENDIX

Table 1a: Stable isotope data of core **SO136-163**

		C. wuellerstorfi		*G. bulloides*		*G. inflata*		*G. truncatulinoides*	
Depth	**Age**	**$\delta^{13}C$**	**$\delta^{18}O$**	**$\delta^{13}C$**	**$\delta^{18}O$**	**$\delta^{13}C$**	**$\delta^{18}O$**	**$\delta^{13}C$**	**$\delta^{18}O$**
(cm)	(ka)	(‰ vs PDB)	(‰ vs PDB)	(‰ vs PDB)	(‰ vs PDB)	(‰ vs PDB)	(‰ vs PDB)	(‰ vs PDB)	(‰ vs PDB)
2	3.7	0.71	3.09	0.14	0.96	0.89	1.67	0.80	1.52
7	6.0	0.46	3.15	0.03	1.61	0.91	1.19	1.04	1.30
12	8.0	0.67	3.31	-0.02	2.23	0.85	1.61	0.45	1.75
17	10.0	0.34	3.88	0.13	2.51	1.07	2.62	0.46	1.58
22	12.0	-0.26	4.74	0.24	2.48	0.96	3.31	0.26	2.20
27	14.0	-0.52	5.02	0.22	3.17	0.99	3.67	0.74	2.83
32	15.7	-0.40	5.06	0.43	3.49	1.31	3.74	0.88	3.58
37	17.5	-0.30	5.06	0.12	3.30	1.02	3.97	1.08	4.02
42	19.2	-0.43	5.07	0.33	3.04	1.12	3.78	1.05	3.85
47	21.0	-0.33	4.95	0.66	3.26	1.10	3.58	1.38	3.75
52	24.9	-0.25	4.79	0.87	3.17	1.24	3.40	1.35	4.01
57	28.8	0.09	4.55	0.47	3.08	1.13	3.47	1.15	3.60
62	32.7	0.28	4.46	0.74	2.88	1.09	3.42	1.32	3.57
67	36.6			0.85	2.96	1.29	3.15	1.34	3.40
72	40.4	0.27	4.41	0.57	2.94	1.25	3.29	1.18	3.21
77	44.3	0.36	4.37	0.73	2.89	1.26	3.33	1.23	3.31
82	48.2	0.06	4.44	0.60	2.87	1.30	3.45	1.14	3.53
87	52.1	-0.53	4.47	0.53	2.94	1.19	3.25	1.10	3.39
92	56.0	0.17	4.42	0.80	3.17	0.94	3.31	1.21	3.61
97	58.3	-0.06	4.46	0.70	3.23	1.12	3.49	1.08	3.59
102	60.6	-0.67	4.66	0.77	3.49	1.09	3.50	1.20	3.72
107	62.9	-0.44	4.66	0.69	3.30	0.97	3.54	1.13	3.56
112	65.1	-0.08	4.37	0.84	3.22	1.26	3.11	1.09	3.73
117	67.4	0.06	4.42	0.92	3.15	1.27	3.27	1.29	3.36
122	69.7	-0.13	4.35	1.09	2.85	1.35	3.23	1.21	3.03
127	72.0	-0.14	4.21	0.90	2.78	1.26	2.97	1.27	3.09
132	74.8	0.00	4.17	0.96	2.83	1.61	3.09	1.45	2.91
137	77.7	0.07	4.01	1.02	2.57	1.61	3.07	1.18	2.89
142	80.5	0.10	3.94	0.92	2.62	1.33	2.58	1.00	2.66
147	83.3	0.02	3.95	0.84	2.67	1.24	2.58	1.14	2.96
152	86.2	-0.04	4.21	0.82	2.91	1.32	3.03	1.50	3.12
157	89.0	-0.35	4.09	0.79	2.67	1.32	2.92	1.34	2.86
162	91.8	-0.08	4.07	0.93	2.75	1.35	2.99	1.31	2.96
167	94.7	0.14	3.87	0.46	2.51	1.34	2.71	1.21	2.72
172	97.5	-0.19	4.04	0.57	2.48	1.28	2.69	1.04	2.64
177	100.3	0.22	3.93	0.85	2.42	1.23	2.59	0.93	2.46
182	103.2	-0.17	4.12	0.58	2.50	1.12	2.72	0.85	2.42
187	106.0	-0.17	4.04	0.67	2.31	1.23	2.68	1.15	2.82
192	108.4	-0.16	4.16	0.67	2.33	1.02	3.02	1.28	2.99
197	110.9	0.38	4.00	0.60	2.50	1.25	2.95	1.20	2.89
202	113.3	-0.34	3.83	0.65	2.42	1.25	2.79	1.19	2.80
207	115.7	0.09	3.64	0.30	2.23	1.19	2.85	1.22	2.59
212	118.1	0.21	3.70	0.55	2.24	1.10	2.74	1.30	2.78
217	120.6	0.34	3.10	-0.08	1.07	1.03	2.27	1.17	2.76
222	123.0	0.23	3.13	-0.27	1.71	0.56	1.42	0.54	1.81
227	124.8	0.32	3.69	-0.36	1.89	0.69	1.22	0.38	1.81
232	126.6	0.11	4.30	-0.01	2.22	0.58	2.65	0.58	2.26
237	128.4	0.07	4.50	-0.08	2.99	0.60	3.36	0.65	3.07
242	130.2	-0.18	4.60	0.17	3.12	0.78	3.48	0.99	3.63
247	132.0	-0.50	5.03	-0.22	3.31	0.67	3.83	1.00	3.61
252	134.7	-0.04	4.82	0.24	3.55	0.81	3.94	0.94	3.92
257	137.4	-0.51	4.83	0.38	3.35	0.87	3.59	0.90	3.61
262	140.1	-0.58	4.76	0.12	3.28	0.75	3.61	0.89	3.61
267	142.9	-0.40	4.70	0.48	3.40	1.00	3.47	0.86	3.45
272	145.6	-0.08	4.82	0.44	3.39	1.14	3.47	0.88	3.49
277	148.3	-0.15	4.75	0.03	3.11	0.84	3.60	0.90	3.35
282	151.0	-0.30	4.65	0.42	3.53	1.06	3.78	0.93	3.81
287	153.7	-0.28	4.68	0.27	3.46	0.74	3.67	0.97	3.80
292	156.4	-0.17	4.78	0.35	3.55	0.58	3.87	0.79	3.89
297	159.1	-0.38	4.71	0.07	3.02	0.85	3.26	0.77	3.29
302	161.9	-0.14	4.53	0.13	3.25	0.96	3.36	1.01	3.30
307	164.6	-0.51	4.62	0.42	3.20	0.66	3.24	0.83	2.95
312	167.3	-0.20	4.30	0.31	2.99	0.96	3.27	0.68	2.98
317	170.0	-0.48	4.64	0.28	2.98	0.63	3.26	0.98	3.41
322	177.0	-0.08	4.72	0.48	3.44	1.00	3.60	0.62	3.33
327	184.0	-0.17	4.26	0.23	3.16	0.66	3.39	0.73	2.99
332	186.4	0.08	4.12	0.05	2.73	0.98	3.02	0.90	2.09
337	188.7	0.13	3.68	0.48	2.29	1.10	2.40	0.44	1.71
342	191.1	-0.03	3.58	-0.08	2.25	1.17	2.87	0.85	2.01
347	193.5	0.25	3.75	0.65	2.35	1.32	2.76	0.74	1.82
352	195.9	0.13	3.92	0.07	2.06	1.26	2.79	0.51	1.48
357	198.2	0.11	3.67	-0.07	2.11	0.91	2.15	0.48	2.06
362	200.6	-0.52	4.32	0.28	2.63	0.99	2.72	0.78	2.90
367	203.0	-0.26	4.51	0.07	2.69	0.85	3.03	0.83	2.69
372	206.3	-0.05	4.35	0.09	2.49	1.07	3.02	0.70	2.76
377	209.7	-0.11	4.08	0.15	2.77	1.01	3.01	1.00	2.63
382	213.0	0.40	3.79	0.32	2.63	1.06	2.73	0.78	2.64
387	221.0	-0.19	4.23	-0.42	1.95	1.22	2.80	0.71	1.82
392	229.0	-0.03	4.17	-0.08	2.49	0.98	3.03	0.50	1.83
397	237.0	0.28	3.33	0.09	2.37	0.63	2.29	0.21	1.88
402	240.7	0.07	4.09	0.20	3.05	0.60	3.18	0.35	2.40
407	244.3	-0.51	4.57	0.21	3.17	0.76	3.52	0.38	2.44
412	248.0	-0.42	4.75	0.22	3.11	0.96	3.59	0.24	2.78
417	250.4	-0.47	4.70	0.10	3.19	1.00	3.52	0.07	2.61
422	252.9	0.18	4.61	0.07	3.03	0.83	3.45	0.41	1.87
427	255.3	-0.70	4.62	0.28	3.02	0.86	3.24	0.43	2.59
432	257.8	-0.27	4.49	0.12	3.09	0.59	3.32	0.24	2.78
437	260.2	-0.42	4.54	0.46	3.17	0.97	3.35	0.08	2.46
442	262.7	-0.52	4.49	0.18	3.25	0.86	3.52	0.35	2.81
447	265.1	-0.82	4.60	0.64	3.08	0.93	3.50	0.12	2.68
452	267.6	-0.35	4.64	0.60	3.40	0.98	3.64	0.12	2.68
457	270.0	-0.65	4.63	0.68	3.37	0.99	3.44	0.27	2.65
462	273.0	-0.38	4.34	1.02	3.11	1.50	3.45		
467	276.0	-0.36	4.55	0.95	2.81	1.26	3.12		
472	279.0	-0.12	4.29	0.63	2.80	1.32	3.24	0.71	2.20
477	282.0	0.14	3.98	0.99	2.67	1.25	2.83	0.76	2.19
482	285.0	0.32	3.97	0.22	2.13	1.20	2.16	0.92	2.23

Table 1a: Stable isotope data of core **SO136-163**

		C. wuellerstorfi		*G. bulloides*		*G. inflata*		*G. truncatulinoides*	
Depth	**Age**	**$\delta^{13}C$**	**$\delta^{18}O$**	**$\delta^{13}C$**	**$\delta^{18}O$**	**$\delta^{13}C$**	**$\delta^{18}O$**	**$\delta^{13}C$**	**$\delta^{18}O$**
(cm)	(ka)	(‰ vs PDB)	(‰ vs PDB)	(‰ vs PDB)	(‰ vs PDB)	(‰ vs PDB)	(‰ vs PDB)	(‰ vs PDB)	(‰ vs PDB)
487	288.0	0.23	3.59	0.70	2.62	1.16	3.31	0.69	2.04
492	289.8	-0.20	4.02	0.79	2.60	1.18	2.63	0.78	1.95
497	291.7	-0.16	4.13	0.88	2.77	1.19	2.49	0.76	2.18
502	293.5	-0.21	4.28	0.68	2.92	1.36	3.03	0.85	2.06
507	295.3	-0.50	4.28	0.74	2.78	1.43	3.12	0.80	2.42
512	297.2	0.08	4.11	0.76	3.08	1.37	3.38	1.04	2.37
517	299.0	0.07	4.30	0.82	2.90	1.32	3.20	0.71	2.48
522	300.8	-0.28	4.19	0.54	2.75	1.30	3.13	0.78	1.96
527	302.7	0.17	3.99	0.44	2.53	1.28	2.92	0.84	2.02
532	304.5	-0.09	4.24	0.87	2.80	1.34	3.03	0.67	1.91
537	306.3	-0.19	3.99	0.77	2.65	1.40	2.92	0.72	1.88
542	308.2	0.15	3.71	0.74	2.07	1.07	2.54	0.78	2.12
547	310.0	-0.05	3.62	0.71	2.01	1.00	2.63	0.71	1.78
552	313.4	-0.17	3.80	0.10	1.78	1.17	2.56	0.72	1.78
557	316.8	-0.07	3.70	0.76	2.10	1.28	2.68	0.49	1.89
562	320.2	-0.46	3.74	0.72	2.14	1.24	2.50	0.79	1.75
567	323.6	0.35	3.47	0.49	2.04	1.22	2.49	0.99	1.50
572	327.0	0.05	3.22	0.30	2.08	0.92	2.19	0.84	1.61
577	329.2	0.07	3.23	-0.13	1.14	0.84	1.77	0.54	1.66
582	331.3	-0.40	3.86	-0.43	1.36	0.69	2.03	0.53	1.88
587	333.5	-0.03	4.07	-0.28	2.39	0.61	2.63	0.49	2.28
592	335.7	-0.76	4.64	-0.29	2.60	0.75	3.05	0.54	2.58
597	337.8	-1.05	4.76	0.19	3.04	0.86	3.68	0.50	3.09
602	340.0	-0.69	4.91	0.29	3.21	1.00	3.73	0.45	3.28
607	342.9	-1.09	4.92	0.14	3.26	0.95	3.54	0.84	2.85
612	345.7	-0.49	4.64	0.01	3.31	0.88	3.68	0.84	2.77
617	348.6	-0.27	4.59	0.49	2.97	1.08	3.38	0.89	2.82
622	351.4	-0.81	4.55	0.63	3.15	0.89	3.49	0.94	2.87
627	354.3	-0.91	4.50	0.50	2.96	1.06	3.35	0.85	2.83
632	357.1	-0.98	4.66	0.39	3.29	1.03	3.62	1.05	3.04
637	360.0	-0.75	4.56	0.25	2.98	1.02	3.47	1.05	2.87
642	361.6	-0.42	4.51	0.25	3.20	0.85	2.72	1.19	3.08
647	363.2	-0.48	4.52	0.47	2.98	1.09	3.27	0.99	2.80
652	364.8	-0.72	4.41	0.66	3.13	1.04	3.09	1.07	2.67
657	366.4	-0.48	4.38	0.42	2.89	1.37	3.21	1.02	2.57
662	368.0	-0.93	4.34	0.74	2.91	1.38	3.30	1.16	2.68
667	369.6	-0.40	4.27	0.50	2.48	1.35	2.90	1.10	2.21
672	371.2	-0.42	4.24	0.43	2.76	1.22	2.89	0.94	2.34
677	372.8	-0.60	4.20	0.92	2.67	1.17	2.81	1.00	2.24
682	374.4	-0.67	4.26	0.88	3.17	1.36	3.01	1.37	2.49
687	376.0	-0.73	4.45	0.50	2.55	1.44	2.85	1.14	2.43
692	378.3	-0.21	4.20	0.24	2.58	1.35	2.69	1.05	2.08
697	380.5	-0.56	4.21	0.76	2.27	1.25	2.85	1.01	2.02
702	382.7	-0.50	4.18	0.45	2.59	1.48	2.73	1.09	2.06
707	385.0	-0.46	4.11	0.96	2.54	1.38	2.62	0.97	2.31
712	387.3	-0.63	4.05	0.29	2.38	1.21	2.57	0.95	2.17
717	389.5	-0.47	4.11	0.96	2.69	1.36	2.79	1.25	2.28
722	391.7	-0.13	4.04	0.92	2.69	1.46	2.75	1.18	2.10
727	394.0	-0.70	4.07	0.71	2.21	1.46	2.49	0.83	1.72
732	396.2	0.36	3.79	0.84	2.43	1.54	2.62	1.36	1.66
737	398.3	0.49	3.65	1.05	1.97	1.65	2.27	1.28	1.62
742	400.5	0.74	3.65	0.84	2.13	1.63	2.26	1.57	1.73
747	402.7	0.73	3.48	0.97	1.77	1.52	2.17	1.34	1.48
752	404.8	0.31	3.21	1.10	1.74	1.50	2.04	1.36	1.42
757	407.0	-0.06	3.41	1.00	1.83	1.57	2.48	1.39	1.59
762	408.9	0.23	3.21	1.24	1.43	1.40	1.93	1.32	1.41
767	410.7	0.03	3.35	0.90	1.49	1.24	1.39	1.23	1.52
772	412.6	-0.01	3.40	0.55	1.75	1.43	1.79	1.24	1.75
777	414.4			0.41	1.45	1.34	1.93	1.16	1.96
782	416.3	-0.16	3.61	0.40	1.85	1.26	2.13	0.82	1.53
787	418.1	-0.11	3.67	0.50	2.32	1.31	2.55	1.15	1.89
792	420.0	-0.20	3.64	0.56	2.03	0.97	2.41	0.91	2.05
797	421.9	-0.24	3.81	0.17	2.71	1.01	2.69	0.95	2.08
802	423.7	0.21	3.85	0.11	2.42	1.12	2.66	0.65	2.12
807	425.6	-0.07	4.08	0.20	2.40	0.67	3.02	0.51	2.24
812	427.4	-0.32	4.47	0.16	2.96	0.68	3.00	0.43	2.36
817	429.3	-0.78	4.82	0.04	3.27	0.78	3.16	0.24	2.68
822	431.1	-0.87	5.10	0.34	3.40	1.01	3.89	0.53	3.03
827	433.0	-0.93	5.15	0.29	3.69	1.20	3.88	1.00	3.38

Table 1b: Sedimentologic data of core **SO136-163**

Depth (cm)	Age (ka)	LSR (cm/kyr)	Carbonate Conc. (wt-%)	Carbonate AR ($g/cm^2/kyr$)	Coarse Carbonate (wt-%)	Fragmentation Ratio (%)
2	3.7	2.5	86.5	1.9	26.0	28.2
7	6.0	2.5	87.5	1.9	27.1	29.7
12	8.0	2.5	85.5	1.9	31.7	
17	10.0	2.5	84.2	1.9	34.6	19.8
22	12.0	2.5	83.6	1.9	26.7	
27	14.0	2.5	81.3	1.8	38.8	22.3
32	15.7	2.8	78.3	1.9	41.2	
37	17.5	2.9	78.0	1.9	44.3	29.5
42	19.2	2.9	76.7	1.9	47.0	
47	21.0	2.6	75.8	1.6	49.3	32.5
52	24.9	1.5	79.9	1.0	49.0	
57	28.8	1.3	78.8	0.9	39.9	23.6
62	32.7	1.3	83.2	1.0	35.8	
67	36.6	1.3	81.5	1.0	33.9	30.4
72	40.4	1.3	81.7	0.9	33.7	
77	44.3	1.3	82.4	0.9	34.9	28.3
82	48.2	1.3	80.2	0.8	32.2	
87	52.1	1.3	82.4	0.9	29.1	21.8
92	56.0	1.4	81.0	0.9	30.8	
97	58.3	2.1	78.4	1.4	27.4	35.9
102	60.6	2.2	76.3	1.4	22.9	
107	62.9	2.2	77.7	1.4	25.1	36.8
112	65.1	2.2	78.2	1.6	24.9	
117	67.4	2.2	81.7	1.5	30.8	30.7
122	69.7	2.2	82.6	1.6	28.4	
127	72.0	2.1	84.8	1.5	28.4	28.9
132	74.8	1.8	86.1	1.4	25.9	
137	77.7	1.8	86.7	1.3	26.1	31.6
142	80.5	1.8	86.2	1.3	22.9	
147	83.3	1.8	84.7	1.2	24.4	34.9
152	86.2	1.8	84.7	1.3	32.0	
157	89.0	1.8	85.8	1.3	35.2	26.1
162	91.8	1.8	84.2	1.3	33.0	
167	94.7	1.8	85.3	1.3	26.5	33.6
172	97.5	1.8	85.4	1.3	25.4	
177	100.3	1.8	81.9	1.2	26.0	33.7
182	103.2	1.8	84.4	1.3	29.3	
187	106.0	1.8	83.0	1.3	27.2	31.4
192	108.4	2.0	84.6	1.5	30.5	
197	110.9	2.1	87.5	1.7	30.6	20.7
202	113.3	2.1	87.0	1.6	28.1	
207	115.7	2.1	88.2	1.6	24.3	26.3
212	118.1	2.1	87.6	1.6	25.3	
217	120.6	2.1	86.2	1.5	27.5	23.5
222	123.0	2.1	84.5	1.6	32.5	
227	124.8	2.7	82.5	1.9	34.3	21.0
232	126.6	2.8	82.7	2.0	27.6	
237	128.4	2.8	83.0	2.2	28.6	17.3
242	130.2	2.8	82.5	2.2	30.1	
247	132.0	2.6	78.6	1.9	22.7	19.9
252	134.7	2.0	79.8	1.4	24.6	
257	137.4	1.8	81.4	1.3	21.1	25.7
262	140.1	1.8	82.3	1.3	23.2	
267	142.9	1.8	80.5	1.2	30.4	22.4
272	145.6	1.8	81.9	1.3	25.8	
277	148.3	1.8	81.8	1.2	24.3	18.3
282	151.0	1.8	84.0	1.3	26.9	
287	153.7	1.8	78.5	1.2	31.9	20.8
292	156.4	1.8	78.3	1.2	39.1	
297	159.1	1.8	75.1	1.2	36.1	24.4
302	161.9	1.8	76.4	1.2	35.4	
307	164.6	1.8	77.2	1.2	34.1	31.0
312	167.3	1.8	75.6	1.2	31.7	
317	170.0	1.6	74.1	1.0	32.0	35.6
322	177.0	0.9	75.1	0.5	29.0	
327	184.0	0.8	74.0	0.5	29.6	41.8
332	186.4	1.9	75.8	1.2	26.6	
337	188.7	2.1	77.4	1.5	25.4	42.6
342	191.1	2.1	80.1	1.4	23.3	
347	193.5	2.1	82.0	1.5	22.6	44.5
352	195.9	2.1	83.6	1.4	28.4	
357	198.2	2.1	82.0	1.6	25.2	40.4
362	200.6	2.1	77.0	1.3	26.6	
367	203.0	2.0	76.2	1.2	34.3	30.4
372	206.3	1.6	76.5	1.0	34.5	
377	209.7	1.5	78.7	1.0	37.0	25.6
382	213.0	1.3	81.5	0.9	38.8	
387	221.0	0.7	83.3	0.5	30.7	30.0
392	229.0	0.6	82.5	0.4	31.7	
397	237.0	0.7	80.8	0.5	31.0	29.7
402	240.7	1.3	82.6	0.9	30.3	
407	244.3	1.4	81.2	1.0	26.2	28.7
412	248.0	1.4	81.1	1.1	20.3	
417	250.4	2.0	82.2	1.4	22.1	36.5
422	252.9	2.0	81.5	1.5	19.7	
427	255.3	2.0	79.1	1.4	24.8	38.1
432	257.8	2.0	77.3	1.3	19.1	
437	260.2	2.0	76.3	1.3	21.3	39.3
442	262.7	2.0	73.8	1.2	21.1	
447	265.1	2.0	70.6	1.1	22.1	38.7
452	267.6	2.0	72.2	1.2	19.5	
457	270.0	2.0	73.9	1.3	16.8	48.9
462	273.0	1.7	76.1	1.1	16.0	
467	276.0	1.7	80.8	1.2	19.6	48.9
472	279.0	1.7	84.4	1.3	16.9	
477	282.0	1.7	88.3	1.4	10.6	60.2
482	285.0	1.7	87.9	1.3	10.0	

Table 1b: Sedimentologic data of core **SO136-163**

Depth (cm)	Age (ka)	LSR (cm/kyr)	Carbonate Conc. (wt-%)	Carbonate AR ($g/cm^2/kyr$)	Coarse Carbonate (wt-%)	Fragmentation Ratio (%)
487	288.0	1.8	86.0	1.3	12.9	44.0
492	289.8	2.6	85.1	2.0	12.3	
497	291.7	2.7	85.1	2.0	15.2	52.8
502	293.5	2.7	84.5	2.0	18.5	
507	295.3	2.7	82.3	1.9	18.0	46.2
512	297.2	2.7	83.3	2.0	24.6	
517	299.0	2.7	86.0	2.1	16.4	40.1
522	300.8	2.7	85.2	2.1	17.1	
527	302.7	2.7	83.5	2.0	13.6	35.9
532	304.5	2.7	82.6	2.0	18.5	
537	306.3	2.7	86.1	2.1	15.8	41.8
542	308.2	2.7	86.6	2.1	13.1	
547	310.0	2.5	86.8	2.1	9.2	45.2
552	313.4	1.6	83.0	1.2	8.4	
557	316.8	1.5	84.2	1.0	8.0	62.0
562	320.2	1.5	87.7	1.2	10.4	
567	323.6	1.5	85.9	1.1	12.0	52.8
572	327.0	1.6	86.0	1.2	16.2	
577	329.2	2.2	87.0	1.7	19.7	41.3
582	331.3	2.3	86.5	1.7	18.2	
587	333.5	2.3	81.3	1.6	20.7	32.2
592	335.7	2.3	81.2	1.5	18.8	
597	337.8	2.3	82.2	1.5	21.9	30.4
602	340.0	2.2	84.7	1.7	23.7	
607	342.9	1.8	87.1	1.4	21.2	18.8
612	345.7	1.8	84.6	1.3	23.5	
617	348.6	1.8	85.7	1.3	20.5	17.8
622	351.4	1.8	85.1	1.3	18.4	
627	354.3	1.8	84.8	1.2	24.0	19.1
632	357.1	1.8	83.8	1.3	19.3	
637	360.0	1.9	85.3	1.4	17.6	20.6
642	361.6	3.0	84.3	2.2	19.5	
647	363.2	3.1	86.0	2.4	19.8	27.6
652	364.8	3.1	87.5	2.4	14.9	
657	366.4	3.1	85.4	2.3	14.4	38.5
662	368.0	3.1	84.8	2.3	16.4	
667	369.6	3.1	88.3	2.4	18.2	34.0
672	371.2	3.1	88.5	2.5	12.2	
677	372.8	3.1	84.7	2.4	11.4	47.4
682	374.4	3.1	86.3	2.3	16.1	
687	376.0	3.0	89.5	2.3	12.3	48.0
692	378.3	2.3	89.4	1.9	11.2	
697	380.5	2.2	89.5	1.8	8.4	43.0
702	382.7	2.2	89.7	1.8	6.3	
707	385.0	2.2	88.9	1.7	9.4	52.4
712	387.3	2.2	88.3	1.7	6.3	
717	389.5	2.2	87.6	1.7	4.3	60.5
722	391.7	2.2	91.3	1.9	6.6	
727	394.0	2.2	92.3	1.9	5.3	59.9
732	396.2	2.3	91.9	1.9	5.1	
737	398.3	2.3	91.2	1.9	4.4	52.7
742	400.5	2.3	90.3	1.8	5.5	
747	402.7	2.3	89.6	1.9	6.3	42.2
752	404.8	2.3	90.1	1.9	6.0	
757	407.0	2.4	90.2	1.9	5.2	46.6
762	408.9	2.6	87.9	2.1	4.6	
767	410.7	2.7	88.8	2.3	5.0	53.6
772	412.6	2.7	87.3	2.1	4.8	
777	414.4	2.7	89.3	2.3	5.8	53.9
782	416.3	2.7	89.4	2.2	7.1	
787	418.1	2.7	91.4	2.2	8.2	34.0
792	420.0	2.7	91.3	2.3	7.9	
797	421.9	2.7	87.8	2.2	8.9	33.6
802	423.7	2.7	88.1	2.1	9.3	
807	425.6	2.7	86.4	2.0	11.1	33.3
812	427.4	2.7	85.6	1.9	12.1	26.2
817	429.3	2.7	86.9	2.2	12.5	23.3
822	431.1	2.7	85.3	2.0	15.6	
827	433.0	2.7	80.9	2.0	22.7	21.2

Table 2a: Stable isotope data of core **SO136-164**

		C. wuellerstorfi		*G. bulloides*	
Depth	**Age**	**$\delta^{13}C$**	**$\delta^{18}O$**	**$\delta^{13}C$**	**$\delta^{18}O$**
(cm)	(ka)	(‰ vs PDB)	(‰ vs PDB)	(‰ vs PDB)	(‰ vs PDB)
2	6.2	-0.15	3.68	0.32	2.89
7	7.5	0.05	3.99		
12	8.9	-0.19	4.63	0.10	2.18
17	10.3	0.38	4.03		
22	11.6	-0.26	4.87	0.47	3.35
27	13.0		5.10		
32	15.2	-0.65	5.17	0.44	3.29
37	17.5	-0.39	5.34		
42	19.8	-0.27	5.10	0.58	3.63
47	22.0	-0.20	5.11		
52	24.2	-0.15	5.02	0.63	3.40
57	26.5	-0.17	5.07		
62	28.7	-0.40	4.83	0.72	3.17
67	31.0	-0.20	4.66		
72	34.4	-0.26	4.68	0.78	3.17
77	37.7	0.03	4.69		
82	41.1	-0.07	4.77	0.86	3.01
87	44.5	-0.16	4.77		
92	47.9	0.20	4.58	0.61	2.89
97	51.2	-0.22	4.52		
102	54.6	-0.08	4.53	0.65	2.88
107	58.0	-0.04	4.58		
112	60.0	-0.37	4.78	0.51	2.96
117	62.0	-0.32	4.56		
122	64.0	-0.67	4.78	0.82	3.35
127	66.0	-0.16	4.83		
132	68.0	-0.22	4.60	0.56	2.93
137	70.0	0.30	4.56		
142	72.8	-0.02	4.23	1.03	2.79
147	75.7	-0.09	4.26		
152	78.5	-0.16	3.94	0.77	2.60
157	81.3	-0.28	4.10		
162	84.2		4.20	0.77	2.80
167	87.0	-0.08	4.37		
172	90.2	-0.01	4.31	0.99	2.79
177	93.3	-0.11	4.21		
182	96.5	0.01	4.25	0.99	2.78
187	99.7	0.13	4.28		
192	102.8	0.10	4.14	0.64	2.68
197	106.0	0.05	4.26		
202	109.1	0.07	4.08	0.82	2.51
207	112.2	-0.08	4.11		
212	115.4	-0.29	3.99	0.98	2.48
217	118.5	0.11	3.58		
222	121.6	0.29	3.55	0.44	2.82
227	124.7	-0.03	3.69		
232	127.9	-0.11	4.58	0.14	3.00
237	131.0	-0.40	4.98		
242	132.9	-0.17	5.08	0.28	3.38
247	134.9	-0.24	5.17		
252	136.8	-0.67	5.03	0.47	3.62
257	138.7	-0.48	5.04		
262	140.6	-0.50	5.09	0.47	3.38
267	142.6	-0.50	5.07		
272	144.5	-0.60	5.00	0.43	3.29
277	146.4	-0.69	5.01		
282	148.4	-0.28	4.98	0.53	3.42
287	150.3	-0.22	4.87		
292	152.2	-0.39	4.86	0.17	3.29
297	154.1	-0.46	4.98		
302	156.1	-0.35	4.97	0.37	3.51
307	158.0	-0.29	5.08		
312	159.4	-0.51	4.96	0.36	3.68
317	160.7	-0.53	4.87		
322	162.1	-0.42	4.72	0.29	3.40
327	163.5	-0.41	4.85		
332	164.8	-0.87	4.77	0.33	3.22
337	166.2	-0.50	4.80		
342	167.5	-0.61	4.60	0.34	3.08
347	168.9	-0.14	4.51		
352	170.3	-0.32	4.71	0.32	2.85
357	171.6	-0.76	4.65		
362	173.0	-0.56	4.75	0.57	3.23
367	177.0	-0.20	4.62		
372	181.0	-0.28	4.54	0.48	3.23
377	185.0	-0.40	4.48		
382	189.0	-0.65	4.07	0.40	2.69
387	193.0	-0.43	3.96		
392	197.0	-0.29	4.06	0.63	2.37
397	199.7	-0.49	4.28		
402	202.3	-0.45	4.66	0.76	2.87
407	205.0	-0.74	4.64		
412	207.7	-0.71	4.70	0.60	3.19
417	210.3	-0.29	4.40		
422	213.0	-0.09	4.01	0.10	2.60
427	220.7				
432	228.3	-0.40	4.45	0.49	2.90
437	236.0	-0.16	4.01		
442	240.3	-0.53	4.63	0.25	2.97
447	244.7	-0.58	4.82		
452	249.0	-0.43	4.85	0.11	3.25
457	250.9	-0.52	4.83		
462	252.8	-0.84	4.88	0.02	3.14
467	254.7	-0.47	4.69		
472	256.6	-0.48	4.72	0.34	3.12
477	258.4	-0.41	4.70		
482	260.3	-0.56	4.71	0.21	3.03

Table 2a: Stable isotope data of core **SO136-164**

		C. wuellerstorfi		*G. bulloides*	
Depth	**Age**	**$\delta^{13}C$**	**$\delta^{18}O$**	**$\delta^{13}C$**	**$\delta^{18}O$**
(cm)	(ka)	(‰ vs PDB)	(‰ vs PDB)	(‰ vs PDB)	(‰ vs PDB)
487	262.2	-0.88	4.64		
492	264.1	-0.70	4.70	0.49	3.33
497	266.0	-0.82	4.81		
502	269.3	-0.94	4.79	0.33	3.19
507	272.5	-0.87	4.73		
512	275.8	-0.88		0.52	3.58
517	279.0	-0.65	4.61		
522	281.8	0.33	4.12	0.97	2.49
527	284.7	-0.32	4.01		
532	287.5	-0.05	4.13	0.58	2.58
537	290.3	-0.52	4.16		
542	293.2	-0.20	4.26	0.74	2.83
547	296.0	-0.37	4.42		
552	299.4	-0.48	4.34	0.68	2.96
557	302.9	-0.37	4.12		
562	306.3	-0.59	4.50	0.46	3.00
567	309.8	-0.09	3.91		
572	313.2	-0.28	4.23	1.00	2.67
577	316.7	-0.34	4.08		
582	320.1	-0.35	3.95	0.72	2.60
587	323.6	-0.39	4.07		
592	327.0	-0.87	3.40	0.89	2.92
597	329.0	-0.18	3.55		
602	331.0	-0.59	3.70	0.71	3.46
607	333.0	-0.78	3.52		
612	335.0	-0.51	4.27	0.46	2.92
617	337.0	-0.67	4.83		
622	339.0	-0.92	5.13	0.83	3.64
627	340.8	-0.79	5.07		
632	342.6	-0.35	4.93	0.70	3.54
637	344.4	-0.90	4.61		
642	346.2	-0.61	4.82	0.44	3.44
647	348.0	-0.99	4.75		
652	349.8	-0.51	4.59	0.81	3.27
657	351.6	-0.48	4.65		
662	353.4	-0.95	4.72	0.67	3.35
667	355.2	-1.24	4.40		
672	357.0	-0.91	4.70	0.96	3.33
677	358.8	-0.91	4.69		
682	360.6	-0.94	4.66	0.88	3.04
687	362.5	-0.58	4.52		
692	364.3	-0.49	4.41	0.75	2.94
697	366.1	-0.49	4.62		
702	367.9	-0.04	4.42	0.94	3.01
707	369.7	-0.21	4.43		
712	371.5	-0.26	4.47	0.89	2.79
717	373.4	-0.14	4.53		
722	375.2	-0.29	4.44	1.08	2.90
727	377.0	-0.27	4.53		
732	381.3	0.00	4.24	0.95	2.41
737	385.5	-0.21	4.28		
742	389.8	0.11	4.23	1.05	2.48
747	394.0	-0.45	4.20	0.62	2.34
752	396.4	0.08	4.08	0.95	2.46
757	398.9	0.14	3.97	0.88	2.22
762	401.3	0.64	3.65	1.13	1.99
767	403.7	0.03	3.92	0.78	1.89
772	406.1	-0.06	3.48	1.42	0.97
777	408.6	0.19	3.49	0.87	0.84
782	411.0	0.43	3.44	0.96	1.26
787	412.9	0.17	3.58	0.15	1.04
792	414.8	0.45	3.79	0.78	2.11
797	416.7	-0.45	3.99		
802	418.7	0.09	4.05	0.80	2.43
807	420.6	-0.54	4.07		
812	422.5	-0.58	4.37	0.02	2.42
817	424.4	-0.59	4.42		
822	426.3	-0.50	4.72	0.63	2.91
827	428.3	-0.66	5.00		
832	430.2	-0.37	5.26	0.41	3.35
837	432.1	-1.07	5.34		
842	434.0	-1.04	5.38	0.53	3.79
847	435.4	-1.28	5.34		
852	436.8	-1.12	5.29	0.42	3.88
857	438.2	-1.00	5.20		
862	439.6	-0.85	5.25	0.79	3.92
867	441.0	-0.48	5.16		
872	442.4	-0.73	5.12	0.88	3.39
877	443.8	-0.80	4.99		
882	445.2	-0.84	4.87	0.49	3.24
887	446.6	-0.91	4.73		
892	448.0	-0.59	4.87	0.86	3.30
897	449.4	-0.90	4.78		
902	450.8	-0.65	4.88	0.67	3.17
907	452.2	-0.82	4.83		
912	453.6	-0.49	4.74	0.37	3.15
917	455.0	-0.30	4.60		
922	457.8	-1.12	4.82	0.63	3.05
927	460.6	-0.34	4.66		
932	463.3	-0.71	4.69	0.48	2.90
937	466.1	-0.25	4.60		
942	468.9	-0.15	4.62	0.58	3.00
947	471.7	-0.17	4.42		
952	474.4	0.14	4.36	1.29	2.53
957	477.2	0.30	4.21		
962	480.0	0.30	4.19		

Table 2b: Sedimentologic data of core **SO136-164**

Depth (cm)	Age (ka)	LSR (cm/kyr)	Carbonate Conc. (wt-%)	Carbonate AR ($g/cm^2/kyr$)	Coarse Carbonate (wt-%)	Fragmentation Ratio (%)
2	6.2	3.6	75.9	2.1	4.9	70.3
7	7.5	3.6		2.3		52.3
12	8.9	3.6	76.6	2.2	13.4	36.5
17	10.3	3.6		2.1		
22	11.6	3.6	74.8	2.1	18.8	30.0
27	13.0	3.0		1.9		
32	15.2	2.3	68.1	1.3	24.8	28.6
37	17.5	2.2		1.2		
42	19.8	2.2	67.0	1.2	20.3	43.2
47	22.0	2.2		1.1		
52	24.2	2.2	62.4	1.0	25.7	52.3
57	26.5	2.2		1.1		
62	28.7	2.2	69.8	1.2	21.8	41.2
67	31.0	2.1		1.1		
72	34.4	1.6	71.7	0.9	22.6	35.3
77	37.7	1.5		0.9		
82	41.1	1.5	73.2	0.8	20.5	32.8
87	44.5	1.5		0.9		
92	47.9	1.5	75.0	0.9	17.5	30.1
97	51.2	1.5		0.9		
102	54.6	1.5	72.8	0.8	19.7	32.1
107	58.0	1.6		0.8		
112	60.0	2.4	68.3	1.3	14.2	36.7
117	62.0	2.5		1.2		
122	64.0	2.5	62.9	1.2	13.0	49.2
127	66.0	2.5		1.2		
132	68.0	2.5	69.2	1.3	15.0	38.9
137	70.0	2.4		1.3		
142	72.8	1.9	74.4	1.1	11.6	44.2
147	75.7	1.8		1.1		
152	78.5	1.8	74.9	1.1	11.3	45.5
157	81.3	1.8		1.0		
162	84.2	1.8	69.1	0.9	12.8	47.3
167	87.0	1.7				
172	90.2	1.6	70.5	0.9	13.9	42.3
177	93.3	1.6				
182	96.5	1.6	75.1	0.9	13.9	43.2
187	99.7	1.6				
192	102.8	1.6	73.3	0.9	13.5	42.4
197	106.0	1.6				
202	109.1	1.6	75.1	1.0	11.2	45.4
207	112.2	1.6				50.5
212	115.4	1.6	72.2	1.0	5.0	65.7
217	118.5	1.6				57.7
222	121.6	1.6	73.0	1.0	9.7	54.7
227	124.7	1.6				
232	127.9	1.6	75.1	0.9	16.2	28.5
237	131.0	1.7				
242	132.9	2.5	74.4	1.6	15.7	34.6
247	134.9	2.6				
252	136.8	2.6	72.0	1.6	13.5	29.0
257	138.7	2.6				
262	140.6	2.6	72.8	1.6	18.2	31.0
267	142.6	2.6				
272	144.5	2.6	71.8	1.5	18.1	30.7
277	146.4	2.6				
282	148.4	2.6	72.7	1.5	19.5	36.6
287	150.3	2.6				
292	152.2	2.6	74.4	1.5	21.6	33.2
297	154.1	2.6				
302	156.1	2.6	72.8	1.5	20.4	34.6
307	158.0	2.7				
312	159.4	3.5	69.2	1.7	20.8	27.2
317	160.7	3.7				
322	162.1	3.7	69.3	1.8	14.2	39.0
327	163.5	3.7				
332	164.8	3.7	57.3	1.4	14.0	55.6
337	166.2	3.7				
342	167.5	3.7	64.1	1.6	17.1	39.9
347	168.9	3.7				
352	170.3	3.7	55.8	1.3	16.3	51.8
357	171.6	3.7				
362	173.0	3.2	47.7	1.0	14.2	55.9
367	177.0	1.6				
372	181.0	1.3	46.5	0.4	8.9	60.1
377	185.0	1.3				
382	189.0	1.3	58.5	0.6	5.4	67.7
387	193.0	1.3				
392	197.0	1.3	62.2	0.9	6.8	56.2
397	199.7	1.8				
402	202.3	1.9	51.8	0.7	9.6	57.9
407	205.0	1.9				
412	207.7	1.9	56.9	0.8	12.6	48.8
417	210.3	1.9				
422	213.0	1.6	70.8	1.1	9.9	52.2
427	220.7	0.8				
432	228.3	0.7	74.0	0.4	13.3	42.7
437	236.0	0.7				
442	240.3	1.1	71.1	0.6	13.9	41.5
447	244.7	1.2				
452	249.0	1.3	71.1	0.8	7.9	46.0
457	250.9	2.5				
462	252.8	2.6	72.9	1.6	9.9	41.6
467	254.7	2.6				
472	256.6	2.6	67.6	1.4	9.3	46.9
477	258.4	2.6				
482	260.3	2.6	68.1	1.4	6.9	39.8

Table 2b: Sedimentologic data of core **SO136-164**

Depth (cm)	Age (ka)	LSR (cm/kyr)	Carbonate Conc. (wt-%)	Carbonate AR ($g/cm^2/kyr$)	Coarse Carbonate (wt-%)	Fragmentation Ratio (%)
487	262.2	2.6				53.5
492	264.1	2.6	47.0	0.8	10.4	63.1
497	266.0	2.5				62.5
502	269.3	1.7	53.3	0.6	15.2	52.6
507	272.5	1.5				64.8
512	275.8	1.5	55.3	0.6	11.7	61.8
517	279.0	1.6				57.9
522	281.8	1.7	78.0	1.1	3.4	52.8
527	284.7	1.8				
532	287.5	1.8	77.8	1.1	3.8	58.5
537	290.3	1.8				
542	293.2	1.8	72.6	1.0	4.8	65.2
547	296.0	1.7				
552	299.4	1.5	60.8	0.6	10.9	64.4
557	302.9	1.5				
562	306.3	1.5	67.5	0.8	8.9	58.7
567	309.8	1.5				
572	313.2	1.5	71.3	0.8	5.3	64.6
577	316.7	1.5				
582	320.1	1.5	62.7	0.6	5.4	68.4
587	323.6	1.5				
592	327.0	1.5	56.8	0.6	5.6	75.5
597	329.0	2.4				69.2
602	331.0	2.5	69.6	1.3	5.3	66.1
607	333.0	2.5				
612	335.0	2.5	71.6	1.5	8.2	52.3
617	337.0	2.5				
622	339.0	2.5	70.3	1.4	11.9	48.5
627	340.8	2.7				
632	342.6	2.8	73.9	1.7	14.5	37.1
637	344.4	2.8				
642	346.2	2.8	68.0	1.6	15.7	33.3
647	348.0	2.8				
652	349.8	2.8	74.1	1.7	9.4	53.0
657	351.6	2.8				
662	353.4	2.8	63.8	1.4	12.6	47.4
667	355.2	2.8				
672	357.0	2.8	68.9	1.5	10.9	47.8
677	358.8	2.8				
682	360.6	2.7	70.0	1.5	10.2	49.1
687	362.5	2.7				
692	364.3	2.7	66.3	1.3	7.2	64.4
697	366.1	2.7				
702	367.9	2.7	71.9	1.5	8.3	50.7
707	369.7	2.7				
712	371.5	2.7	68.8	1.4	6.3	58.3
717	373.4	2.7				
722	375.2	2.7	77.3	1.7	6.3	56.2
727	377.0	2.5				
732	381.3	1.4	77.2	0.8	3.1	61.0
737	385.5	1.2				
742	389.8	1.2	77.9	0.8	3.3	62.8
747	394.0	1.3				
752	396.4	1.9	69.5	1.0	4.4	72.9
757	398.9	2.1				
762	401.3	2.1	77.1	1.3	2.0	63.6
767	403.7	2.1				
772	406.1	2.1	68.8	1.0	2.3	56.2
777	408.6	2.1				
782	411.0	2.1	74.8	1.3	1.4	66.7
787	412.9	2.5				
792	414.8	2.6	84.8	1.8	2.4	54.7
797	416.7	2.6				
802	418.7	2.6	83.0	2.0	3.8	48.8
807	420.6	2.6				
812	422.5	2.6	80.6	1.8	4.7	46.1
817	424.4	2.6				
822	426.3	2.6	79.7	1.8	5.6	33.1
827	428.3	2.6				
832	430.2	2.6	76.8	1.7	4.6	
837	432.1	2.6				
842	434.0	2.7	68.3	1.6	9.1	
847	435.4	3.5				
852	436.8	3.6	59.4	1.7	9.5	
857	438.2	3.6				
862	439.6	3.6	52.5	1.4	8.2	
867	441.0	3.6				
872	442.4	3.6	74.9	2.3	6.7	
877	443.8	3.6				
882	445.2	3.6	84.6	2.9	5.9	
887	446.6	3.6				
892	448.0	3.6	81.3	2.6	5.7	
897	449.4	3.6				
902	450.8	3.6	72.8	2.2	6.0	
907	452.2	3.6				
912	453.6	3.6	75.5	2.3	6.4	
917	455.0	3.3				
922	457.8	2.0	62.8	0.9	8.6	
927	460.6	1.8				
932	463.3	1.8	66.7	0.9	6.8	
937	466.1	1.8				
942	468.9	1.8	69.0	0.9	7.2	
947	471.7	1.8				
952	474.4	1.8	82.7	1.3	3.0	
957	477.2	1.8	78.3	1.1	3.0	
962	480.0	1.8	80.6	1.2	2.4	

Table 3: Stable isotope data of core **MD97-2108**

		C. wuellerstorfi		*G. bulloides*	
Depth	**Age**	**$\delta^{13}C$**	**$\delta^{18}O$**	**$\delta^{13}C$**	**$\delta^{18}O$**
(cm)	(ka)	(‰ vs PDB)	(‰ vs PDB)	(‰ vs PDB)	(‰ vs PDB)
1	4.0	0.74	3.23	-0.23	2.31
8	6.0	0.60	3.11	-0.10	1.64
14	7.7			-0.22	1.92
20	9.4	0.57	3.86	-0.30	2.16
26	11.1	0.26	4.13	-0.54	2.69
31	12.6	0.39	4.22	-0.47	3.15
36	14.0	0.40	4.54	-0.47	3.13
41	14.9	0.47	4.52	-0.30	2.96
46	15.7	0.52	4.49	-0.17	3.15
51	16.6	0.30	4.46	-0.33	3.00
56	17.4	0.23	4.50	-0.13	3.17
61	18.3			0.11	3.24
66	19.1			0.11	3.31
71	20.0	0.28	4.70	0.20	3.03
76	24.3	0.45	4.05	0.72	3.17
81	28.7	0.42	4.41	0.48	3.07
86	33.0	0.57	3.83	0.33	2.93
91	36.5	0.64	4.19	0.67	2.87
96	40.0	0.71	4.17	0.48	2.93
101	43.5	0.70	4.26	0.41	2.64
106	47.0	0.66	3.82	0.45	2.80
111	50.5	0.66	4.15	0.08	2.55
116	54.0	0.57	3.83	0.27	2.80
121	56.4	0.45	3.99	0.34	2.76
126	58.8			-0.02	2.72
131	61.1	0.68	4.24	0.47	3.01
136	63.5	0.38	4.56	0.66	3.10
141	65.9	0.63	4.15	0.51	2.78
146	68.3	0.63	4.21	0.28	2.91
151	70.6	0.45	4.15	0.36	2.92
156	73.0	0.62	4.06	0.29	2.83
161	75.0			0.29	2.48
166	77.0			0.50	3.02
171	79.0	0.58	4.10	0.17	2.71
176	81.0	0.61	3.88	0.36	2.90
181	83.0	0.44	4.02	0.18	2.76
186	85.0	0.42	3.90	0.14	2.75
191	87.0	0.47	4.18	0.35	2.77
196	93.7	0.63	3.65	0.23	2.69
201	100.3	0.60	3.73	-0.02	2.91
206	107.0	0.21	4.00	0.36	2.61
211	110.0	0.46	3.76	0.23	2.65
216	113.0	0.67	3.53	0.03	2.37
221	116.0	0.43	3.60	0.16	2.15
226	119.0	0.26	3.92	-0.20	1.88
231	122.0	0.63	3.26	-0.43	1.93
236	124.0	0.39	3.79	-0.25	1.60
241	126.0	0.07	4.75	-0.57	2.21
246	128.0	0.00	4.59	-0.61	1.62
251	130.0	0.26	4.55	-0.42	2.68
256	132.0	0.04	4.51	-0.49	3.41
261	134.0	0.01	4.80	-0.39	3.57
266	137.1	0.02	4.78	-0.63	3.48
271	140.2	0.06	4.90	-0.14	3.61
276	143.3	0.05	4.40	-0.31	3.54
281	146.4	-0.04	4.80	-0.58	3.11
286	149.5	-0.09	4.63	-0.24	3.30
291	152.6			-0.42	3.12
296	155.7			-0.50	3.06
301	158.8	0.06	4.49	-0.27	3.01
306	161.9	0.20	4.14	-0.69	2.73
311	165.0	0.32	4.04	-0.26	2.96
316	175.5	-0.04	4.82	0.04	2.90
321	186.0	0.36	3.88	-0.28	2.80
326	188.5	0.47	3.55	0.07	2.59
331	191.0	0.52	3.31	-0.01	2.29
336	193.5	0.34	3.44	-0.04	2.49
341	196.0	0.33	3.54	-0.33	2.50
346	198.5	0.37	3.17	-0.07	2.40
351	201.0	0.06	4.10	-0.63	2.55
356	206.8	0.27	4.14	-0.66	2.60
361	212.5	0.07	3.99	-0.64	2.44
366	218.3	-0.12	4.06	-0.62	2.47
371	224.0	0.16	4.34	-0.33	2.93
376	226.4	-0.09	4.29	-0.74	2.56
381	228.8	0.00	4.24	-0.10	3.08
386	231.2	0.36	3.78	0.05	2.80
391	233.6	0.25	4.02	-0.19	2.51
396	236.0	0.39	4.18	-0.16	2.38
401	237.8	0.44	3.97	-0.05	2.50
406	239.7	0.25	4.28	-0.39	2.60
411	241.5			-0.25	2.90
416	243.3	0.29	4.39	-0.47	2.74
421	245.2			-0.46	3.15
426	247.0	0.11	4.66	-0.51	3.21
431	252.9	-0.01	4.67	-0.61	3.23
436	258.7	-0.05	4.63	-0.17	3.46
441	264.6			-0.20	3.32
446	270.4	-0.03	4.46	-0.16	3.43
451	276.3	-0.22	4.76	-0.27	3.18
456	282.1	0.40	4.16	0.20	2.92
461	288.0	0.50	4.29	0.48	2.91
466	289.3	0.25	4.15	0.35	2.76
471	290.7	0.34	4.30	0.28	2.87
476	292.0	0.15	4.44	0.12	2.81
481	293.3	0.26	4.44	0.24	2.86
486	294.7	0.20	4.40	0.34	2.94

Table 3: Stable isotope data of core **MD97-2108**

		C. wuellerstorfi		*G. bulloides*	
Depth	**Age**	**$\delta^{13}C$**	**$\delta^{18}O$**	**$\delta^{13}C$**	**$\delta^{18}O$**
(cm)	(ka)	(‰ vs PDB)	(‰ vs PDB)	(‰ vs PDB)	(‰ vs PDB)
491	296.0	0.32	4.58	0.38	3.04
496	299.0	0.26	4.45	0.19	2.84
501	302.0	0.35	4.51	0.21	2.94
506	305.0	0.29	4.13	0.26	2.83
511	308.0	0.30	4.40	0.54	2.81
516	311.0	0.39	4.03	0.37	2.65
521	314.0	0.46	4.01	0.08	2.66
526	317.0	0.14	4.36	0.21	2.39
531	319.2	0.38	3.76	0.09	2.40
536	321.4	0.36	3.81	0.18	2.47
541	323.6			0.26	2.43
546	325.8	0.07	4.55	0.27	2.19
551	328.0	0.11	3.56	-0.01	2.30
556	329.6	-0.85	4.45	-0.21	2.15
561	331.1	0.14	4.07	0.12	2.56
566	332.7	-0.19	4.78	-0.16	2.50
571	334.3	0.13	4.24	-0.12	2.87
576	335.9	-0.09	4.44	-0.19	3.17
581	337.4			0.12	3.34
586	339.0	-0.45	4.70	0.08	3.09
591	340.3	-0.96	4.73	0.04	3.53
596	341.7	-1.02	4.76	0.36	3.61
601	343.0	-0.21	4.81	0.53	3.62
606	344.3	-0.44	4.77	0.28	3.64
611	345.7	-0.51	4.48	0.26	3.74
616	347.0	0.16	4.30	0.26	3.21
621	348.3	0.06	4.82	0.39	3.47
626	349.7	0.07	4.54	0.39	3.24
631	351.0	-0.90	4.53	0.36	3.46
635	352.6	0.00	4.73	0.60	3.47
641	355.0	0.26	3.83	0.54	3.35
646	357.0	0.14	4.59	0.56	3.53
651	358.9	0.28	4.67	0.42	3.37
656	360.9	0.56	4.53	0.41	3.20
661	362.9	0.38	4.67	0.49	3.24
666	364.9	0.27	4.58	0.69	3.14
671	366.9	0.46	4.54	0.46	3.14
676	368.9	0.38	4.61	0.61	3.01
681	370.8	-0.42	4.45	0.48	3.29
686	372.8	0.47	4.35	0.49	3.07
691	374.8			0.56	2.87
694	376.0	-0.05	4.79	0.59	2.94
701	378.6	0.43	3.90	0.48	3.03
706	380.5	0.59	4.10	0.16	2.85
711	382.4	0.09	4.29	0.49	2.96
716	384.2	0.54	3.99	0.71	2.95
721	386.1	0.64	4.16	0.82	3.06
726	388.0	0.69	3.93	0.44	3.16
731	389.8	0.62	3.96	0.76	2.92
736	391.7	0.37	4.27	0.67	3.03
741	393.6	0.84	3.82	0.75	2.68
746	395.4	0.76	3.77	1.02	2.49
751	397.3	0.74	3.62	0.67	2.75
756	399.2	0.63	3.79	0.83	2.48
761	401.0	0.62	4.08	0.72	2.68
766	402.9	0.57	3.70	0.88	2.35
771	404.8	0.68	3.43	0.94	2.34
777	407.0	0.61	3.46	0.57	2.38
781	409.0	0.43	3.39	0.60	2.01
786	411.4	0.58	3.44	0.80	2.14
791	413.9	0.63	3.58	0.68	2.17
796	416.3	0.55	3.83	0.55	2.42
801	418.8	0.49	3.86	0.49	2.80
806	421.2	0.53	3.77	0.28	2.30
811	423.7	0.57	4.41	0.12	2.90
816	426.1	0.66	3.85	-0.08	3.00
821	428.6	0.65	3.96	0.18	3.36
826	431.0	0.25	4.82	-0.15	3.22
831	433.5	0.32	4.86	-0.09	3.76
836	435.9	-0.10	4.94	0.14	3.57
841	438.4	0.11	4.52	-0.05	3.30
846	440.8			0.14	3.39
851	443.2	-0.06	4.71	0.13	3.30
856	445.7	0.51	4.42	0.36	3.48
861	448.1	0.25	4.74	0.42	3.18
866	450.6	0.31	4.66	0.79	3.23
871	453.0	0.55	4.25	0.84	3.23
876	455.5	0.77	4.41	0.96	3.17
881	457.9	0.62	4.31	0.88	2.99
886	460.4	0.63	4.48	0.98	3.19
891	462.8	0.55	4.27	1.13	3.12
896	465.3	0.68	4.32	1.13	3.12
901	467.7	0.85	4.46	1.14	2.90
906	470.2	0.89	4.10	0.95	2.70
911	472.6	0.92	4.06	1.06	2.81

Table 4: Stable isotope data and sedimentologic data of core **SO136-162**

			C. wuellerstorfi		*G. bulloides*		Carbonate		Coarse
Depth	**Age**	**LSR**	**$\delta^{13}C$**	**$\delta^{18}O$**	**$\delta^{13}C$**	**$\delta^{18}O$**	**Conc.**	**AR**	**Carbonate**
(cm)	(ka)	(cm/kyr)	(‰ vs PDB)	(‰ vs PDB)	(‰ vs PDB)	(‰ vs PDB)	(wt-%)	(g/cm^2/kyr)	(wt-%)
2	5.0	3.0	0.23	3.29	0.02	1.18	88.8	2.3	26.5
7	6.7	3.0	0.54	3.36	0.14	1.08	89.1	2.3	32.8
12	8.3	3.0	-0.08	4.32	-0.17	1.68	86.7	2.3	36.0
17	10.0	3.0	-0.02	4.35	-0.61	1.63	85.4	2.3	37.5
22	11.7	3.0	-0.32	4.70	-0.09	2.68	83.8	2.2	40.8
27	13.3	3.0	-0.37	4.66	-0.24	2.60	85.0	2.2	50.2
32	15.0	2.8	-0.48	5.00	0.12	3.08	84.7	1.9	53.2
37	17.8	1.9	-0.55	5.03	0.31	3.24	83.2	1.4	56.6
42	20.6	1.8	-0.22	4.75	-0.02	3.18	80.6	1.2	58.9
47	23.4	1.8	-0.19	4.80	0.09	2.86	84.0	1.2	57.9
52	26.2	1.8	-0.21	4.67	-0.03	2.85	82.6	1.2	62.7
57	29.0	1.7	-0.03	4.61	0.15	2.89	85.7	1.2	61.3
62	33.5	1.2	-0.16	4.57	0.13	2.72	85.7	0.9	51.3
67	38.0	1.1	-0.03	4.47	0.10	2.73	85.9	0.9	50.3
72	42.5	1.1	-0.11	4.49	0.33	2.79	85.2	0.9	47.4
77	47.0	1.1	-0.14	4.47	0.33	2.75	86.7	0.9	46.7
82	51.5	1.1	-0.28	4.53	-0.29	2.49	82.8	0.8	48.6
87	56.0	1.2	-0.20	4.50	0.03	2.73	83.6	0.9	40.8
92	58.4	2.0	-0.58	4.61	0.50	3.15	79.7	1.3	37.3
97	60.8	2.1	-0.47	4.68	0.35	3.09	78.9	1.5	32.2
102	63.2	2.1	-0.69	4.54	0.40	3.51	80.5	1.4	26.4
107	65.6	2.1	-0.30	4.67	0.78	3.49	86.2	1.7	25.9
112	68.0	2.0	-0.18	4.50	0.33	3.00	85.2	1.6	34.1
117	70.9	1.8	-0.18	4.30	1.00	2.97	88.7	1.4	36.5
122	73.7	1.8	-0.39	4.09	1.00	3.12	86.4	1.4	32.1
127	76.6	1.8	0.09	4.20	0.90	2.94	89.2	1.4	33.0
132	79.4	1.8	-0.16	3.98	0.48	2.65	87.1	1.4	30.6
137	82.3	1.8	-0.40	3.94	0.82	2.63	87.9	1.4	30.5
142	85.1	1.8	-0.35	4.03	0.71	2.91	83.3	1.3	33.3
147	88.0	1.7	-0.22	4.29	0.80	2.96	88.8	1.4	41.6
152	91.0	1.7	-0.12	4.10	0.65	2.80	87.5	1.3	41.9
157	94.0	1.7	-0.08	4.06	0.54	2.75	89.1	1.4	34.8
162	97.0	1.7	0.32	3.99	0.48	2.66	88.5	1.3	32.8
167	100.0	1.7	-0.02	3.97	0.51	2.75	88.4	1.3	33.8
172	103.0	1.7	0.01	4.00	0.20	2.56	86.7	1.3	35.7
177	106.0	1.7	-0.22	4.23	0.46	2.61	86.3	1.3	33.9
182	108.7	1.8	-0.38	4.16	0.62	2.89	86.7	1.5	35.0
187	111.3	1.9	0.04	4.07	0.49	2.70	87.9	1.5	34.2
192	114.0	1.9	-0.17	3.97	0.62	2.79	86.7	1.5	30.7
197	116.7	1.9	0.28	3.83	0.18	2.34	87.3	1.5	28.1
202	119.3	1.9	-0.05	4.11	-0.26	1.42	86.8	1.4	32.1
207	122.0	1.8	0.25	3.22	-0.70	1.14	87.1	1.4	37.2
212	125.0	1.7	0.06	3.51	-0.53	1.74	86.1	1.3	31.8
217	128.0	1.7	-0.37	4.80	-0.26	2.67	89.0	1.4	31.7
222	131.0	1.7			-0.15	3.72	84.6	1.4	37.3
227	134.0	1.6	-0.30	5.04	-0.02	3.63	86.2	1.3	35.2
232	137.3	1.5	-0.54	4.99	0.14	3.79	81.3	1.2	30.9
237	140.7	1.5	-0.53	4.82	0.28	3.62	83.7	1.1	30.3
242	144.0	1.5	-0.73	4.92	-0.05	3.56	82.4	1.1	32.8
247	147.3	1.5	-0.56	4.78	0.33	3.57	85.7	1.1	36.8
252	150.7	1.5	-0.69	4.82	0.19	3.52	82.7	1.1	35.7
257	154.0	1.6	-0.62	4.73	0.11	3.55	85.6	1.2	35.0
262	156.2	2.2	-0.59	4.90	0.22	3.85	81.7	1.5	36.7
267	158.4	2.3	-0.64	4.89	0.17	3.70	86.3	1.7	38.0
272	160.6	2.3	-0.77	4.83	-0.08	3.61	80.8	1.5	47.9
277	162.8	2.3	-0.67	4.62	0.10	3.10	83.2	1.6	42.3
282	165.0	2.0	0.11	4.07	0.03	3.20	82.8	1.4	33.9
287	171.2	1.0	-0.30	4.40	0.25	3.11	81.2	0.7	35.8
292	177.5	0.8	-0.05	4.26	0.13	3.21	78.7	0.5	40.3
297	183.7	0.8	-0.16	4.29	0.39	3.02	85.9	0.6	41.9
302	190.0	0.9	0.12	3.94	0.22	2.77			
307	192.3	2.0	-0.18	4.13	-0.24	2.07	86.9	1.5	30.3
312	194.7	2.1	-0.15	3.98	-0.48	2.00			
317	197.0	2.1	-0.48	4.33	-0.35	2.93	89.1	1.8	34.3
322	199.3	2.1	-0.64	4.56	0.09	3.13	84.9	1.7	42.9
327	201.7	2.1	-0.29	4.61	0.01	3.32	88.7	1.8	28.1
332	204.0	2.1	-0.62	4.62	-0.17	3.48	84.7	1.7	24.4

Table 5: Stable isotope data and sedimentologic data of core **SO136-155**

			C. wuellerstorfi		*G. bulloides*		Carbonate		Coarse
Depth	**Age**	**LSR**	**$\delta^{13}C$**	**$\delta^{18}O$**	**$\delta^{13}C$**	**$\delta^{18}O$**	**Conc.**	**AR**	**Carbonate**
(cm)	(ka)	(cm/kyr)	(‰ vs PDB)	(‰ vs PDB)	(‰ vs PDB)	(‰ vs PDB)	(wt-%)	(g/cm^2/kyr)	(wt-%)
0	5.0	3.5			0.01	1.12	93.1	2.7	40.3
5	6.4	3.5	0.61	3.22	-0.01	1.44	93.2	3.1	36.4
10	7.9	3.5	0.35	3.41	-0.02	1.20	93.1	2.9	36.8
15	9.3	3.5	0.22	4.13	-0.47	1.49	91.9	2.9	35.8
20	10.7	3.5	0.19	4.00	-0.48	1.35	92.2	2.9	40.1
25	12.1	3.5	0.15	4.37	-0.47	2.36	91.0	2.9	43.3
30	13.6	3.5	-0.30	4.77	-0.93	2.57	92.5	2.8	53.3
35	15.0	3.2	-0.56	5.06	-0.66	2.84	89.0	2.3	52.7
40	18.0	1.9	-0.10	4.89	-0.57	3.19	90.2	1.5	50.8
45	21.0	1.7	-0.02	5.01	-0.52	3.26	90.1	1.3	49.7
50	24.0	1.7	-0.15	4.80	-0.48	2.82	90.5	1.5	57.3
55	27.0	1.7	0.48	4.62	-0.61	2.78	90.4	1.3	64.1
60	30.0	1.7	0.07	4.50	-0.40	2.78	91.6	1.4	56.3
65	33.0	1.6	0.33	4.26	-0.15	2.77	90.1	1.4	56.2
70	36.9	1.3	0.38	4.52	-0.16	2.75	89.2	1.1	48.1
75	40.7	1.3	-0.01	4.60	-0.32	2.62	90.3	1.3	44.4
80	44.6	1.3	0.28	4.58	-0.42	2.61	90.0	1.1	48.2
85	48.4	1.3	0.08	4.21	-0.37	2.67	89.9	1.2	46.1
90	52.3	1.3	0.19	4.25	-0.16	2.50	89.6	1.1	48.1
95	56.1	1.3	0.21	4.23	-0.67	2.49	91.2	1.2	47.4
100	60.0	1.4	-0.41	4.54	-0.44	2.62	89.6	1.2	45.0
105	61.8	2.6	-0.24	4.52	-0.34	2.82	89.3	2.3	40.9
110	63.6	2.8	-0.20	4.61	-0.12	3.22	86.3	2.5	35.9
115	65.4	2.8	-0.99	4.45	-0.21	2.98	88.3	2.6	29.2
120	67.2	2.8	-0.49	4.68	0.11	3.09	89.0	2.4	30.9
125	69.0	2.7	-0.25	4.30	-0.22	2.81	90.8	2.4	32.8
130	71.3	2.2	0.15	4.19	0.22	2.69	91.1	2.0	39.6
135	73.6	2.2	0.00	4.01	0.17	2.76	90.8	1.9	35.8
140	75.9	2.2	0.31	4.19	0.21	2.62	91.3	2.0	37.0
145	78.3	2.2	0.25	3.92	0.04	2.27	92.5	1.9	34.8
150	80.6	2.2	-0.22	3.96	0.18	2.01	92.5	2.0	37.1
155	82.9	2.2	0.00	3.82	0.06	2.27	91.6	1.9	36.3
160	85.2	2.2	-0.09	4.32	-0.05	2.35	90.7	1.7	39.4
165	87.5	2.2	-0.04	4.07	0.13	2.35	91.5	1.9	45.8
170	89.8	2.2	0.21	4.05	0.30	2.46	92.0	2.0	46.8
175	92.1	2.2	-0.10	4.06	0.07	2.40	92.0	2.0	42.7
180	94.4	2.2	-0.07	4.19	0.22	2.48	91.0	1.9	35.7
185	96.8	2.2	0.16	3.87	-0.01	2.01	91.9	1.9	40.4
190	99.1	2.2	0.18	3.86	-0.03	2.29	91.5	1.8	41.0
195	101.4	2.2	0.00	3.80	-0.14	1.92	90.9	1.8	37.2
200	103.7	2.2	0.23	3.86	0.04	2.22	91.0	1.8	40.0
205	106.0	2.2	-0.06	4.10	-0.14	2.18	91.8	1.9	37.7
210	108.1	2.3	0.47	4.04	0.38	2.48	91.0	2.1	38.1
215	110.3	2.3	0.16	3.69	0.24	2.63	91.8	2.1	40.7
220	112.4	2.3	0.39	3.61	0.45	2.39	93.3	2.1	34.3
225	114.6	2.3	0.40	3.54	0.09	2.07	93.5	2.1	38.8
230	116.7	2.3	0.14	3.77	0.20	2.04	93.2	2.0	37.0
235	118.9	2.3	0.21	3.39	-0.38	1.09	93.2	1.7	36.0
240	121.0	2.3	0.34	3.28	-0.21	1.27	92.0	2.0	38.7
245	123.2	2.3	0.00	3.98	-0.63	1.20	90.4	1.9	38.7
250	125.4	2.3	-0.09	3.65	-0.66	1.19	91.4	2.0	39.3
255	127.6	2.3	0.16	4.09	-0.68	1.96	92.0	2.0	38.1
260	129.8	2.3	-0.51	4.75	-0.71	2.73	91.1	2.0	40.4
265	132.0	2.3	-0.20	4.92	-0.97	2.45	89.5	1.8	50.2
270	134.2	2.3	-0.21	4.83	-0.78	3.05	88.0	1.9	44.8
275	136.4	2.3	-0.77	4.86	-0.61	3.20	91.5	2.0	46.4

Table 6: Stable isotope data and sedimentologic data of core **MD97-2107**

			C. wuellerstorfi		*G. bulloides*		Carbonate		Coarse
Depth	**Age**	**LSR**	**$\delta^{13}C$**	**$\delta^{18}O$**	**$\delta^{13}C$**	**$\delta^{18}O$**	**Conc.**	**AR**	**Carbonate**
(cm)	(ka)	(cm/kyr)	(‰ vs PDB)	(‰ vs PDB)	(‰ vs PDB)	(‰ vs PDB)	(wt-%)	(g/cm^2/kyr)	(wt-%)
1	3.0	2.9	0.32	3.61	0.70	2.49	86.8	2.3	31.7
4	4.0	2.9	0.57	3.30	0.36	2.82	92.3	2.5	29.8
9	5.7	2.9	0.49	3.56	0.23	2.34	87.1	2.2	30.5
14	7.5	2.8	0.37	3.18	0.18	2.53	90.1	2.3	30.8
19	9.3	2.7	0.38	3.61	-0.21	2.38	86.8	2.1	34.4
24	11.3	2.5	-0.16	4.68	-0.02	2.39	90.3	2.1	27.8
29	13.4	2.3	-0.26	4.59	-0.31	2.65	87.4	1.8	39.1
34	15.6	2.2	-0.19	4.85	-0.11	3.07	88.3	1.7	36.5
39	18.0	2.0	-0.35	5.22	-0.18	3.61	85.3	1.5	39.1
44	20.6	1.8			0.24	3.52	84.2	1.4	42.7
49	23.4	1.7	-0.19	4.52	0.40	3.80	81.5	1.2	47.0
54	26.3	1.7	-0.09	4.76	0.42	3.46	83.0	1.2	45.7
59	29.4	1.6	-0.04	4.31	0.67	3.58	85.2	1.2	52.3
64	32.5	1.6	0.21	4.45	0.46	3.46	88.0	1.3	46.7
69	35.6	1.6	0.21	3.75	0.70	3.65	87.0	1.2	44.2
74	38.7	1.6	0.10	4.59	0.58	3.45	88.2	1.3	43.4
79	41.8	1.6	-0.14	4.46	0.56	3.31	89.1	1.3	39.2
84	44.8	1.7	-0.19	4.37	0.25	3.17	87.8	1.3	38.8
89	47.7	1.8	0.33	4.48	0.47	3.35	89.6	1.5	41.4
94	50.5	1.9	0.17	4.43	0.21	3.24	87.2	1.5	41.5
99	53.0	2.1	-0.29	4.12	0.22	3.27	86.8	1.6	42.2
104	55.3	2.2	-0.35	4.58	0.13	3.24	85.6	1.7	41.0
109	57.5	2.4	-0.63	4.63	0.18	3.46	85.9	1.9	39.5
114	59.4	2.6	-0.17	4.56	0.25	3.64	86.8	2.0	35.4
119	61.3	2.8	-0.28	4.69	0.45	3.74	86.2	2.1	28.6
124	63.1	2.9	-0.40	4.44	0.58	3.53	88.5	2.3	28.4
129	64.8	2.9	0.05	4.35	0.72	3.59	86.8	2.3	28.3
134	66.5	2.9	-0.17	4.40	0.64	3.21	89.9	2.4	30.0
139	68.2	2.9	0.05	4.51	0.64	3.21	87.4	2.2	33.7
144	70.0	2.7	0.12	4.36	0.91	3.12	87.8	2.2	37.1
149	71.9	2.6	0.07	3.95	0.86	3.16	87.3	2.0	32.3
159	75.8	2.4	0.08	3.99	0.58	3.00	89.7	2.0	33.1
164	78.0	2.3	0.20	3.97	0.39	2.99	92.5	2.0	31.2
169	80.1	2.3	0.11	4.00	0.54	2.77	88.9	1.8	37.8
174	82.4	2.2	-0.19	4.12	0.46	2.93	89.8	1.8	35.1
179	84.7	2.2	-0.12	4.29	0.41	3.11	90.7	1.8	40.5
184	87.0	2.1	-0.13	4.24	0.66	3.13	87.7	1.7	48.4
189	89.4	2.1	0.12	4.15	0.73	3.30	91.7	1.8	38.7
194	91.8	2.1	0.12	4.12	0.48	3.05	86.6	1.6	44.3
199	94.3	2.0	-0.23	4.17	0.29	2.82	89.8	1.7	38.8
204	96.7	2.0	0.12	3.98	0.53	2.99	88.8	1.6	37.6
209	99.2	2.0	0.23	4.10	0.52	3.03	89.7	1.7	39.5
214	101.6	2.0	0.00	4.23	0.50	3.11	92.0	1.8	32.3
219	104.1	2.1	0.16	4.00	0.54	3.02	91.8	1.8	33.0
224	106.5	2.1	-0.02	4.16	0.35	3.20	92.0	1.8	37.5
229	108.8	2.1	0.07	4.16	0.51	3.04	93.0	1.9	36.2
234	111.1	2.2	-0.05	4.00	0.52	2.87	91.1	1.9	38.8
239	113.4	2.3	0.19	3.89	0.35	2.95	91.3	1.9	39.6
244	115.5	2.4	0.16	3.75	0.32	2.57	93.3	2.1	38.8
249	117.6	2.5	0.01	3.54			89.3	2.0	30.6
255	120.0	2.6	0.09	2.88	-0.31	1.89	89.0	2.1	33.0
259	121.5	2.7	-0.57	3.24	-0.16	2.85	89.3	2.2	32.4
264	123.3	2.7	-0.33	4.66	-0.17	3.45	88.4	2.2	38.7
269	125.2	2.7	-0.16	3.79	-0.15	3.14	86.5	2.1	31.1
274	127.1	2.5	-0.55	4.60	-0.02	3.81	86.6	1.9	27.7
279	129.2	2.3	-0.28	4.43	0.03	3.42	86.3	1.8	27.4
284	131.4	2.1	-0.53	4.71	0.08	3.49	86.5	1.6	26.0
289	134.0	1.8	-0.55	4.88	0.19	3.72	85.4	1.4	30.5
294	136.9	1.7	-0.65	4.58	0.00	3.44	86.8	1.3	39.7
299	140.1	1.5	-0.34	4.68	-0.02	3.61	87.7	1.2	42.1
304	143.4	1.4	-0.16	4.83	0.10	3.66	86.8	1.1	41.2
309	147.0	1.4	-0.32	4.92	-0.03	3.65	84.7	1.0	44.1
314	150.6	1.4	-0.40	4.37	-0.16	3.61	85.6	1.0	43.9
319	154.3	1.4	-0.12	4.09	-0.07	3.68	81.8	1.0	46.1
324	158.0	1.4	-0.30	4.69	-0.12	3.51	84.7	1.0	48.7
329	161.6	1.4	-0.56	4.40	-0.11	3.35	83.3	1.0	42.7
334	165.1	1.4	-0.18	4.44	0.01	3.19	84.3	1.1	47.9
339	168.5	1.5	-0.28	4.34	-0.15	3.22	82.8	1.1	43.8
344	171.8	1.5	-0.40	4.54	0.17	3.37	84.1	1.1	40.3
349	175.0	1.6	-0.22	4.60	0.18	3.09	85.8	1.2	43.3
354	178.1	1.6	-0.27	4.44	0.36	3.35	85.6	1.2	44.0
359	181.1	1.7	-0.12	4.11	0.19	2.90	86.4	1.3	45.5
364	184.0	1.8	0.06	4.00	0.21	2.74	87.4	1.4	46.3
369	186.8	1.8			0.18	3.04	86.4	1.4	50.5
374	189.5	1.9	-0.47	4.25	0.18	2.89	89.6	1.6	40.4
379	192.1	1.9	-0.12	3.60	-0.04	2.55	87.5	1.5	39.5
384	194.6	2.0	0.09	3.58	0.05	2.67	87.8	1.6	47.8
389	197.1	2.0	-0.42	3.75	0.09	2.44	90.0	1.7	36.1
394	199.6	2.0	-0.67	4.13	-0.06	2.90	88.2	1.6	35.2
399	202.0	2.0	-0.21	4.17	-0.12	3.11	85.6	1.6	41.4

Table 7: Stable isotope data of core **FRG94-003**

			C. wuellerstorfi		*G. bulloides*	
Depth	**Age**	**LSR**	**$\delta^{13}C$**	**$\delta^{18}O$**	**$\delta^{13}C$**	**$\delta^{18}O$**
(cm)	(ka)	(cm/kyr)	(‰ vs PDB)	(‰ vs PDB)	(‰ vs PDB)	(‰ vs PDB)
0	4.0	2.3	0.57	3.38	-0.76	0.17
5	6.2	2.3	0.53	3.41	0.05	0.98
10	8.3	2.3	0.52	4.12	0.01	1.07
15	10.5	2.3	-0.03	4.62	-0.42	2.01
20	12.7	2.3	0.33	3.56	0.00	2.36
25	14.8	2.3	0.08	4.78	0.04	2.66
30	17.0	2.0	-0.05	5.04	0.03	2.80
35	23.6	1.0	0.21	4.58	0.01	2.54
40	30.2	0.8	0.35	4.67	-0.45	2.26
45	36.8	0.8	0.24	4.49	0.27	2.53
50	43.3	0.8	0.17	4.49	0.39	2.63
55	49.9	0.8	0.23	4.21	0.13	2.52
60	56.5	0.8	0.19	4.02	0.35	2.76
65	63.1	0.8	0.25	4.49	0.11	2.38
71	71.0	0.8	0.30	4.22	0.53	2.33
75	74.6	1.1	0.07	3.88	0.19	2.00
80	79.1	1.1	0.14	3.93	0.13	1.68
90	88.0	1.1	0.24	4.17	0.19	1.97
95	93.5	0.9	0.41	3.31	-0.11	1.40
100	99.0	0.9	0.23	3.93	0.16	1.94
110	110.0	0.9	0.26	3.74	-0.39	1.50
115	115.5	0.9	0.15	3.80	0.33	1.86
120	121.0	1.0	0.41	3.12	-0.18	1.61
125	123.0	2.3	0.53	3.21	-0.32	0.92
130	125.0	2.5	0.15	3.76	-0.23	1.17
135	127.0	2.5	0.26	3.89	-0.40	0.92
140	129.0	2.5	-0.15	4.67	-0.44	1.55
145	131.0	2.2	0.03	5.09	-0.69	2.05
150	135.7	1.2	0.05	5.07	-0.71	2.63
155	140.3	1.1	-0.34	4.29	-0.69	2.88
160	145.0	1.1	-0.34	4.79	-0.49	2.84
165	149.7	1.1	-0.18	4.73	-0.44	2.94
168	152.5	1.1	-0.19	4.71	-0.55	2.77
172	156.2	1.1	-0.11	4.83	-0.52	2.70
175	159.0	1.1	-0.14	4.88	-0.01	2.92
180	162.4	1.4	-0.30	4.44	-0.10	3.32
185	165.8	1.5	-0.21	4.48	-0.40	2.96
190	169.2	1.5	-0.28	4.13	-0.45	2.87
195	172.6	1.5	-0.14	4.58	-0.08	3.04
200	176.0	1.3	0.15	4.46		
205	184.0	0.7	-0.25	4.57		
210	192.0	0.7	0.07	3.40		
215	195.7	1.3	0.08	3.93		
220	199.3	1.4	-0.04	4.01		
225	203.0	1.2	-0.21	4.55		
230	213.5	0.6	0.11	3.70		
235	224.0	0.5	-0.14	4.31		
240	228.7	1.0	-0.09	4.29		
250	238.0	1.0	-0.86	3.45		
255	248.0	0.5	-0.46	4.66		
262	264.8	0.4	-0.11	4.22		
265	272.0	0.5	-0.41	4.44		
270	278.0	0.8	-0.54	4.16		
280	290.0	0.9	0.24	4.09		
285	292.7	1.7	-0.15	4.34		
290	295.4	1.8	0.06	4.19		
295	298.1	1.8	-0.03	4.21		
300	300.9	1.8	0.09	4.23		
305	303.6	1.8	0.26	3.97		
310	306.3	1.8	0.16	3.83		
315	309.0	1.6	0.09	3.70		
320	316.3	0.8	-0.16	4.14		
325	323.7	0.7	0.28	3.86		
330	331.0	0.8	0.02	3.78		
335	334.1	1.5	-0.52	4.63		
340	337.3	1.6	-0.22	4.59		
346	341.1	1.6	-0.15	4.79		
350	343.6	1.6	-0.20	4.69		
355	346.7	1.6	-0.29	4.70		
360	349.8	1.6	-0.37	4.67		
365	353.0	1.6	-0.43	4.75		
370	356.1	1.6	-0.43	4.54		
373	358.0	1.6	-0.17	4.77		
377	360.5	1.6	-0.37	4.63		
380	362.4	1.6	-0.37	4.47		
385	365.6	1.6	-0.21	4.60		
390	368.7	1.6	-0.34	4.28		
395	371.9	1.6	-0.23	4.30		
400	375.0	1.5	-0.44	4.50		
410	385.0	1.1	-0.03	4.43		
415	390.0	1.0	-0.29	4.45		
420	395.0	1.0	-0.51	4.42		
425	400.0	0.9	0.29	2.94		
435	414.0	0.8	0.14	4.14		
440	421.0	0.7	0.50	3.70		
445	428.0	0.7	0.22	4.38		
450	435.0	0.8	-0.26	4.46		
460	440.8	1.6	-0.09	4.24		
465	443.7	1.7	0.25	4.08		
469	446.0	1.7	0.32	3.89		

Table 8: Stable isotope data of core **SO136-061**

			C. wuellerstorfi	
Depth (cm)	**Age** (ka)	**LSR** (cm/kyr)	**$\delta^{13}C$** (‰ vs PDB)	**$\delta^{18}O$** (‰ vs PDB)
2	4.0	4.9	1.88	2.48
4	4.4	4.9	1.54	3.22
6	4.8	4.9	1.69	4.26
8	5.2	4.9	1.73	2.86
10	5.6	4.9	1.62	3.31
12	6.0	4.9	1.52	2.62
14	6.4	4.9	1.83	3.14
16	6.9	4.9	1.66	2.81
18	7.3	4.9	1.73	2.60
20	7.7	4.9	1.68	2.73
22	8.1	4.9	1.73	3.18
24	8.5	4.9	1.79	3.82
26	8.9	4.9	1.73	3.12
28	9.3	4.9	1.94	4.06
30	9.7	4.9	1.89	2.85
32	10.1	4.9	1.68	2.91
34	10.5	4.9	1.62	3.73
36	10.9	4.9	1.68	3.61
38	11.3	4.9	1.73	3.30
40	11.7	4.9	1.62	4.11
42	12.1	4.9	1.56	4.06
44	12.6	4.9	1.70	2.97
46	13.0	4.9	1.70	3.99
48	13.4	4.9	1.62	3.98
50	13.8	4.9	1.73	4.22
52	14.2	4.9	1.53	4.11
54	14.6	4.9	1.75	4.20
56	15.0	4.0	1.66	4.47
58	17.4	1.3	1.73	4.37
60	19.9	0.8	1.69	4.22
62	22.3	0.8	1.93	4.06
64	24.7	0.8	1.95	3.71
66	27.1	0.8	1.83	4.12
68	29.6	0.8	1.56	4.03
70	32.0	0.8	1.82	3.87
72	34.4	0.8	1.71	3.91
74	36.9	0.8	1.98	3.96
76	39.3	0.8	1.84	3.81
78	41.7	0.8	2.04	3.94
80	44.1	0.8	1.94	3.94
82	46.6	0.8	1.84	3.90
84	49.0	0.8	1.82	4.11
86	51.4	0.8	1.78	4.27
88	53.9	0.8	1.96	3.87
90	56.3	0.8	2.01	3.59
92	58.7	0.8	1.86	3.88
94	61.1	0.8	1.70	3.97
96	63.6	0.8	1.85	4.12
98	66.0	0.9	2.06	3.78
100	67.0	1.9	2.00	4.04
102	68.0	2.0	1.76	3.79
104	69.0	2.0	2.05	3.74
106	70.0	2.0	1.98	3.19
108	71.0	2.0	1.81	3.78
110	72.0	2.0	1.73	3.47
112	73.0	2.0	1.74	3.80
114	74.0	2.0	1.94	3.38
116	75.0	2.0	1.92	3.31
118	76.0	2.0	1.77	3.41
120	77.0	2.0	2.05	3.46
122	78.0	2.0	1.98	3.56
124	79.0	2.0		
126	80.0	2.0	2.00	3.39
128	81.0	2.0	1.81	3.25
130	82.0	2.0		
132	83.0	2.0	2.10	3.49
134	84.0	2.0	2.04	3.38
136	85.0	2.0	2.05	3.41
138	86.0	2.0		
140	87.0	2.0	2.05	3.29
142	88.0	2.0	1.93	3.51
144	89.2	1.7	2.05	3.43
146	90.4	1.7	1.72	3.15
148	91.6	1.7	1.97	3.36
150	92.8	1.7	1.75	3.28
152	94.0	1.7	1.87	3.26
154	95.2	1.7	1.71	3.01
156	96.4	1.7	1.88	3.18
158	97.6	1.7	1.79	3.33
160	98.8	1.7	1.76	3.37
162	100.0	1.7	1.78	3.15
164	101.2	1.7	1.82	2.98
166	102.4	1.7	1.77	3.48
168	103.6	1.7	1.86	3.36
170	104.8	1.7	1.78	3.31
172	106.0	1.6	1.72	3.70
174	107.3	1.5	1.80	3.50
176	108.7	1.5	1.83	3.38
178	110.0	1.5	1.43	2.78
180	111.3	1.5	1.78	2.77
182	112.7	1.5	1.79	3.05
184	114.0	1.5	1.84	2.95
186	115.3	1.5	1.51	3.21
188	116.7	1.5	1.80	3.05
190	118.0	1.5	1.40	2.71
192	119.3	1.5	1.67	3.63
194	120.7	1.5	1.15	3.03

Table 8: Stable isotope data of core **SO136-061**

			C. wuellerstorfi	
Depth (cm)	**Age** (ka)	**LSR** (cm/kyr)	**$\delta^{13}C$** (‰ vs PDB)	**$\delta^{18}O$** (‰ vs PDB)
196	122.0	1.5	1.54	3.00
198	123.3	1.5	1.34	2.13
200	124.7	1.5	1.02	2.54
202	126.0	1.5	1.58	3.37
204	127.3	1.5	1.69	3.08
206	128.7	1.5	1.53	3.67
208	130.0	1.3	1.62	4.38
210	133.1	0.8	1.42	1.73
212	136.2	0.6	1.55	4.34
214	139.3	0.6	1.38	3.53
216	142.4	0.6	1.53	2.75
218	145.6	0.6	1.50	4.37
220	148.7	0.6	1.34	3.81
224	154.9	0.6	1.70	3.45
226	158.0	0.6	1.58	3.98

Table 9: Stable isotope and sedimentologic data of core **SO136-111**

			C. wuellerstorfi		*N. pachyderma*		Carbonate	Biog. Silica
Depth	**Age**	**LSR**	**$\delta^{13}C$**	**$\delta^{18}O$**	**$\delta^{13}C$**	**$\delta^{18}O$**	**Conc.**	**Conc.**
(cm)	(ka)	(cm/kyr)	(‰ vs PDB)	(‰ vs PDB)	(‰ vs PDB)	(‰ vs PDB)	(wt-%)	(wt-%)
2	3.2	5.5	3.59	0.16	1.27	3.16	34.7	
7	4.1	5.5	3.61	0.36	1.11	3.05	35.8	
12	5.0	5.5	3.56	0.38	1.07	3.17	32.8	
17	5.9	5.5	3.76	0.16	1.06	3.12	34.3	
22	6.8	5.5	3.90	0.03	1.03	3.30	36.3	
27	7.7	5.5	3.74	0.17	0.94	3.23	40.0	
32	8.6	5.5	4.15	-0.15	0.66	3.60	42.2	
37	9.5	5.5	4.21	0.06	0.77	3.62	42.4	
42	10.4	5.5	4.38	0.24	0.88	3.79	36.7	
47	11.4	5.5			0.76	3.81	32.8	
52	12.3	5.5	5.21	-0.43	0.65	4.03	31.7	
57	13.2	5.5			0.59	4.20	25.7	
62	14.1	5.5	5.24	-0.88	0.38	4.36	23.9	
67	15.0	5.1	5.20	-0.37	0.16	4.52	25.8	
72	16.6	3.4	5.06	-0.14	0.34	4.39	29.4	
77	18.2	3.1	5.17	-0.48	0.28	4.42	32.3	
82	19.8	3.1			0.39	4.33	34.6	
87	21.4	3.1			0.41	4.30	33.2	
92	23.0	3.0			0.34	4.29	28.4	
97	25.9	2.4					26.5	
102	28.7	1.8			0.41	4.15	32.8	
107	31.6	1.7			0.40	4.28	27.3	
112	34.5	1.7			0.42	4.19	26.3	
117	37.4	1.7			0.46	4.15	27.3	
122	40.3	1.7			0.51	4.24	32.3	
127	43.1	1.7			0.37	4.27	31.8	
132	46.0	1.7			0.41	4.24	23.2	
137	48.9	1.7			0.41	4.17	31.9	
142	51.7	1.7			0.37	4.30	31.8	
147	54.6	1.7			0.49	4.14	23.4	
152	57.5	1.7			0.48	4.20	27.6	
157	60.4	1.7			0.45	4.20	25.7	
162	63.3	1.7			0.19	4.29	22.4	
167	66.1	1.7			0.36	4.21	24.5	
172	69.0	1.9			0.33	4.16	33.3	
177	70.3	3.6			0.48	3.99	35.6	
182	71.6	3.9			0.47	4.04	38.7	
187	72.9	3.9			0.70	3.86	36.1	
192	74.1	3.9			0.66	3.90	38.2	
197	75.4	3.9			0.80	3.73	32.2	
202	76.7	3.9			0.74	3.88	31.9	
207	78.0	3.9			0.64	3.81	23.0	
212	79.3	3.9			0.68	3.81	21.8	
217	80.6	3.9			0.74	3.58	18.3	
222	81.9	3.9			0.60	3.73	19.5	
227	83.1	3.9			0.70	3.69	24.6	
232	84.4	3.9			0.63	3.81	25.4	
237	85.7	3.9			0.51	3.98	30.9	
242	87.0	4.1			0.55	4.17	25.1	
247	87.8	6.2			0.47	3.89	25.8	
252	88.5	6.6			0.49	3.80	21.2	
257	89.3	6.6			0.68	3.93	21.4	
262	90.0	6.6			0.67	3.82	20.9	
267	90.8	6.6			0.70	3.83	21.8	
272	91.6	6.6			0.65	3.80	17.8	
277	92.3	6.6			0.66	3.83	18.7	
282	93.1	6.6			0.69	3.72	18.4	
287	93.8	6.6			0.73	3.79	16.6	
292	94.6	6.6			0.74	3.84	16.1	
297	95.4	6.6			0.67	3.88	17.9	
302	96.1	6.6			0.69	3.85	18.9	
307	96.9	6.6			0.57	3.68	18.5	
312	97.6	6.6					17.1	
317	98.4	6.6					16.3	
322	99.2	6.6			0.54	3.73	14.5	
327	99.9	6.6			0.49	3.76	14.3	
332	100.7	6.6			0.47	3.65	16.0	
337	101.4	6.6			0.45	3.70	17.2	
342	102.2	6.6			0.57	3.82	21.8	
347	103.0	6.6			0.52	3.94	29.7	
352	103.7	6.6			0.45	3.90	25.0	
357	104.5	6.6			0.57	4.00	24.7	
362	105.2	6.6			0.51	4.00	19.8	
367	106.0	6.4			0.53	4.08	25.7	
372	107.0	5.2			0.50	4.05	31.3	
377	108.0	5.0			0.45	3.98	27.7	
382	109.0	5.0			0.48	3.85	21.6	41.9
387	110.0	5.0			0.57	3.83	23.5	41.8
392	111.0	5.0			0.48	3.12	28.8	20.2
397	112.0	5.0			0.54	3.81	29.1	45.2
402	113.0	5.0			0.62	2.90	30.3	47.4
407	114.0	5.0			0.65	3.06	29.8	50.5
412	115.0	5.0			0.61	2.75	31.3	47.7
417	116.0	5.0			0.45	2.62	34.0	46.0
422	117.0	5.0			0.61	2.65	32.8	43.2
427	118.0	5.0			0.48	2.69	31.3	42.7
432	119.0	5.0			0.38	2.66	32.3	42.2
437	120.0	5.0			0.37	2.77	30.8	45.4
442	121.0	5.0			0.46	2.66	30.1	45.0
447	122.0	5.0			0.37	2.81	27.8	48.8
452	123.0	5.0			0.52	2.77	29.8	42.8
457	124.0	5.0			0.51	2.84	35.2	34.0
462	125.0	5.0			0.14	2.81	45.7	36.3
467	126.0	5.0			0.07	2.87	53.0	9.0
472	127.0	5.0			0.27	3.13	48.8	12.7
477	128.0	5.0			0.15	3.19	43.0	13.3
482	129.0	5.0			0.41	3.72	29.8	18.8

Table 9: Stable isotope and sedimentologic data of core **SO136-111**

			C. wuellerstorfi		*N. pachyderma*		Carbonate	Biog. Silica
Depth	**Age**	**LSR**	**$\delta^{13}C$**	**$\delta^{18}O$**	**$\delta^{13}C$**	**$\delta^{18}O$**	**Conc.**	**Conc.**
(cm)	(ka)	(cm/kyr)	(‰ vs PDB)	(‰ vs PDB)	(‰ vs PDB)	(‰ vs PDB)	(wt-%)	(wt-%)
487	130.0	5.0					15.3	15.5
492	131.0	5.0			0.16	4.14	10.6	19.2
497	132.0	5.0			0.00	4.33	12.8	23.3
502	133.0	4.3			-0.04	4.52	15.1	22.4
507	136.2	2.0			0.01	4.32	15.0	36.0
512	139.4	1.6			-0.09	4.43	11.0	22.2
517	142.6	1.6			0.26	4.39	8.5	18.7
522	145.8	1.6			0.08	4.36	3.4	
527	148.9	1.6			0.17	4.26	4.8	
532	152.1	1.6			-0.03	4.33	5.8	
537	155.3	1.6			-0.08	3.98	7.2	
542	158.5	1.6			0.07	4.19	3.7	
547	161.7	1.6			0.15	4.13	2.6	
552	164.9	1.6			0.01	4.03	1.8	
557	168.1	1.6			0.31	4.33	3.1	
562	171.2	1.6			0.25	4.24	6.0	
567	174.4	1.6			0.21	3.96	10.6	
572	177.6	1.6			0.29	3.78	11.8	
577	180.8	1.6			0.12	3.89	9.7	
582	184.0	1.7			0.37	3.90	7.1	
587	185.3	3.5			0.33	3.39	6.4	
592	186.7	3.7			0.25	3.62	9.0	
597	188.0	3.7			0.38	3.54	10.6	
602	189.3	3.7			0.51	3.70	11.2	
607	190.7	3.7			0.31	3.31	13.4	
612	192.0	3.7			0.45	3.38	13.8	
617	193.3	3.7			0.36	3.07	13.8	
622	194.7	3.7			0.23	3.30	14.1	
627	196.0	3.6			0.19	3.20	12.8	
632	197.8	2.9			0.11	3.09	11.9	
637	199.6	2.8			0.41	3.31	11.0	
642	201.4	2.8			0.26	3.51	12.1	
647	203.2	2.8			0.31	3.09	12.3	
652	205.1	2.8			0.33	3.29	12.2	
657	206.9	2.8			0.38	3.17	13.9	
662	208.7	2.8			0.32	3.33	14.4	
667	210.5	2.8			0.31	3.14	15.5	
672	212.3	2.8			0.22	3.21	19.1	
677	214.1	2.8			0.29	3.31	18.0	
682	215.9	2.8			0.32	3.09	17.7	
687	217.7	2.8			0.37	3.17	17.8	
692	219.6	2.8			0.29	3.52	26.9	
697	221.4	2.8					24.5	
702	223.2	2.8			0.14	3.85	18.5	
707	225.0	2.9			0.10	3.87	14.8	
712	226.3	3.7			0.14	3.93	7.5	
717	227.6	3.8			0.29	3.45	6.4	
722	228.9	3.8			0.41	3.34	12.0	
727	230.2	3.8			0.52	3.27	22.4	
732	231.6	3.8			0.55	3.39	32.3	
737	232.9	3.8			0.58	3.36	36.4	
742	234.2	3.8					40.9	
747	235.5	3.8					33.8	
752	236.8	3.8			0.39	3.30	39.5	
757	238.1	3.8			0.28	2.90	37.5	
762	239.4	3.8			0.34	3.34	44.8	
767	240.7	3.8			0.29	3.34	40.8	
772	242.1	3.8			0.24	3.90	16.8	
777	243.4	3.8			0.33	3.38	3.2	
782	244.7	3.8			0.13	3.37	5.8	
787	246.0	3.1			-0.28	4.25	10.3	
792	254.7	1.0			-0.25	4.30	9.5	
797	263.3	0.6			-0.43	4.28	1.9	
802	272.0	0.8					1.1	
807	277.0	0.9					2.5	
812	282.0	1.1					2.3	
817	287.0	1.2					1.2	
822	292.0	1.3					1.0	
827	296.6	1.4					1.0	
832	299.8	1.5					2.9	
837	302.9	1.6					6.5	
842	306.0	1.6					0.9	
847	309.1	1.6					7.4	
852	312.3	1.7					5.4	
857	315.4	2.2					4.3	
862	317.4	2.6					10.8	
867	319.1	2.9			0.17	3.07	19.8	
872	320.7	3.0			0.36	2.98	21.8	
877	322.4	3.0			0.14	3.06	25.6	
882	324.1	3.0			0.18	2.71	26.3	
887	325.8	3.0			0.16	2.85	24.8	
892	327.5	3.0					26.0	
897	329.2	3.0					25.8	
902	330.9	3.0			0.19	2.94	46.2	
907	332.6	3.0			0.13	3.44	52.0	
912	334.3	3.0			0.16	3.86	3.5	
917	336.0	3.0			-0.10	4.14	5.5	
922	337.7	3.0					0.9	
927	339.4	3.0					0.8	
932	341.1	3.0					1.0	
937	342.8	3.0					1.1	
942	344.5	3.0					1.0	
947	346.2	3.0					1.4	

Table 10: Stable isotope data of core MD97-2109

			C. wuellerstorfi	
Depth (cm)	**Age** (ka)	**LSR** (cm/kyr)	**$\delta^{13}C$** (‰ vs PDB)	**$\delta^{18}O$** (‰ vs PDB)
3	4.2	5.0	1.72	2.56
8	5.2	5.0	1.29	2.30
13	6.2	5.0	1.77	3.58
18	7.2	5.0	1.80	2.41
23	8.1	5.0	1.66	2.75
28	9.1	5.0	1.71	3.19
33	10.1	5.0	1.61	3.04
38	11.1	5.0	1.79	2.91
43	12.1	5.0	1.70	3.36
48	13.0	5.0	1.59	3.45
53	14.0	5.0	1.83	3.86
58	15.0	4.0	1.99	4.29
63	23.3	1.2	1.74	3.88
68	31.7	0.6	2.07	3.35
73	40.0	0.6	1.90	3.89
78	46.0	0.8	1.61	4.00
83	52.0	0.8	1.98	4.04
88	58.0	0.8	1.78	3.87
93	64.0	0.8	1.83	4.15
98	70.0	0.9	2.18	3.31
103	71.7	2.7	2.03	3.30
108	73.4	2.9	2.21	3.45
113	75.1	2.9	1.76	3.63
118	76.8	2.9	1.94	3.29
123	78.5	2.9	2.23	3.57
128	80.2	2.9	1.99	3.43
133	81.9	2.9	2.03	3.55
138	83.6	2.9	2.08	3.24
143	85.3	2.9	2.03	3.53
148	87.0	2.9	2.05	3.60
153	88.7	3.0	2.09	3.36
158	90.3	3.0	2.17	3.32
163	92.0	3.0	2.09	3.27
168	93.7	3.0	2.12	3.48
173	95.3	3.0	1.99	3.45
178	97.0	3.0	1.99	3.43
183	98.7	3.0	1.86	3.39
188	100.3	3.0	1.93	3.49
193	102.0	3.0	1.91	3.42
198	103.7	3.0	1.99	3.47
203	105.3	3.0	1.99	3.41
208	107.0	2.9	1.97	3.61
213	109.3	2.3	1.81	3.72
218	111.6	2.2	1.74	3.00
223	113.9	2.2	1.53	2.57
228	116.2	2.2	1.50	2.58
233	118.5	2.2	1.38	2.47
238	120.8	2.2	1.16	2.40
243	123.1	2.2	1.64	3.10
248	125.4	2.2	1.15	2.41
253	127.7	2.2	1.76	3.05
258	130.0	1.9	1.66	3.80
263	135.6	1.1	1.56	3.27
268	141.2	0.9	1.76	3.31
273	146.8	0.9	1.68	3.18
278	152.4	0.9	1.52	3.35
283	158.0	0.9	2.06	3.81
288	162.0	1.2	1.74	3.65
293	166.0	1.3	1.81	3.41
298	170.0	1.3	2.01	3.59

Table 11: Stable isotope data of core **SO136-011**

			C. wuellerstorfi	
Depth (cm)	**Age** (ka)	**LSR** (cm/kyr)	**$\delta^{13}C$** (‰ vs PDB)	**$\delta^{18}O$** (‰ vs PDB)
1	0.00	10.9		
5	0.37	10.9		
9	0.74	10.9	0.63	2.73
13	1.11	10.9		
17	1.47	10.9		
21	1.84	10.9	0.37	2.38
25	2.21	10.9	0.89	2.75
29	2.58	10.9		
33	2.95	10.9		
37	3.32	10.9		
41	3.68	10.9	0.86	2.54
45	4.05	10.9	0.61	2.64
49	4.42	10.9		
53	4.79	10.9	0.36	3.11
57	5.16	10.9	0.39	2.93
61	5.53	10.9	0.68	2.92
65	5.89	10.9	0.69	2.97
69	6.26	10.9	0.66	3.00
73	6.63	10.9	0.79	2.97
77	7.00	10.9	0.22	2.60
81	7.37	10.9	0.68	2.65
85	7.74	10.9		
89	8.11	10.9	0.08	3.58
93	8.47	10.9		
97	8.84	10.9	0.53	3.62
101	9.21	10.9	0.53	3.55
105	9.58	10.9	0.32	3.36
109	9.95	10.9		
113	10.32	10.9	0.31	3.88
117	10.68	10.9	0.52	3.57
121	11.05	10.9	0.69	3.77
125	11.42	10.9	0.14	3.92
129	11.79	10.9	0.29	4.00
133	12.16	10.9	0.21	4.11
137	12.53	10.9	0.28	4.32
141	12.90	10.9	0.26	4.00
145	13.26	11.7	0.30	4.08
149	13.63	11.7	0.39	4.10
153	14.00	11.7	0.20	4.34
157	14.34	11.7	0.08	4.31
161	14.69	11.7	-0.21	4.12
165	15.03	11.7	0.25	4.11
169	15.37	11.7		
173	15.71	11.7	0.02	4.33
177	16.06	11.7	0.35	3.89
181	16.40	11.7	0.25	4.34
185	16.74	11.7	0.09	4.38

Table 12: Stable isotope data of core **SO136-003**

			C. wuellerstorfi	
Depth (cm)	**Age** (ka)	**LSR** (cm/kyr)	**$\delta^{13}C$** (‰ vs PDB)	**$\delta^{18}O$** (‰ vs PDB)
0	3.0	2.6	1.06	2.23
6	5.3	2.6	1.32	2.19
10	6.9	2.6	1.15	2.05
14	8.4	2.6		
18	10.0	2.6	1.04	2.32
22	11.6	2.6	1.06	3.61
28	13.9	2.6	0.77	3.94
31	15.1	2.6	0.87	3.90
36	17.0	2.7	0.74	3.71
40	18.1	3.4	0.88	3.71
47	20.1	3.5	1.02	3.79
60	23.8	3.5	0.92	3.81
64	25.0	3.5	0.99	3.62
68	26.1	3.5	1.01	3.80
72	27.2	3.5	0.68	3.41
76	28.4	3.5		
80	29.5	3.5	1.06	3.51
84	30.6	3.5	0.82	3.27
88	31.8	3.5	1.01	3.49
91	32.6	3.5	0.95	3.12
96	34.0	3.5	1.23	3.52
100	35.2	3.5	1.22	3.57
104	36.3	3.5	1.16	3.53
108	37.5	3.5	1.07	3.45
112	38.6	3.5	1.12	3.38
116	39.7	3.5	1.09	3.56
120	40.9	3.5	1.20	3.43
124	42.0	3.5	1.06	3.57
128	43.3	3.1	1.04	3.27
130	44.0	3.1	0.99	3.55
134	45.3	3.1	1.02	3.19
138	46.6	3.1	1.25	3.20
142	47.9	3.1	0.66	3.61
146	49.2	3.1	0.58	3.42
150	50.5	3.1	1.03	3.06
154	51.8	3.1	1.11	3.19
158	53.1	3.1	0.72	3.42
164	55.0	3.1	0.94	3.25
168	56.3	3.1	0.68	3.37
170	57.0	3.1	0.82	3.54
176	59.0	3.1	0.86	3.57
180	60.3	3.1	0.72	3.42
184	61.6	3.1	0.68	3.59
192	64.2	3.1	0.81	3.47
196	65.5	3.1	0.84	3.40
200	66.8	3.1	0.97	3.37
204	68.1	3.1	0.80	3.65
212	70.7	3.1	0.98	3.26
216	72.0	3.1		
220	73.3	3.0	0.87	2.97
224	74.7	3.0	0.88	2.23
227	75.7	3.0	1.26	3.17
229	76.3	3.0	1.07	3.25
238	79.3	3.0	0.89	2.52
242	80.7	3.0	1.03	3.19
246	82.0	3.0	0.83	3.01
250	83.3	3.0	1.12	2.65
258	86.0	3.0	0.73	3.15
266	88.5	3.2	1.03	3.05
274	91.0	3.2	0.66	2.84
278	92.3	3.2	0.94	2.79
282	93.5	3.2	1.27	2.63
290	96.0	3.2	0.96	2.81
294	97.3	3.2	0.99	2.62
298	98.5	3.2		
306	101.0	3.2	1.09	2.68
310	102.3	3.2	1.00	2.96
314	103.5	3.2	1.25	2.77
318	104.8	3.2		
322	106.0	2.9	0.97	3.04
326	108.7	1.7	0.85	2.94
332	112.7	1.5	0.93	2.76
336	115.3	1.5	1.08	2.31
340	118.0	1.5	1.08	1.95
346	122.0	1.6	0.94	1.80
352	124.1	2.7	0.92	1.92
360	126.9	2.9	0.93	3.35
364	128.2	2.9	0.97	3.06
368	129.6	2.9	0.78	3.68
372	131.0	3.0	0.65	3.86
376	132.2	3.4	0.78	3.89
380	133.3	3.4	0.84	3.76
384	134.5	3.4	0.73	3.71
388	135.7	3.4	0.80	3.68
392	136.8	3.4	0.61	3.86
396	138.0	3.4	0.75	3.75
398	138.6	3.4	0.50	3.98
402	139.7	3.4	0.64	3.72
406	140.9	3.4	0.72	3.77
410	142.0	3.4	0.66	3.81
414	143.2	3.4	0.72	3.70
418	144.4	3.4	1.01	3.46
422	145.5	3.4		
426	146.7	3.4	0.77	3.34
429	147.6	3.4	0.70	3.78
432	148.4	3.4	0.85	3.58
436	149.6	3.4	0.80	3.61

Table 12: Stable isotope data of core **SO136-003**

			C. wuellerstorfi	
Depth (cm)	**Age** (ka)	**LSR** (cm/kyr)	**$\delta^{13}C$** (‰ vs PDB)	**$\delta^{18}O$** (‰ vs PDB)
440	150.7	3.4	0.59	3.56
444	151.9	3.4	0.81	3.81
448	153.1	3.4	0.45	3.66
452	154.2	3.4	0.48	3.68
456	155.4	3.4	0.87	3.46
461	156.8	3.4		
465	158.0	3.5	0.93	3.60
469	158.9	4.2	0.65	3.49
473	159.8	4.4	0.49	3.40
477	160.8	4.4	0.70	3.46
481	161.7	4.4	0.57	3.47
485	162.6	4.4	0.54	3.42
489	163.5	4.4	0.64	3.22
493	164.4	4.4	0.56	3.26
497	165.3	4.4	0.84	3.14
501	166.25	4.4	0.8	3.2
505	167.2	4.4	0.43	3.21
509	168.1	4.4	0.63	3.20
513	169.0	4.0	0.89	3.47
517	170.9	2.4	0.57	3.46
521	172.8	2.1	0.56	3.48
525	174.6	2.1	0.50	3.43
529	176.5	2.1	0.58	3.52
533	178.4	2.1	0.87	3.25
537	180.3	2.1	0.43	3.14
545	184.0	2.2	0.53	2.92
557	189.2	2.3	1.20	2.36
561	190.9	2.3	1.19	2.44
569	194.4	2.3	1.06	2.20
573	196.1	2.3		
589	203.0	2.3	0.63	2.80

Table 13: Stable isotope data and sedimentologic data of core **ELT35-002**

			C. wuellerstorfi		Carbonate		Coarse	Fragmentation
Depth	**Age**	**LSR**	**$\delta^{13}C$**	**$\delta^{18}O$**	**Conc.**	**AR**	**Carbonate**	**Ratio**
(cm)	(ka)	(cm/kyr)	(‰ vs PDB)	(‰ vs PDB)	(wt-%)	($g/cm^2/kyr$)	(wt-%)	(%)
5	3.0	2.5	2.72	3.36	90.4	1.0	59.2	7.9
9	4.6	2.5	2.73	3.37	90.5	0.9	56.1	7.0
14	6.6	2.5	2.78	3.42	91.8	1.0	57.3	5.4
18	8.2	2.5	3.32	3.96	91.4	1.0	58.7	4.3
26	11.4	2.5	3.66	4.30	87.2	1.0	60.3	3.4
35	15.0	2.6	4.07	4.71	92.7	1.0	58.5	6.4
45	18.4	2.9	4.03	4.67	85.1	1.7	76.7	9.6
55	21.8	2.9	3.87	4.51	88.1	1.6	74.2	4.5
65	25.2	2.9	4.02	4.66	86.1	1.5	70.3	6.3
75	28.6	2.9	3.89	4.53	88.0	1.5	70.5	5.4
85	32.0	2.8	3.42	4.06	88.8	1.3	64.3	4.0
95	36.6	2.3	3.61	4.25	91.0	1.1	66.5	4.8
105	41.2	2.2	3.50	4.14	90.9	1.0	64.1	5.6
115	45.8	2.2	3.46	4.10	90.2	1.1	67.0	3.8
125	50.4	2.2	3.56	4.20	91.3	1.1	68.4	4.2
135	55.0	2.2	3.50	4.14	90.3	1.0	62.4	5.0
145	58.7	2.6	4.01	4.65	86.0	0.8	52.2	11.9
150	60.6	2.7	4.16	4.80	81.9	0.9	56.1	9.3
155	62.5	2.7	3.76	4.40	83.1	1.0	59.9	8.1
165	66.2	2.7	4.37	5.01	81.4	1.5	75.3	16.8
175	70.0	2.6	3.76	4.40	84.1	1.4	73.8	14.8
185	74.1	2.4	3.02	3.66	87.7	1.2	68.4	8.0
195	78.3	2.4	3.33	3.97	82.8	1.1	68.0	6.5
205	82.4	2.4	3.21	3.85	89.0	1.3	70.7	7.3
211	84.9	2.4	3.38	4.02	79.7	0.8	53.3	6.2
216	87.0	2.2	3.92	4.56	87.7	1.0	66.9	10.2
225	93.9	1.4	3.54	4.18	85.7	0.6	60.7	20.0
235	101.6	1.3	3.66	4.30	80.4	0.4	47.3	10.2
242	107.0	1.3	4.01	4.65	81.8	0.4	52.4	25.0
246	111.3	1.0	3.62	4.26	91.1	0.1	21.1	26.8
251	116.6	0.9	2.79	3.43	93.0	0.1	18.4	19.4
256	122.0	1.1	2.75	3.39	90.3	0.1	16.5	23.3
265	124.8	3.0	3.04	3.68	89.6	0.4	25.4	18.6
275	127.9	3.2	3.53	4.17	85.0	0.7	39.6	9.5
285	131.0	3.2	4.01	4.65	86.9	0.8	42.1	18.8
295	134.0	3.3	3.48	4.12	68.1	1.4	66.4	5.7
305	137.0	3.3	3.89	4.53	84.3	1.6	67.2	7.7
315	140.0	3.3	4.24	4.88	80.2	1.6	69.6	7.8
325	143.0	3.3	3.89	4.53	79.1	1.7	71.5	
336	146.3	3.3	3.90	4.54	85.5	1.6	66.5	9.9
345	149.0	3.3	4.00	4.64	87.7	1.6	68.6	
355	152.0	3.3	3.43	4.07	88.0	1.7	69.1	7.3
365	155.0	3.3	4.03	4.67	85.4	1.6	68.8	
375	158.0	3.2	4.12	4.76	88.0	1.7	71.7	11.8
385	162.0	2.6	4.01	4.65	87.2	1.2	67.0	
395	166.0	2.5	3.89	4.53	88.5	1.3	71.3	11.6
405	170.0	2.5	3.86	4.50	82.6	1.4	74.8	
415	174.0	2.5	4.12	4.76	84.9	1.1	65.2	11.3
425	178.0	2.5	4.07	4.71	89.4	1.1	64.0	
435	182.0	2.4	4.26	4.90	85.2	1.0	63.5	12.1
445	187.5	1.9	3.61	4.25	77.7	0.9	69.4	12.8
455	193.0	1.8	3.67	4.31	82.6	0.6	54.8	18.7
465	198.5	1.8	3.96	4.60	85.0	0.7	59.2	13.3
475	204.0	1.8	3.77	4.41	84.5	0.8	61.8	
485	209.5	1.8	3.89	4.53	84.2	0.6	54.9	12.2
495	215.0	1.8	3.76	4.40	81.9	0.8	63.5	
505	220.5	1.8	3.94	4.58	80.8	0.6	56.4	8.0
515	226.0	2.0	4.12	4.76	78.0	0.8	65.3	10.1
525	228.9	3.3	3.71	4.35	85.7	1.4	63.5	
535	231.7	3.5	3.89	4.53	88.4	1.2	55.2	15.2
545	234.6	3.5	3.47	4.11	85.7	1.5	63.9	
555	237.4	3.5	3.58	4.22	83.1	1.6	65.9	9.2
565	240.3	3.5	3.82	4.46	86.2	1.5	63.7	7.7
575	243.1	3.5	3.66	4.30	87.0	1.4	59.1	9.8
585	246.0	3.5	4.02	4.66	83.5	1.3	56.3	10.0

Table 14: Stable isotope data and sedimentologic data of core **ELT39-043**

			C. wuellerstorfi		Carbonate		Coarse	Fragmentation
Depth	**Age**	**LSR**	**$\delta^{13}C$**	**$\delta^{18}O$**	**Conc.**	**AR**	**Carbonate**	**Ratio**
(cm)	(ka)	(cm/kyr)	(‰ vs PDB)	(‰ vs PDB)	(wt-%)	($g/cm^2/kyr$)	(wt-%)	(%)
5	4.0	1.3	0.39	3.61	93.7	0.2	19.0	23.7
10	8.0	1.3	0.05	4.29	96.3	0.4	36.9	
15	12.0	1.3	-0.06	4.50	91.5	0.5	43.3	11.5
20	16.0	1.1	-0.20	4.97	93.7	0.5	54.5	
25	25.8	0.6	-0.03	4.81	91.8	0.3	57.4	12.5
30	35.5	0.5	-0.07	4.59	95.3	0.3	58.3	
35	45.3	0.5	-0.18	4.60	94.8	0.3	56.0	9.0
40	55.0	0.6	0.21	4.49	93.6	0.3	55.8	
45	59.7	1.0	-0.30	4.66	90.8	0.5	54.5	7.5
50	64.3	1.1	-0.09	4.63	87.7	0.4	48.7	
55	69.0	1.0	-0.08	4.63	91.3	0.4	42.6	22.8
60	75.0	0.9	0.15	4.32	86.0	0.3	41.3	
65	81.0	0.8	0.06	4.30	88.3	0.2	37.3	21.2
70	87.0	0.9	-0.13	4.46	91.8	0.3	35.2	
75	91.9	1.0	0.23	4.23	87.2	0.3	33.0	25.8
80	96.7	1.0	0.28	4.21	88.7	0.3	35.9	
85	101.6	1.0	0.24	4.23	90.8	0.3	30.9	26.0
90	106.4	1.0	0.28	4.05	87.9	0.3	32.9	
95	111.3	1.0	0.03	4.29	90.2	0.3	31.1	22.7
100	116.1	1.0	0.06	3.92	89.2	0.2	29.0	
105	121.0	1.1	0.03	3.79	88.0	0.2	28.1	23.1
110	124.7	1.3	0.14	4.06	89.9	0.4	34.5	
115	128.5	1.3	-0.50	4.63	89.3	0.5	42.4	12.6
120	132.2	1.3	-0.21	4.33	87.7	0.5	49.0	
125	136.0	1.2	-0.55	4.79	88.7	0.5	51.5	14.5
129	143.6	0.6	-0.30	4.79	89.8	0.3	50.3	
135	155.0	0.5	-0.17	4.60	88.1	0.2	49.8	18.3
140	164.5	0.5	-0.62	4.64	85.4	0.2	48.0	
145	174.0	0.5	-0.76	4.70	84.2	0.2	45.8	19.2
149	180.2	0.6	-0.58	4.60	82.6	0.2	40.9	
155	189.6	0.6	-0.80	4.32	84.3	0.2	37.2	25.2
160	197.4	0.6	0.01	4.61	85.7	0.2	34.1	
165	205.2	0.6	-0.60	4.57	86.5	0.2	36.0	23.7
170	213.0	0.6	-0.38	4.40	88.3	0.2	39.4	
175	222.0	0.6	-0.25	4.54	87.3	0.2	40.0	22.6
180	231.0	0.6	-0.26	4.81	87.8	0.2	37.4	
185	240.0	0.6	-0.54	4.77	84.8	0.2	37.9	20.0
190	249.0	0.6	-0.66	4.95	84.5	0.2	35.7	
195	254.5	0.9	-0.46	4.89	83.6	0.2	34.6	21.3
200	259.9	0.9	-0.50	4.73	87.8	0.2	34.1	
205	265.4	0.9	-0.69	4.79	88.0	0.2	33.4	28.1
210	270.8	0.9	-0.66	4.76	86.1	0.2	32.1	
215	276.3	0.9	-0.79	4.88	88.3	0.2	30.8	22.8
220	281.7	0.9	-0.64	4.54	87.6	0.2	26.8	
225	287.2	0.9	-0.84	4.25	89.3	0.2	23.8	26.6
230	292.6	0.9	-0.20	4.45	89.8	0.2	20.4	
235	298.1	0.9	-0.28	4.53	88.9	0.1	16.1	28.6
240	303.5	0.9	-0.18	4.45	88.5	0.1	12.7	
245	309.0	0.9	-0.75	3.90	90.7	0.1	9.9	35.4
250	314.0	1.0	0.35	4.25	91.3	0.1	8.4	
255	319.0	1.0	-0.72	4.99	91.4	0.1	7.6	34.3
260	324.0	1.0	0.35	4.17	91.6	0.1	8.9	
265	329.0	1.0	0.23	4.10	90.9	0.1	9.6	33.2
270	334.0	1.0	-0.44	4.70	90.7	0.1	11.2	
275	339.0	0.9	-0.51	5.04	85.6	0.1	11.7	34.8
280	348.7	0.6	-0.52	5.06	82.8	0.1	13.2	
285	358.3	0.5	-0.03	4.81	84.0	0.1	13.9	40.9
290	368.0	0.5	-0.12	4.67	88.9	0.0	10.4	
295	377.7	0.5	-0.32	4.41	88.6	0.0	8.6	46.5
300	387.3	0.5	0.15	4.51	89.0	0.0	7.8	
305	397.0	0.6	0.01	4.39	91.6	0.0	8.0	39.5
309	401.1	0.9	0.67	3.88	92.2	0.1	8.5	
315	407.3	1.0	-0.53	4.74	93.8	0.1	8.5	31.4
320	412.5	1.0	0.34	4.11	93.0	0.1	11.9	
325	417.7	1.0	0.31	4.24	95.0	0.1	15.7	37.1
330	422.8	1.0	-0.07	4.39	92.0	0.2	20.0	
335	428.0	1.0	-0.39	4.65	89.0	0.2	24.7	32.0
340	433.2	1.0	-0.64	4.78	84.8	0.2	24.2	
345	438.3	1.0	-0.18	4.75	81.0	0.2	27.6	44.7
350	443.5	1.0	-0.54	4.73	82.1	0.2	28.3	
355	448.7	1.0	-0.81	4.63	85.6	0.2	30.2	31.1
360	453.8	1.0	-0.93	4.85	86.5	0.2	31.4	

Table 15: Stable isotope data and sedimentologic data of core **ELT45-077**

			G. bulloides		Carbonate		Coarse
Depth	**Age**	**LSR**	**$\delta^{13}C$**	**$\delta^{18}O$**	**Conc.**	**AR**	**Carbonate**
(cm)	(ka)	(cm/kyr)	(‰ vs PDB)	(‰ vs PDB)	(wt-%)	($g/cm^2/kyr$)	(wt-%)
6	3.0	2.2	0.27	2.46	86.1	1.7	22.2
10	4.8	2.2	0.18	2.82	88.3	1.7	27.4
15	7.1	2.2	0.16	2.49	87.2	1.7	34.1
20	9.4	2.2	0.23	2.56	74.4	1.3	38.8
25	11.7	2.2	-0.11	3.29	68.4	1.2	46.3
30	14.0	1.8	0.31	3.77	49.5	0.6	42.6
35	32.0	0.5	0.45	3.78	46.1	0.1	25.9
40	50.0	0.3	0.13	3.46	37.5	0.1	40.5
45	68.0	0.3	0.36	3.40	40.9	0.1	36.5
50	70.8	1.6	0.38	3.04	48.2	0.5	35.5
55	73.6	1.8	0.84	2.86	68.3	0.9	30.6
60	76.4	1.8	0.56	2.82	71.7	1.0	34.9
65	79.2	1.8	0.51	2.66	71.2	1.0	26.2
70	82.0	1.8	0.41	2.80	74.4	1.1	27.6
75	84.8	1.8	0.44	2.89	73.6	1.1	32.0
79	87.0	1.6	0.17	2.97	65.9	0.8	29.2
85	94.5	0.9	0.05	2.80	46.6	0.3	29.6
90	100.7	0.8	-0.12	2.86	36.1	0.2	48.8
95	107.0	0.8	0.35	2.98	54.1	0.3	38.2
100	110.8	1.2	0.48	2.86	64.1	0.6	37.3
105	114.7	1.3	0.62	2.84	79.7	0.9	39.7
110	118.5	1.3	0.30	2.65	83.9	1.0	36.3
115	122.3	1.3	0.14	2.70	85.0	1.0	38.6
120	126.2	1.3	-0.13	3.04	80.2	0.9	40.8
125	130.0	1.1	-0.26	3.22	70.4	0.6	49.4
130	142.7	0.5	-0.10	3.23	57.7	0.2	46.4
135	155.5	0.4	-0.15	3.40	54.2	0.1	47.4
140	168.2	0.4	-0.35	3.31	63.2	0.2	49.7
145	181.0	0.4	0.15	3.34	52.2	0.1	48.1
150	192.0	0.4	-0.03	3.09	45.1	0.1	37.9
156	205.2	0.5	0.50	3.10	41.7	0.1	35.3
160	214.0	0.5	0.57	2.85	44.8	0.1	28.6
165	225.0	0.5	0.64	3.25	50.5	0.2	30.1
170	236.0	0.5	0.45	2.68	59.9	0.2	31.5
175	239.3	1.4	0.65	2.91	58.8	0.6	26.2
180	242.5	1.5	0.09	3.10	66.2	0.8	22.4
185	245.8	1.5	0.13	3.30	65.5	0.8	27.1
190	249.0	1.4	0.20	3.46	51.3	0.5	37.6
195	256.0	0.8	-0.05	3.50	54.7	0.3	32.9
200	263.0	0.7	0.07	3.49	52.7	0.3	28.7
205	270.0	0.7	0.49	3.20	66.6	0.4	19.2
210	277.0	0.7	0.08	3.58	75.3	0.4	20.3
215	284.0	0.7	0.45	2.98	77.9	0.5	15.3
220	292.0	0.6	0.88	2.87	75.7	0.4	12.6
225	300.0	0.6	0.43	2.92	80.3	0.4	14.2
230	308.0	0.6	0.63	2.62	80.7	0.4	10.2
235	316.0	0.7	0.27	3.19	85.4	0.5	8.5
240	320.4	1.1	0.05	2.91	85.1	0.8	8.8
245	324.8	1.1	0.08	2.94	84.1	0.8	9.4
250	329.2	1.1	0.03	3.02	88.2	0.9	16.3
255	333.6	1.1	-0.19	3.10	84.5	0.8	16.7
260	338.0	1.1	-0.04	3.51	74.7	0.7	13.3
265	342.3	1.2	0.21	3.53	62.3	0.5	12.1
270	346.7	1.2	0.19	3.26	69.7	0.6	11.0
275	351.0	1.0	-0.35	3.14	35.7	0.2	14.0
280	361.5	0.6	0.02	3.41	40.5	0.1	12.7
285	372.0	0.5	0.52	3.28	61.2	0.2	11.2
290	382.5	0.5	0.86	2.98	73.2	0.3	8.2
295	393.0	0.5	1.04	3.15	76.3	0.3	8.5
300	400.0	0.7	0.99	2.81	79.7	0.5	8.8
305	407.0	0.7	1.33	2.87	82.7	0.5	9.5
310	414.0	0.7	1.08	2.80	84.0	0.5	11.4
315	419.2	0.9	1.09	3.01	83.7	0.7	14.5
320	424.5	1.0	0.99	3.17	86.4	0.7	16.6
325	429.8	1.0	0.77	3.14	86.2	0.7	14.5
330	435.0	0.9	0.83	3.21	86.5	0.7	15.3
335	441.1	0.8	0.49	3.06	87.2	0.7	17.9
340	447.1	0.8	1.03	3.32	89.8	0.7	19.1
345	453.2	0.8	1.04	3.23	90.7	0.7	26.0
350	459.3	0.8	0.45	3.06	90.3	0.7	32.7
355	465.3	0.8	0.29	2.98	90.2	0.7	41.6
360	471.4	0.8	-0.05	2.90	86.4	0.6	46.5
367	479.9	0.8	-0.24	2.89	86.7	0.6	46.1
372	485.9	0.8	-0.12	2.95	83.2	0.6	42.8
377	492.0	0.8	0.05	3.12	61.7	0.4	33.4
383	499.3	0.8	-0.32	2.92	59.7	0.4	32.3
387	504.1	0.8	0.04	2.80	61.5	0.4	31.4
391	509.0	0.8	-0.06	2.80	63.0	0.4	28.2
395	513.8	0.8	-0.07	2.70	71.1	0.5	28.6
400	519.9	0.8	-0.40	2.59	72.4	0.5	35.9
405	526.0	0.8	-0.25	2.53	75.7	0.5	39.1
410	532.0	0.8	-0.74	2.90	59.7	0.4	35.6
415	538.1	0.8	-0.67	2.81	44.1	0.2	30.9
420	544.1	0.8	-0.53	2.90	58.7	0.3	39.7
425	550.2	0.8	-0.40	2.97	45.7	0.2	29.1
430	556.3	0.8	-0.37	2.78	43.1	0.2	30.5
435	562.3	0.8	-0.64	2.64	38.9	0.2	34.4
440	568.4	0.8	-0.85	2.53	77.5	0.5	37.2
445	574.5	0.8	-1.20	2.58	70.1	0.5	36.7
450	580.5	0.8			53.8	0.3	36.7
455	586.6	0.8	-0.66	2.38	72.3	0.5	23.8
460	592.7	0.8	-0.38	2.52	79.7	0.6	19.7
465	598.7	0.8	-0.35	2.57	71.2	0.5	16.4
470	604.8	0.8	-0.33	2.87	57.7	0.3	20.9
475	610.9	0.8	-0.16	2.45	67.4	0.4	20.0
480	616.9	0.8	-0.55	2.66	62.1	0.4	21.7
485	623.0	0.8	-0.89	2.99	68.5	0.4	21.0

EIDESSTATTLICHE ERKLÄRUNG

Hiermit erkläre ich an Eides statt, dass die Abhandlung mit dem Titel „Changes in ocean circulation and carbonate chemistry in the Australian sector of the Southern Ocean during the last 500,000 years“ - abgesehen von der Beratung durch den Betreuer - nach Inhalt und Form meine eigene Arbeit ist.

Diese Arbeit hat an keiner anderen Stelle im Rahmen eines Prüfungsverfahrens vorgelegen.

Arne Sturm Kiel, den 14.12.2003